INFORMATION TO USERS

This manuscript has been reproduced from the microfilm master. UMI films the text directly from the original or copy submitted. Thus, some thesis and dissertation copies are in typewriter face, while others may be from any type of computer printer.

The quality of this reproduction is dependent upon the quality of the copy submitted. Broken or indistinct print, colored or poor quality illustrations and photographs, print bleedthrough, substandard margins, and improper alignment can adversely affect reproduction.

In the unlikely event that the author did not send UMI a complete manuscript and there are missing pages, these will be noted. Also, if unauthorized copyright material had to be removed, a note will indicate the deletion.

Oversize materials (e.g., maps, drawings, charts) are reproduced by sectioning the original, beginning at the upper left-hand corner and continuing from left to right in equal sections with small overlaps.

Photographs included in the original manuscript have been reproduced xerographically in this copy. Higher quality 6" x 9" black and white photographic prints are available for any photographs or illustrations appearing in this copy for an additional charge. Contact UMI directly to order.

Bell & Howell Information and Learning
300 North Zeeb Road, Ann Arbor, MI 48106-1346 USA

UMI®
800-521-0600

Department of Civil Engineering and Applied Mechanics
McGill University, Montreal

A Thesis submitted to the Faculty of Graduate Studies and Research in partial fulfilment of the requirements of the degree of Master in Civil Engineering

"Centrifuge Modelling of LNAPL Transport in Partially Saturated Granular Medium"

Gennaro Esposito (Master Science)
Candidate Master Engineering

March, 1998

ABSTRACT

This thesis presents the experimental modelling of *Light Non-Aqueous Phase Liquids* transport in partially saturated with water sand using centrifuge tests, which were carried out at the Geotechnical Centrifuge facility located at Delft Technical University (The Netherlands). The experimentation consisted of a two-dimensional three-phase flow (air, water, Light Non-Aqueous Phase Liquids) in an unsaturated sand for two values of porosity. The Light Non-Aqueous Phase Liquids used in this research was a multigrade motor oil. The modelling of a two-dimensional flow and the use of a transparent strong-box enabled the direct observations of the experiments. Scaling laws developed in connection with other studies available in the literature were used. Tests were conducted at two different gravity accelerations, 20*g* and 30*g*, in order to verify, by means of the "*modelling of models*" technique, the similitude between the different experiments. The thesis covers details of the experimental methodologies and the measurement techniques which where used to evaluate the final water and LNAPL content in the experiments.

RESUME'

Ce mémoire discute l'analyse du transport LNAPL dans un sable partiellement saturé avec l'aide de testes centrifuge éxécutés à l'Université Delft de Technologie (aux Pays-Bas). L'expérience consistait en un model bidimensionnel de flux en trois phases (air, eau, LNAPL) dans un sable insaturé ayant deux valeurs de porosité. Deux accélérations gravitationnelle furent utilisées dans le but de vérifier, avec la méthode de "*modélisation des modèles*", la similitude entre différent modèles. Le mémoire présente les détails des méthodes expérimentales et des techniques de mesure qui furent utilisées pour évaluer le contenu final d'eau et de LNAPL dans les modèles. Les modèles centrifuges indique aussi le configuration des panaches de migration du LNAPL.

ACKNOWLEDGMENTS

The author wishes to express his gratitude to his thesis supervisor, Prof. A.P.S. Selvadurai, Department of Civil Engineering and Applied Mechanics, McGill University, for his guidance and his suggestions concerning this research. The author would especially like to thank Dr. H.G.B. Allersma, Geotechnical Laboratory, Delft Technical University (The Netherlands), for his suggestions during the experimental part of this research. The author also wishes to acknowledge the assistance of the technical staff of the Geotechnical Laboratory of Delft Technical University. In particular, the centrifuge tests was done with expert help of Mr. De Visser. The author would like to thank his colleges and friends Robert Iasenza, Holly Burton, Hamed Javaheri, Mira Rao, and Angela Seferta, for their assistance in reviewing drafts of the thesis. Thanks are also due to the Festen family who provided essential assistance during the stay in The Netherlands. Dr. J.E. Festen is thanked for her continuous support and encouragement throughout the duration of the work. Finally, the author wishes to thank his family for the assistance, support, and encouragement provided during the course of this work.

TABLE OF CONTENTS

LIST OF FIGURES

LIST OF TABLES

LIST OF SYMBOLS

C is solute concentration ($Kg \cdot m^{-3}$)

μ_f is fluid viscosity ($Pa \cdot sec$)

D_m is the coefficient of molecular diffusion ($m^2 \cdot t^{-1}$)

S is mass of adsorbed solute per unite volume ($Kg \cdot m^{-3}$)

v is the Darcian velocity ($m \cdot sec^{-1}$)

σ is the fluid-particle surface tension ($Pa \cdot sec$)

ρ_f is fluid density ($Kg \cdot m^{-3}$)

g is gravitational acceleration ($m \cdot sec^{-2}$)

l is characteristic microscopic length (m)

L is characteristic macroscopic length (m)

k_c is the first-order reaction rate constant (sec^{-1})

t is time (sec)

k is the intrinsic permeability of the medium (m^2)

N is the acceleration factor (N-times the earth's gravity)

v is the kinematics viscosity ($m^2 \cdot \sec^{-1}$)

k_f is the fluid relative permeability factor for the fluid based on its saturation

1. INTRODUCTION

1.1 GENERAL

The environmental damage caused by the release of hazardous chemical substances into the ground is a problem of major concern. Sources of chemical release range from abandoned hazardous waste disposal sites to leaking storage tanks located both above ground and underground. Currently, considerable resources have been directed to carrying out research on this specific topic. One such research area is the development of physical and numerical models for the study of contaminant flows through soils.

Predicting the transport of contaminants in the subsurface and in underground water has proven to be extremely challenging exercise. Accurate predictions of transport of pollutants in subsurface environments is important in assessing the risk of the exposure of the public to the contaminants and for the purpose of evaluating various remediation scenarios.

When considering the transport of *Non-Aqueous Phase Liquids* (NAPLs) in the subsurface, density and viscosity of the NAPL are of prime interest (Corapcioglu and Hossain, 1986). NAPLs are oily substances that exist in a liquid state in contact with water. Density of immiscible fluid relative to water is the parameter which delineates *light non-aqueous phase liquids* (LNAPLs) from *dense non-aqueous phase liquids* (DNAPLs),

(i.e. the "floaters" from the "sinkers".) Viscosity is a measure of the resistance of a fluid to stress induced flow. A less viscous fluid will penetrate a porous medium more readily. Fluids with densities higher than and viscosities lower than water will be more mobile in the subsurface than water.

However, other variables make the NAPL flow in the subsurface more complex. Consider for example the hypothetical NAPL contaminated subsurface scenario shown in Figure 1.1 (Abriola and Pinder, 1985). Initially, the NAPL contaminant enters the unsaturated soil and begins to infiltrate downwards under the effect of the gravity. The NAPL can be composed of a single contaminant or of multiple contaminants. It is less common that the pollutant may be introduced into the subsurface as the soluble portion of an aqueous phase (Abriola and Pinder, 1985). The vertical migration is coupled to horizontal movement due to diffusion and capillary suction (Mitchell, 1994). Around the contaminated region, a gaseous shell of chemical vapor may develop due to the volatilization of lighter components (Abriola and Pinder, 1985).

If the contaminant volume is sufficiently large, the NAPL may reach the capillary fringe. There, part of the contaminant can dissolve in the surrounding groundwater forming a plume of contaminated water which extends outwards from the central polluted zone. The dissolved phase may become part of the ground water system and can migrate along with the water phase. The non-aqueous phase liquid which does not dissolve can still be driven downwards if it possesses an adequate hydraulic gradient. If a sufficient quantity is present, undissolved non-aqueous phase liquid may finally reach the water table. At this

point, the water surface can be depressed by the weight of the contaminant. When the water table is

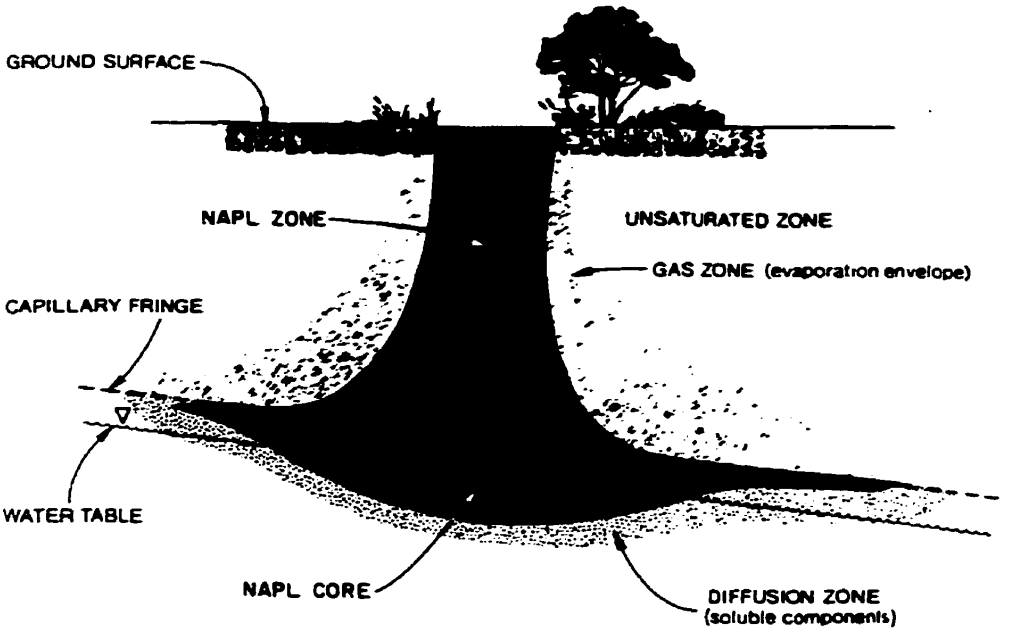

Figure 1.1 Schematic representation of lighter than water NAPL movement through the unsaturated and into the saturated zone (Abriola and Pinder, 1985)

non-horizontal, the non-aqueous phase liquid may move on the top of it following its slope. As shown in Figure 1.2 (Pinder and Abriola, 1986), non-aqueous phase liquids with density greater than water can continue migrating downwards until they encounter an impervious boundary. There, the dense non-aqueous phase liquids can spread over the impermeable geologic formation and move following the slope of the impervious boundary. However, most of the contaminant remains trapped in the unsaturated zone

due to the action of capillary forces (Abriola and Pinder, 1985). This non-aqueous phase liquid may be a source of contamination to either infiltrating rain water or rising ground water. The gaseous shell is also source of further contamination due to dissolution by infiltrating rain water.

Finally, the NAPL flow in unsaturated soils is made even more complicated by the seasonal movement of the water table. When the water table moves, it leaves residual NAPL behind it. If the water table rises faster than NAPL, "pockets" of free oil might also be left below the water table. In this thesis, the movement of light non-aqueous phase liquid in unsaturated sand is considered.

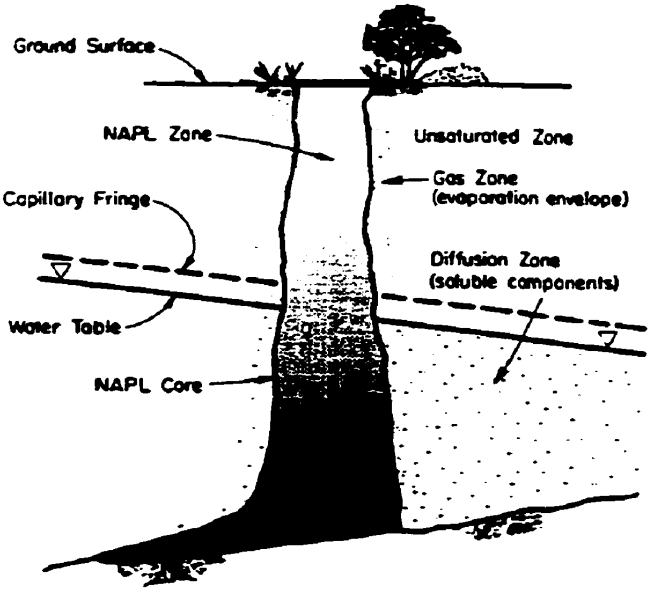

Figure 1.2 Schematic representation of heavier than water NAPL movement through the unsaturated and into the saturated zone (Pinder and Abriola, 1986)

1.2 APPLICATION OF CENTRIFUGE MODELLING

To quantify some of the phenomena described in the previous section and to forecast contaminant migration, both mathematical and physical models have been considered in the literature. Mathematical models of non-aqueous phase liquid flow and transport which take into account a variety of flow and transport processes are difficult to use and invariably require a numerical solution procedure. Alternatively, simpler mathematical models admit closed form solutions but require a large number of constraints to reduce the analysis to analytically manageable forms (Pinder and Abriola, 1985). Numerical models can provide good solutions for contaminant flows in saturated soils. When considering partially saturated soils, however, the transport processes are non-linear. Furthermore, it is difficult to characterize the *in situ* parameters governing transport processes. Thus, numerical solutions can provide estimates which can possess wide variability. In such instances, the flow of non-aqueous phase liquid flow through partially saturated soils may be better examined by recourse to physical models.

For partially saturated soils, a convenient and efficient physical model is a geotechnical centrifuge (Cooke and Mitchell, 1991). In this technique, prototype dimensions are scaled down, but the soil used in the model is identical to that of the prototype. This implies that by changing the acceleration of the model to equal the scale factor multiplied by the acceleration due to the earth's gravity field, it is possible to reproduce the gravity induced stress at any point of the prototype with the inertial mass induced stress at any point of the model (Mitchell, 1991). This is true if the boundary conditions are identical at all similar

points. The resulting changes in the soil properties of the model that occur due to the stress, will occur in the same way as they would in the prototype. Since the physical distances are reduced in the model, the time scale involved is reduced to equal the square of the scale factor.

The advantages of using a geotechnical centrifuge are both in the possibility of physical modelling which involves an extremely reduced time scale, and in the simulation of the actual effective stress field. The actual effective stress field is difficult to reproduce in a permeability test using a normal bench scale test. The centrifuge modelling described above would be an accurate way of defining the soil stress field.

Concerns related to delayed chemical effects can be overcome by testing at different time scales and comparing the results obtained. If the results are similar at different time scales, it can be assumed that they are similar at any time scale, including the real time. This procedure is called "modelling of models" (Mitchell, 1991). Moreover, since the time scale is reduced in the model, it is possible to carry out a large number of tests relatively quickly.

Another characteristic of geotechnical centrifuge modelling is that the model may be enhanced by the use of equipment that allows for direct observation of the soil behavior. In this research, video cameras and image processing technique were used to provide further information. Thus, a large amount of information may be obtained from centrifuge modelling. This data can be used to "calibrate" numerical models. Therefore, the

combined use of centrifuge modelling and numerical methods can provide satisfactory evaluations of the non-aqueous phase liquid movement in the subsurface.

1.3 OBJECTIVES

The primary aim of this research is to obtain information about light non-aqueous phase liquid movement in partially saturated sand using centrifuge models. In particular, attention is restricted to a two-dimensional situation where a light non-aqueous phase liquid is allowed to seep from a line source. The two-dimensional geometry of the model combined with the use of a transparent strong-box should allow the direct observation of the LNAPL transport in the porous medium. The influence of the porosity of the sand on the LNAPL flow and the effect of the capillary fringe and water table on the NAPL distribution are also investigated.

2. LITERATURE REVIEW

2.1 INTRODUCTION

The movement of non-aqueous phase liquids in porous media was first studied by petroleum reservoir engineers. They often examined the behavior of the two-phase system (water and non-aqueous phase liquid) to understand the mechanics of the movement of the oil in reservoirs. More recently, geoenvironmental engineers have conducted studies in this area to better understand the transport of organic phases in subsurface environments. Contamination by organic compounds is recognized as one of the main causes of pollution of soils and groundwater.

If the NAPL movement starts from near the ground surface, the NAPL may seep through unsaturated soils. In this case, due to the partial saturation of the soil, a three-phase flow occurs. Common LNAPLs are gasoline, diesel fuel, and motor oil. In this research, the LNAPL used in this study is Shell Multigrade motor oil 15W/40. DNAPLs include chlorinated hydrocarbons, such as, for example, trichloroethylene (Cl_3CH).

The NAPL can be composed of multiple compounds having different properties, as is the case with gasoline which is a mixture of up to 200 hundred different organic compounds (Corapcioglu and Baehr, 1987). NAPLs can be partially soluble in water, so that a dissolved phase as well as a non aqueous phase may be present (Schwille, 1981, 1984,

1988; Fetter, 1993). In the partially saturated zone of the soil, the NAPL can partition into the air as vapor phase (Baehr, 1987). If the non-aqueous phase liquid has a density greater than water, then it can flow below the water table resulting in a two-phase flow. Another factor which affects the NAPL migration in a porous medium is the interfacial tension of the liquids involved in the flow. The transport of each phase can be governed by both advection and diffusion which are, in turn, governed by gravity effects, pressure and concentration gradients. Finally, in addition to dispersion and diffusion, compounds can be involved in adsorption and chemical and biological degradation processes (Fetter, 1993).

Several analytical and numerical models are available in literature to describe a three-phase flow. Because of the extreme complexity of the phenomenon, these models are not completely exhaustive and the theoretical and computational modelling of three-phase flow is at present an hydrogeological challenge. Pinder and Abriola (1986) elaborated a model which utilizes 27 independent partial differential equations to obtain a comprehensive NAPL flow model.

2.2 BASIC CONCEPTS OF MULTI-PHASE FLOW

2.2.1 Saturation Ratio and Wettability

The saturation ratio of a fluid is the fraction of total pore space available that is filled with the liquid:

$$q = \frac{Fluid\ Volume}{Void\ Volume} \qquad (2.1)$$

The total of the saturation ratios for all the fluids present, including air, add up to 1.0 (Fetter, 1993). When a liquid is in contact with an other substance, such as an immiscible liquid or a solid, it possesses energy at the separation surface between the two substances. Such interfacial energy is due to the difference in degree of attraction between molecules of the substance to itself at the liquid surface, compared with the degree of attraction for molecules of the other substance. This energy is also called interfacial tension, and is defined as the amount of work necessary to separate a unit area of one substance from another, along the interface (Fetter, 1993). Thus, the interfacial tension has the units of work. Given three substances, two fluids, G and L, and a solid, S, the interfacial tension between any two substances (σ_{ij}) is schematically shown in Figure 2.1. The interfacial angle between the two fluids is given in equation (2.2), which is referred to as Young's equation:

$$\cos\theta = \frac{\sigma_{SG} - \sigma_{SL}}{\sigma_{GL}} \qquad (2.2)$$

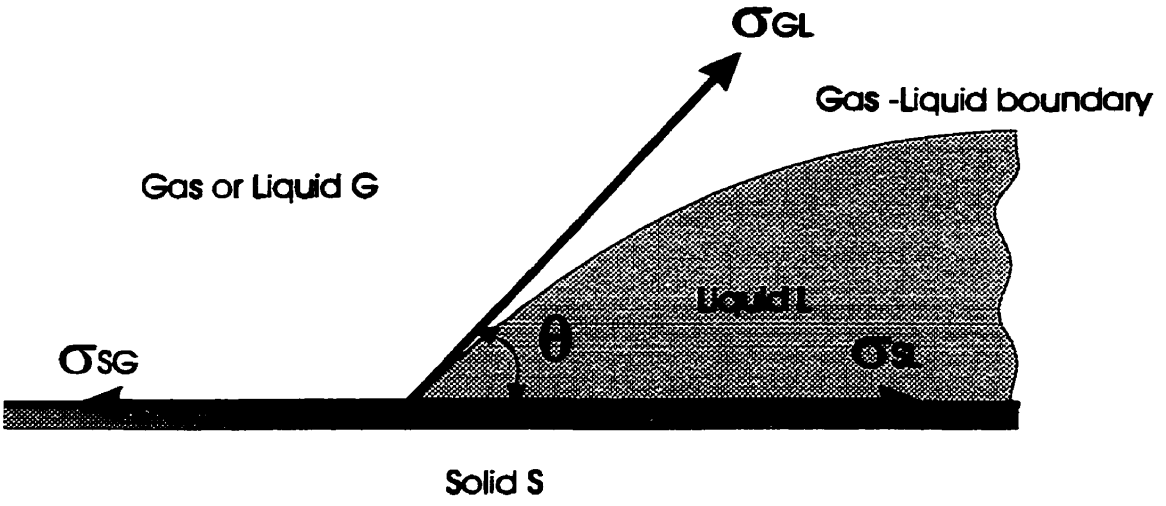

Figure 2.1 Interfacial Tensions between a solid surface, a wetting liquid surface, L, and a non-wetting liquid or gas phase, G.

By convention, θ is measured through the denser fluid. Owing to the different chemical-physical characteristics, when two fluids are in contact on a solid surface, one of the two tends to spread over, or wet, the whole surface available. This fluid is called wetting phase, whereas the other is non-wetting phase. In Figure 2.1, fluid L is the wetting phase. If the interfacial angle θ is greater than 90 degrees, then fluid G would be the wetting-phase. In general, in water-NAPL systems, water tends to be the wetting phase. If the solid medium is completely dry, the first fluid to spread over it would be the wetting phase: then it is possible to have oil-wet (or NAPL-wet) systems and water-wet systems. In nature, however, it is difficult to find a complete dry soil. Soils which appear completely dry may have water held to them by capillary forces (Fetter, 1993). When the water content is below the residual saturation, the water located between two grains forms

pendular rings. Despite the small volume, such water content is sufficient to consider the soil water-wet. Then, it is reasonable to consider most of the natural case NAPL releases onto the ground surface as water-wet. In this research, the sand models are water-wet, the air is the non-wetting phase, and the LNAPL is the intermediate-wetting phase, since it is assumed to spatially separate the wetting and the non-wetting phase (Stone, 1973).

2.2.2 Capillary Pressure

Since this study aims to model a three-phase flow in a partially saturated sand, it is useful to define the concept of *capillary pressure*. When two immiscible fluids are in contact, the pressure of each fluid measured close to the interfacial surface is not the same. This causes the formation of a curved separation surface. The difference in pressure is referred to as the capillary pressure. Given a wetting fluid having a pressure P_W, a non wetting fluid having pressure a P_{NW}, then the capillary pressure is

$$P_C = P_W - P_{NW} \qquad (2.3)$$

In an unsaturated soil, the pressure of the capillary water is negative.

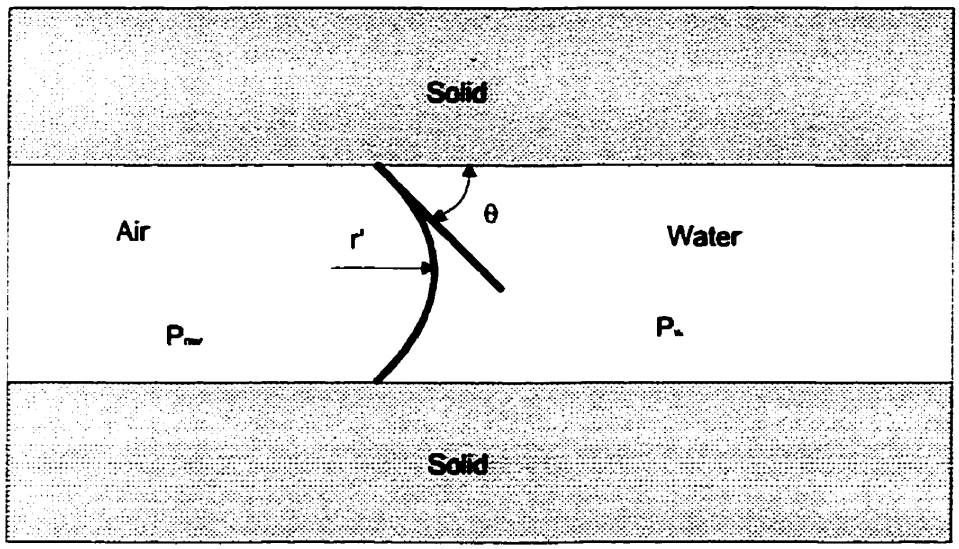

Figure 2.2 Radius of curvature for a spherical capillary interface.

Figure 2.2 shows the curved surface for a spherical air-water interface. The capillary pressure is directly proportional to the interfacial tension (σ) and inversely proportional to the radius of curvature (r'), as shown in equation (2.4):

$$P_C = \frac{2\sigma}{r'} \qquad (2.4)$$

Furthermore, the radius of curvature depends upon the amount of each fluid present in the system and upon the pore size. The capillary pressure is then a function of, (i) the properties of the two immiscible fluids, (ii) the proportion of wetting and non-wetting phases present in the porous medium, and (iii) the macroscopic geometry of the void

spaces in the soil. The latter is a soil characteristic that cannot easily be described mathematically (Fetter, 1993).

Usually, the capillary pressure is expressed as a function of the saturation ratio. Figure 2.3 shows an ideal capillary pressure - wetting fluid saturation curves for two-phase flow. It is interesting to note that the drainage (drying curve) and the imbibition (wetting curve) do not follow the same path and displays a hysterisis. Since, for a given porous medium, the capillary pressure - saturation relationships depend on the specific immiscible fluid, such relationships have to be determined experimentally. Two additional definitions should also be noted. The *irreducible wetting fluid saturation* is the ultimate value of wetting fluid saturation at which no more of the wetting fluid will be displaced by the non-wetting fluid. The *residual non-wetting fluid saturation* is the saturation value at which no more of the non-wetting fluid will be displaced by the wetting fluid.

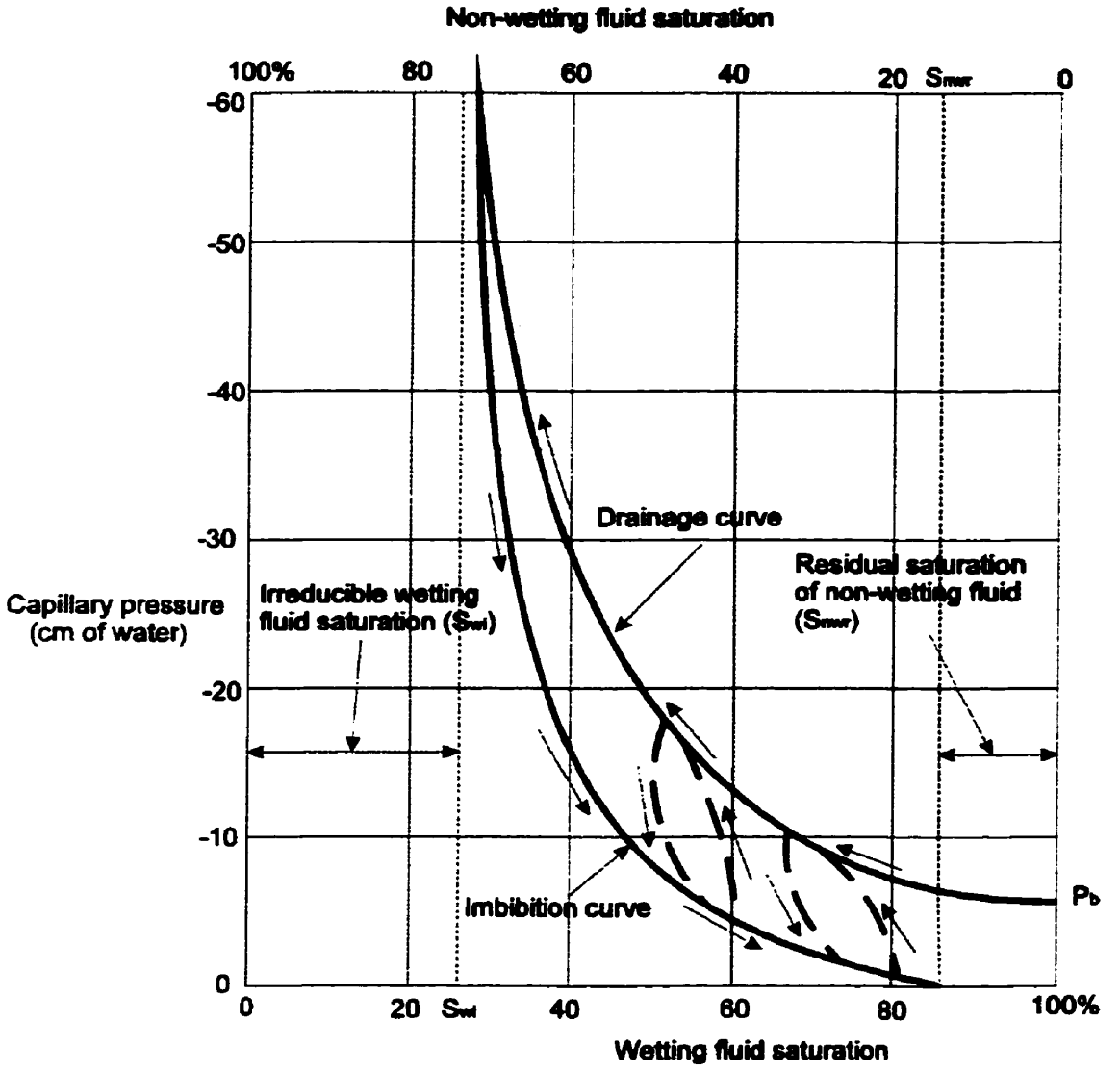

Figure 2.3 Capillary pressure-wetting fluid saturation curves for two-phase flow (Fetter, 1993)

In Figure 2.3, the drainage curve starts off at a wetting fluid saturation ratio of 1.0, and a non-zero capillary pressure, P_b. This pressure is called *bubbling pressure*, and is the value of pressure that the non-wetting fluid has to reach in order to displace the wetting fluid. In this study, the capillary pressure - saturation ratio relationship is expressed as fluid height above the water table against the fluid content. This choice enabled the

performance of simpler experimental measurement procedures. The total soil fluid potential is

$$\Phi = P_C + \rho_F g z \quad (2.5)$$

where

Φ	is fluid potential in terms of energy per unit volume
P_C	is the matric potential measured as capillary pressure,
ρ_F	is the fluid density
g	the acceleration of gravity
z	is the elevation above a reference plane

If equation (2.5) is divided by $\rho_F g$, the soil fluid potential Φ (expressed as energy per unit weight, which also has units of length) is obtained: i.e..

$$\Phi = \frac{P_C}{\rho_F g} + z = h + z \quad (2.6)$$

In (2.6), h, the pressure potential, is the matric potential with units of length (typically measured in cm.) A typical unsaturated soil profile expressed as capillary height against saturation is shown in Figure 2.4 (Abdul, 1988). In correspondence with the top of the unsaturated zone, the water is held at the irreducible water saturation. Such a case is called *pendular water*. As the water content begins to increase, the water is called

funicular water. Finally, there is the capillary fringe where the water is close to 100 percent of saturation. The top of the capillary zone, is not a smooth surface but is an extremely irregular fringe. This is because the capillary height depends upon the radius of the capillary tube, which is variable in a natural porous media. The inflection point of the unsaturated curve gives the approximate location of the top of the capillary fringe (Bear, 1972).

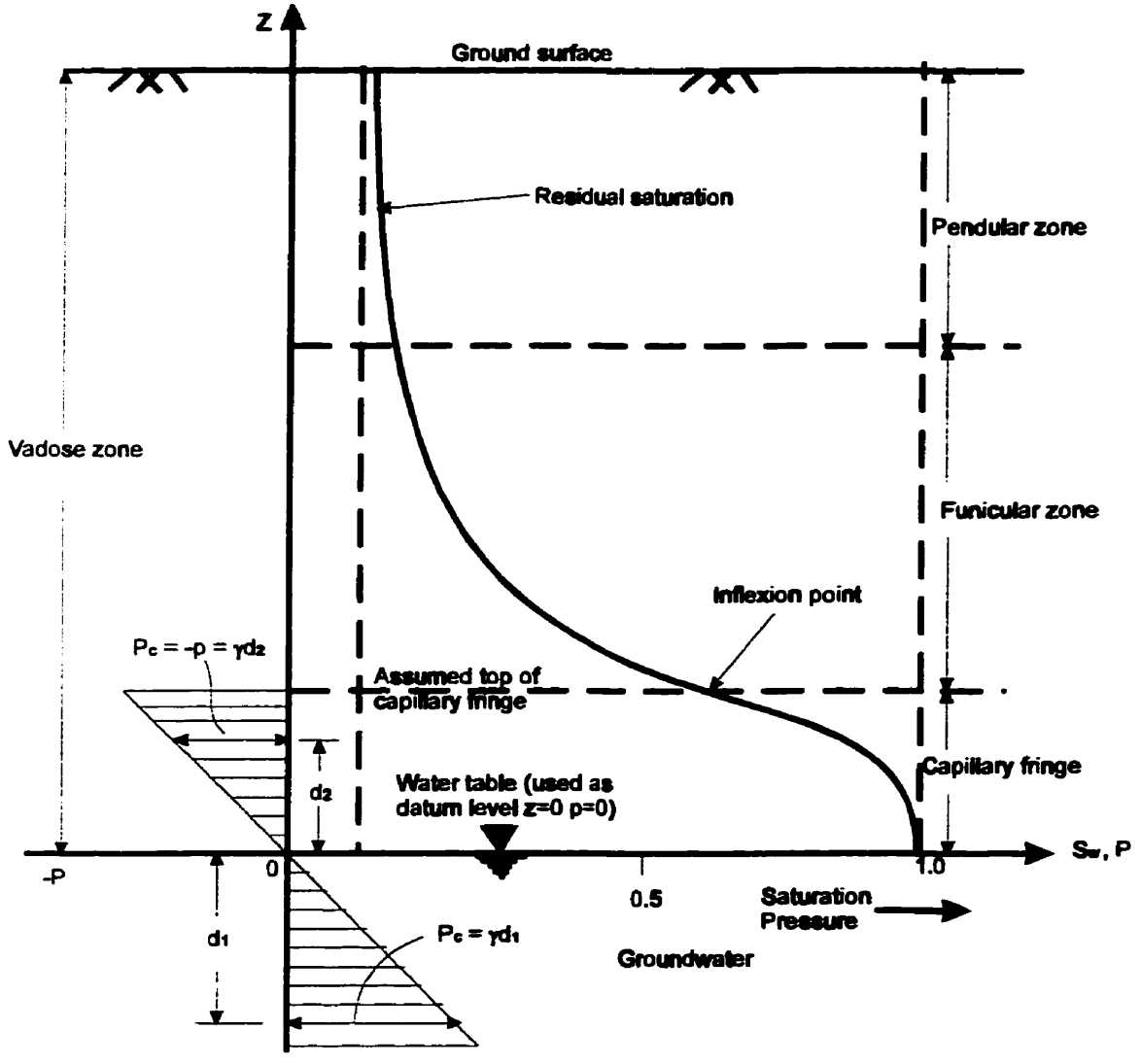

Figure 2.4 Vertical distribution of water in the vadose zone in the absence of non-aqueous phase liquids (Abdul, 1988)

2.2.3 Simultaneous Flow of Immiscible Fluids

In multi-phase flows, Darcy's law for the steady-state saturated flow of the phase i in the presence of another phase is given as

$$v_i = -\frac{k_i \rho_i g}{\mu_i} \times \frac{dh_i}{dl} \qquad (2.7)$$

where,

v_i	is the velocity of the fluid i $(m \cdot sec^{-1})$
k_i	is the effective permeability of the medium to the fluid i (m^2)
μ_i	is the dynamic viscosity of the fluid i $(Pa \cdot sec)$
ρ_i	is the density of the fluid i $(kg \cdot m^{-3})$
l	is the spatial variable (m)
g	is the earth's acceleration $(m \cdot sec^{-2})$
h_i	is the head of the fluid i (m)

In equation (2.6), the term $\frac{k_i \rho_i g}{\mu_i}$ is the hydraulic conductivity of the fluid i expressed as a ratio of the effective permeability of the medium to the viscosity of the fluid i. The effective permeability depends on the structure of the porous medium involved, on the intrinsic permeability k of the medium to a single-phase fluid completely saturating it, and on the saturation. The effective permeability can be written as

$$k_i = k_{ri} \times k \qquad (2.8)$$

where k_{ri} is the relative permeability of the porous medium to fluid i. Using equation (2.8), equation (2.7) can be written as

$$v_i = -\frac{k_{ri} k_i \rho_i g}{\mu_i} \times \frac{dh_i}{dl} \qquad (2.9)$$

In three-dimensional flows, the hydraulic head is function of all three dimensions: $h = h(x, y, z)$. Thus, the gradient of the head is a vector and the Darcy's law, (2.9), can be re-written as

$$v = -\frac{k_{ri} k_i \rho_i}{\mu_i} \times \nabla h_i \qquad (2.10)$$

where v is the velocity vector and $\nabla = i\frac{\partial}{\partial x} + j\frac{\partial}{\partial y} + k\frac{\partial}{\partial z}$ is the gradient operator. If equation (2.9) is applied to the water flow in an unsaturated porous medium, and air being the stagnant non-wetting phase at pressure equal to zero, it can be shown that:

$$v_w = -\frac{k_w(\theta)}{\mu_w} \nabla(-P_C + \gamma_w z) \qquad (2.11)$$

where

v_w	is the water velocity ($m \cdot sec^{-1}$)
P_C	is the capillary pressure which is equal to the negative pressure of the pressure in the water (Pa)
$k_w(\theta)$	is the permeability function of the moisture content (m^2)
γ_w	is the water unit weight ($N \cdot m^{-3}$)
z	is the potential height (m)
μ_w	is the water dynamic viscosity ($Pa \cdot sec$)

Thus, the effective permeability, $k_w(\theta)$, is not a constant as in the case of saturated flow and the following relation can be written:

$$K_w(\theta) = \frac{k_w(\theta)\rho_w g}{\mu_w} \qquad (2.12)$$

where $k_w(\theta)$ is the effective (water) hydraulic conductivity. P_C is also a function of the volumetric liquid content, θ, and therefore the relationship $P_c = P_c(\theta)$ is not an unique one. Then, owing to the hysteresis, the history of wetting and drying can play an important role in the analysis of flow problems (Bear, 1973).

2.3 NAPL PARTITIONING

Residual NAPL components in the vadose zone can partition into the vapor phase as well as a soluble phase in the capillary water. The degree of partitioning of each component depends upon the relative volatility of the non-aqueous phase and its solubility in water (Fetter, 1993). These two factors are related by *Henry's law* which states that in dilute aqueous solutions there is a linear relationship between the air phase concentration and the aqueous concentration of the component. The proportionality between the two quantities can be expressed both by means of the *Henry's law constant* (L.atm/*mol*) or by means of the *water-air partition coefficient*, which is the ratio of the aqueous solubility of a substance (*mg/l* at a given temperature) to the saturated vapor concentration of the pure phase of the substance (*mg/l*) (Baehr, 1987). Thus, in the vadose zone, for example, a low water-air partition coefficient implies that the NAPL favours the vapor-phase relative to aqueous phase. In contrast, high water-air partition coefficient indicates that the NAPL compound favours the water-phase. If the NAPL is a mixture of different compounds, the water-air partition coefficients for each compounds are necessary to describe the behavior of the NAPL.

3. CONVENTIONAL THEORY OF CENTRIFUGE MODELLING

3.1 INTRODUCTION

In most geotechnical applications, the stresses due to gravity effects are an important consideration. The use of centrifuge technique allows the study of such stresses by resort to smaller scale models of the structure which is subjected to higher gravity fields. For example, if a model which is 1/100 the scale of a prototype is subjected to a gravity field 100 times than of earth's gravity, then the stresses in the model are identical to those that can act in the prototype at similar locations. The earliest recorded use of a centrifuge to model gravity stresses is due to Philips (1869). He observed that a 1g scale model of a structure was not sufficiently accurate to examine structures involving large constructions where gravity stresses formed the major aspect of the stress distribution. By using the centrifugal acceleration, the weight of the construction could be effectively increased and, consequently, the forces in the model would be similar to the forces of the prototype. The idea of using a centrifuge to increase the stresses in a model was not put into practice until the 1930's. Significant applications of centrifuge technique to problems in soil mechanics were made in Russia in the late 1930's (Pokrovsky and Fiodorov, 1936). Centrifuge techniques were applied to the study of a number of problem in geotechnical engineering including the stability of slopes, pressures under foundations, settlement of foundations, and the development of pressure on buried culverts and pipes.

Since the end of the 1960's the use of the centrifuge for modelling problems in geotechnical engineering has become more and more wide spread and the geotechnical centrifuge has been developed as a tool for modelling geotechnical phenomena. Mikasa and Takada (1973) used the 1 m radius centrifuge of the Osaka City University, Japan, to

demonstrate the validity of the Mikasa's consolidation equation (1973) derived in terms of strains of clay. The first results obtained from the centrifuge modelling was the observed relationships between the degree of consolidation and time which illustrated a linear relationship when the obtained experimental points were plotted in a prototype scale. Another result was that in contrast to the results obtained with conventional odometer tests, the secondary consolidation for the investigated clays was negligible.

Mandel *et al.* (1975) performed studies related to the stability of cylindrical and spherical cavities at medium and large depths using the centrifuge of the Laboratoire de Mecanique des Solides of Ecole Polytechnique, France. Experimental studies were undertaken in order to validate and supplement calculation related to the theoretical limit state analysis. Models were built with different materials, which satisfied Tresca, and Mohr-Coulomb failure criteria ($\phi \neq 0$, $c \neq 0$), in order to provide a whole range of conditions. For Tresca materials, cohesive, and frictional materials, centrifuge results were found to be in good agreement with the analytical models. For Coulomb soils, studies provided only a complementary tool to theoretical analysis.

Yamaguchi *et al.* (1977) used the centrifuge of the Tokyo Institute of Technology, Japan, to study the bearing capacity of shallow foundations. A series of loading tests was carried out in an attempt to explain de Beer's scale effect of a footing on the bearing capacity of dense sand from the view point of progressive failure. They found that the bearing capacity factor decreased with the increase of γB, where γ is the unit weight of the sand, and B is the breadth of the footing. Their final conclusion was that the assumption of constant shearing strains adopted in existing bearing capacity theories overestimates the bearing capacity of dense sand and this was regarded as unacceptable.

Boon and Craig (1978) used centrifuge modelling to demonstrate the importance of the scale effect in the design of anchors. They found that the small scale models tested at *1g* gave considerably higher values of pullout capacity than similar models tested in the centrifuge at *Ng* (where *N* is the acceleration factor in the centrifuge model) so as to simulate prototypes of dimensions *N* times those of the model.

The centrifuge has been previously adapted as a tool for the modelling of contaminant transport problems. Arulanadan *et al.* (1988) modelled the transport of a non-reactive pollutant in different soils by using the centrifuge of the University of California at Davis, USA. The scaling laws for the particular phenomenon were derived and tested under different gravity's accelerations. The results showed that capillary effects, adsorption, and advection could be properly scaled in the model. The dispersion process was, instead, not similar both in model and prototype if the Peclet number, the ratio of the product of fluid velocity and length and molecular diffusion, was greater than unity.

Mitchell and Stratton (1994) modelled an instantaneous 2000 *l* surface spill of a light oil on dry sand. Four scaling factors, between 19 and 50 gravities were used to demonstrate that the contaminant movement is independent of the model scale. After one year (prototype time), the 2000 *l* of oil contaminated a volume equal to 20 m^3 of sand and reached a maximum depth of 4 *m*. The maximum measured oil content measured in the sand was close to 7 percent by weight.

Allersma *et al.* (1996) investigated the sliding behavior of "spudcans" in base footings for offshore exploration structures in layered soil by using the geotechnical centrifuge of Delft Technical University, The Netherlands. Several interesting phenomena could be observed in the centrifuge tests. It appeared that more than full embedment penetration was needed to reach the maximum bearing capacity. A spike-shaped tip reduced the bearing capacity

especially in situations where a rough spudcan had a higher bearing capacity than a smooth footing. Test on the sliding capacity showed that the sliding check as described in the *Recommended Practice for Site Specific Assessment of Mobile Jack-Up Units* is applicable to restricted loading conditions and may therefore be too optimistic.

3.2 THE CENTRIFUGE

3.2.1 Dynamics of the centrifuge

In problems where the mechanical effects are important, stress dependent strength and deformability characteristics can be adequately modelled via centrifuge techniques. Thus, when gravity induced forces through soils are considered, the centrifuge techniques offer a means of examining such processes.

In this section, we present a brief account of the dynamics of the centrifuge and the scaling laws for the modelling of mechanical and transport processes appropriate to geotechnical and geoenvironmental problems.

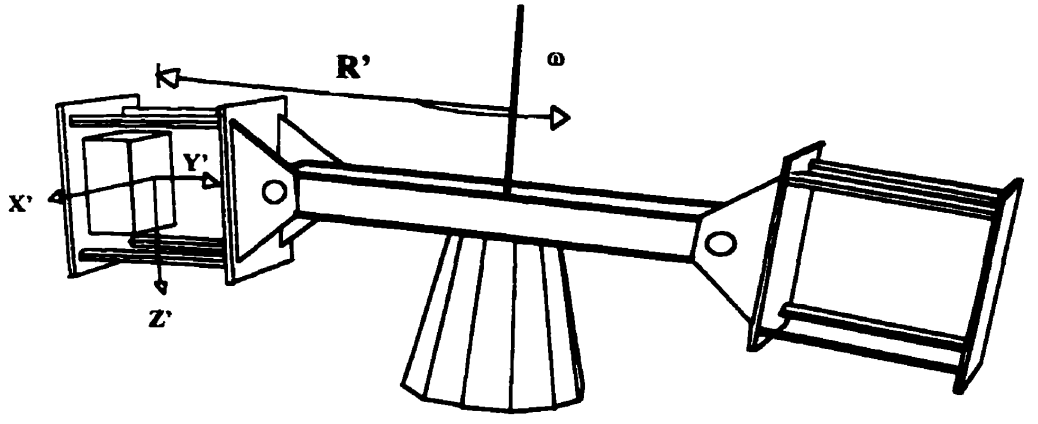

Figure 3.1 Axis orientation in the centrifuge (Stuit, 1995).

In order to increase the self weight of the sample in the centrifuge by a factor N, the model is held in equilibrium in steady flight in a centrifuge with angular velocity ω at a radius R, as shown in Figure 3.1 (Stuit, 1995).

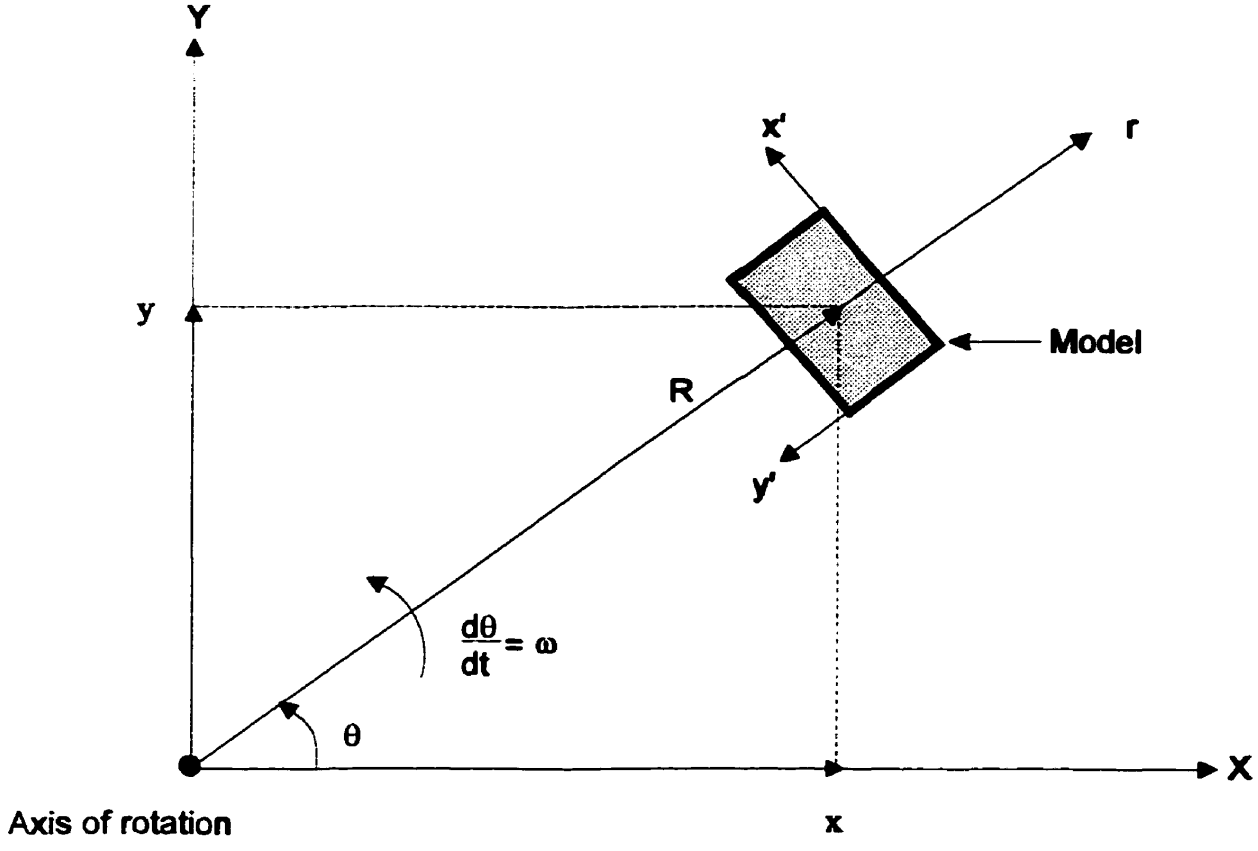

Fig. 3.2 Global polar coordinates of the model and the local coordinates of the model.

The location of the sample at a distance R from the central axis of the centrifuge as shown in Figure 3.2, given in polar co-ordinates, is:

$$\begin{aligned} x &= x\left[R(t),\ \theta(t)\right] = R(t)\cos\theta(t) \\ y &= y\left[R(t),\ \theta(t)\right] = R(t)\sin\theta(t) \end{aligned} \qquad (3.1)$$

The components of the local linear velocity of the model are given by:

$$\begin{aligned} \frac{dx}{dt} &= \frac{\partial x}{\partial R}\cdot\frac{dR}{dt} + \frac{\partial x}{\partial \theta}\cdot\frac{d\theta}{dt} = \frac{dR}{dt}\cos\theta - R\frac{d\theta}{dt}\sin\theta \\ \frac{dy}{dt} &= \frac{\partial y}{\partial R}\cdot\frac{dR}{dt} + \frac{\partial y}{\partial \theta}\cdot\frac{d\theta}{dt} = \frac{dR}{dt}\sin\theta - R\frac{d\theta}{dt}\cos\theta \end{aligned} \qquad (3.2)$$

Similarly, the components of the acceleration are given by

$$\begin{aligned} \frac{d^2x}{dt^2} &= \frac{d^2R}{dt^2}\cos\theta - 2\frac{dR}{dt}\frac{d\theta}{dt}\sin\theta - R\frac{d^2\theta}{dt^2}\sin\theta - R\left(\frac{d\theta}{dt}\right)^2\cos\theta \\ \frac{d^2y}{dt^2} &= \frac{d^2R}{dt^2}\sin\theta - 2\frac{dR}{dt}\frac{d\theta}{dt}\cos\theta - R\frac{d^2\theta}{dt^2}\cos\theta - R\left(\frac{d\theta}{dt}\right)^2\sin\theta \end{aligned} \qquad (3.3)$$

Considering the global coordinates (x and y) and the local coordinates of the centrifuge model (x' and y') we have

$$\begin{pmatrix} x' \\ y' \end{pmatrix} = \begin{bmatrix} -\sin\theta & \cos\theta \\ -\cos\theta & -\sin\theta \end{bmatrix} \begin{pmatrix} x \\ y \end{pmatrix} \qquad (3.4)$$

With this transformation the total components of the local velocities in the centrifuge are given by

$$\begin{pmatrix} \frac{dx'}{dt} \\ \frac{dy'}{dt} \end{pmatrix} = \begin{bmatrix} -\sin\theta & \cos\theta \\ -\cos\theta & -\sin\theta \end{bmatrix} \begin{pmatrix} \frac{dx}{dt} \\ \frac{dy}{dt} \end{pmatrix} \qquad (3.5)$$

Considering (3.2) and (3.5) we obtain

$$\begin{aligned} \frac{dx'}{dt} &= +R\frac{d\theta}{dt} = R\omega \\ \frac{dy'}{dt} &= -\frac{dR}{dt} = v_R \end{aligned} \qquad (3.6)$$

where ω is the angular velocity of the centrifuge arm and v_R is the velocity in the direction of the centrifuge arm. The components of the local acceleration can similarly be obtained by using the transformation

$$\begin{pmatrix} \frac{d^2x'}{dt^2} \\ \frac{d^2y'}{dt^2} \end{pmatrix} = \begin{bmatrix} -\sin\theta & \cos\theta \\ -\cos\theta & -\sin\theta \end{bmatrix} \begin{pmatrix} \frac{d^2x}{dt^2} \\ \frac{d^2y}{dt^2} \end{pmatrix} \qquad (3.7)$$

which gives

$$\frac{d^2x'}{dt^2} = 2\left(\frac{dR}{dt}\right)\left(\frac{d\theta}{dt}\right) + R\frac{d^2\theta}{dt^2} \qquad (3.8a)$$

$$\frac{d^2y'}{dt^2} = -\frac{d^2R}{dt^2} + R\left(\frac{d\theta}{dt}\right)^2 \qquad (3.8b)$$

The different terms of the these equations are known as follows:

$$2\left(\frac{dR}{dt}\right)\left(\frac{dq}{dt}\right) = 2v_R\omega = \text{Coriolis effect} \qquad (3.8c)$$

$$R\frac{d^2\theta}{dt^2} = \text{Tangential acceleration of the model} \qquad (3.8d)$$

$$-\frac{d^2R}{dt^2} = \text{Radial acceleration of the model} \qquad (3.8e)$$

$$R\left(\frac{d\theta}{dt}\right)^2 = R\omega^2 = \text{Centrifugal acceleration, which is applied to the model} \qquad (3.8f)$$

The terms (3.8d) and (3.8e) are the horizontal and vertical shaking of the model respectively, which relevant to simulation of earthquake motion. The term (3.8f) for the centrifugal acceleration is the acceleration needed to increase the self weight of the model in the centrifuge. The factor N for the self weight increase is given by

$$N = R\omega^2/g \qquad (3.9)$$

where g is the acceleration due to gravity (9.81 m/s^2). The term (3.8c) is called the Coriolis effect. This term induces an error in certain cases involving centrifuge modelling. When a radial velocity, v_R, occurs in the centrifuge model, an additional tangential acceleration develops. A vertical velocity in the centrifuge model occurs when, for example, sand is rained in the centrifuge, or during the driving of piles or when the soil body of a slope suddenly moves. At low radial velocities, for example when a fluid flow is laminar, the Coriolis effect can be neglected. Stuit (1995) suggests that the radial velocity, v_R, should be lower than 5 % of the centrifuge rotational velocity, ωR, which implies at the most an extra acceleration of 10 % in the tangential direction of the model.

A further error in the centrifuge can be as a result of the acceleration not being constant over the height of the model. The acceleration in the centrifuge depends on the radius, which varies over the height of the sample. For example, the free surface of the model has zero normal and shear stress. When the required test acceleration is defined at the base of the sample, the acceleration in the sample is lower since the arm, R, to the center of the centrifuge is shorter. The soil pressures in the model are in that case lower than the soil pressures in the prototype of the model (Figure 3.3). The vertical stress at the base of the centrifuge model is the result of the soil weight of the soil layers above. For a homogeneous soil sample with constant unit weight, γ, the vertical stress at the base of the sample is:

$$\sigma_{v,base} = \int_{R-h}^{R} \gamma r\, \omega^2\, dr = \frac{\gamma \omega^2}{2} h\,(2R-h) \quad (3.10)$$

In the prototype situation $\sigma_{v,base} = \gamma \omega^2 Rh$, where $w^2 R$ is the acceleration of the sample. When the test acceleration is referred to the upper surface layer of the soil sample the vertical stress at the base of the sample is higher than the prototype stress by:

$$\sigma_{v,base} = \int_{R}^{R+h} \gamma r\, \omega^2\, dr = \frac{g \omega^2}{2} h\,(2R+h) \quad (3.11)$$

Figure 3.3 shows an example of the distribution of vertical stresses in a centrifuge sample. In this diagram the height of the sample is one fifth of the centrifuge radius. The solid line in the Figure indicates the linear distribution of the vertical stresses in the modelled prototype. In case of the first dashed line (line I) in Figure 3.3, the radius of the model is defined at the base of the sample. The stresses in the model are underestimated compared

to the actual stresses in the prototype. When the centrifuge radius is defined at the upper surface the stresses will be overestimated (line II).

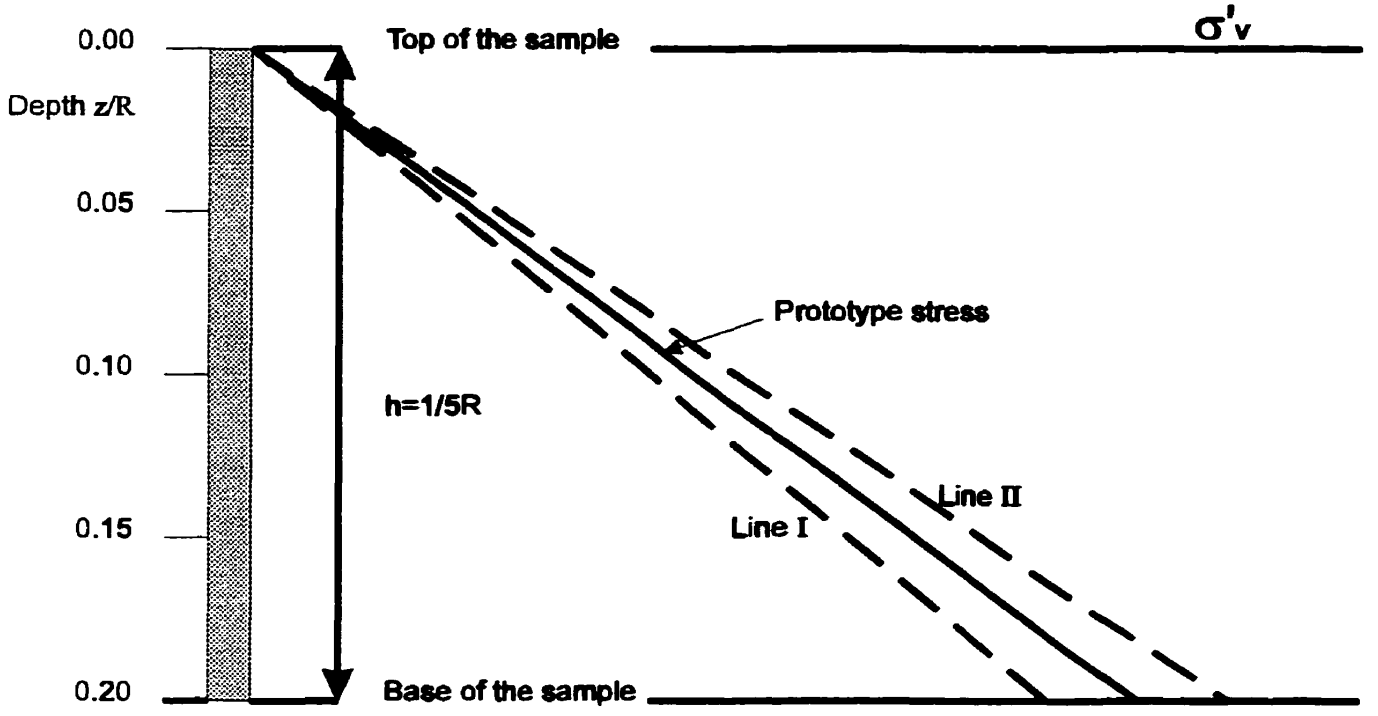

Figure 3.3 Error in the vertical stresses in a centrifuge model

I = underestimated stresses when R is defined at the sample bottom

II = overestimated stresses when R is defined at the sample surface

If a model height is chosen as, for instance, one fifth of the centrifuge radius, this does not mean that the error is 20 per cent. In the most unfavorable situations, when the radius is defined at the bottom of the sample, the maximum error of the stresses is only 10 per cent (equation (3.10) and (3.11)). The error in the vertical stresses is about 5 per cent when the radius is defined at a depth of 2/3 of the height of the sample.

3.2.2 Scaling laws

Model laws are relationships between the physical variables of the reduced model test and of those of the full scale of prototype problem. These model laws can be based on either dimensional analysis or the differential equations that govern the phenomena in question. Both methods allow determination of the model relationships for all the independent variables of a problem. The relationship between the prototype and the model is given for each variable and relationship involved in the phenomenon as a dimensionless factor. In this approach it is important that all the significant variables are taken into account. Often, not all of the variables are independent and different model relationships are required for the same variable. This leads to a distorted interpretation of the test, resulting in errors called *scale effects*.

The model scaling factor π of a parameter is defined as the model value divided by the prototype value of that parameter. Assuming that the centrifugal acceleration is N times g, then the scaling factor for the model lengths, π_L, for example, is $1/N$ and for the model acceleration, π_a is N. The density, particle size, and the stress have a scale factor equal to unity. In most cases it is realistic to use the prototype material for the soil model in the centrifuge. Table 3.1 lists the basic scaling relations which have been extensively employed in previous research in centrifuge modelling (Arulanandan *et al.*, 1985; Cooke and Mitchell, 1991; Illangasekare *et al.*, 1991; Knight and Mitchell, 1996).

Table 3.1 Scale factors

Quantity	*Symbol*	$\frac{\textit{Model dimensions}}{\textit{Prototype dimensions}}$	*Scaling factor*
Length	L	$1/N$	π_L
Displacement	u	$1/N$	π_u
Area	A	$1/N^2$	π_A
Volume	V	$1/N^3$	π_V
Strain	ε	1	π_ε
Force	F	$1/N^2$	π_F
Stress	σ	1	π_σ
Density	ρ	1	π_ρ
Mass	m	$1/N^3$	π_m
Acceleration	a	N	π_a
Velocity	v	N	π_v
Frequency	f	N	π_f
Energy	E	$1/N^3$	π_E

The use of identical materials in the prototype and the model enables the issue of material property scaling to be by-passed. In a geometrically similar model the soil will be subjected to the same stresses as in the prototype and hence will develop the same strains. However, this assumption gives contradictory scaling results for the soil parameters, which could have its influence on the interpretation of the behavior of the soil. Figures 3.4a and 3.4b (Stuit, 1995) show the soil particles of an idealized sand. Figures 3.4a and b respectively illustrate the sand in the prototype and the centrifuge models. The sand particles shown in Figure 3.4a are sketched at their normal size, while the particles of the

model sand shown in Figure 3.4b are sketched according to the scaling relation of the length of the particles. It can be seen that, relatively, the particles of the model sand are larger, and this can have an influence on certain mechanisms in the soil, for instance the width of a shear band as indicated in both Figures 3.4a and 3.4b. The error caused by this effect is referred as *grain size effect*.

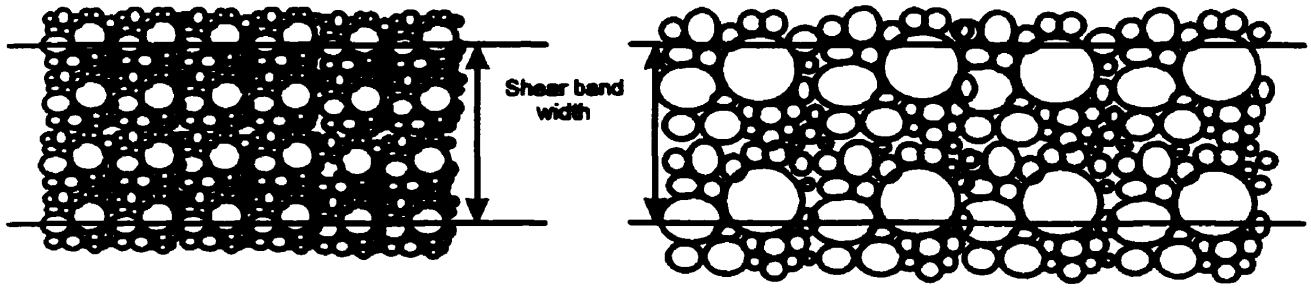

(a) (b)

Figure 3.4 Scaling influence on the dimensions of sand particles: (a) sand in the model; (b) sand in the prototype (Stuit, 1995).

In soil-structure interaction problems, the error of the grain size effect is minimized by choosing the dimension of the test structure large enough compared to the size of the sand grains. A so called "*grain size ratio*" is introduced which is defined as the typical structural length, L, over the mean grain size, d_{50}. There are no significant errors when the width of the structure is greater than 30 times the mean particle diameter (Stuit, 1995).

3.3 SCALING LAWS IN A THREE-PHASE FLOW

In this section the centrifuge scaling laws for a multi-phase flow in unsaturated soils are discussed. It is convenient, however, to begin the discussion from the point of view of the migration of water-soluble components in soils. In such cases, the migration is treated as a two-phase flow: the contaminant is dissolved in water (the wetting phase), and air is the non-wetting phase. Many authors have developed scaling laws for both saturated and unsaturated water-soluble contaminant transport. Arulanandan *et al.* (1988), and Cooke and Mitchell (1991), analyzed the effect of nine dimensionless numbers on the similitude between prototype and model in dissolved contaminant flows.

$$\pi_1 = \frac{C}{\rho_f} \quad \textit{(concentration number)}$$

$$\pi_2 = \frac{\rho_f v l}{\mu_f} \quad \textit{(Reynolds number)}$$

$$\pi_3 = \frac{vt}{L} \quad \textit{(advection number)}$$

$$\pi_4 = \frac{D_m t}{L^2} \quad \textit{(diffusion number)}$$

$$\pi_5 \quad \frac{S}{\rho_f} \quad \textit{(adsorption number)}$$

$$\pi_6 = \frac{gt^2}{l} \quad \textit{(dynamic efects number)}$$

$$\pi_7 = \frac{vl}{D_m} \quad \textit{(Peclet number)}$$

$$\pi_8 = k_c t \quad \textit{(chemical effects number)}$$

where,

C	is solute concentration ($Kg \cdot m^{-3}$)
μ_f	is dynamic fluid viscosity ($Pa \cdot sec$)
D_m	is the coefficient of molecular diffusion ($m^2 \cdot t^{-1}$)
S	is mass of adsorbed solute per unit volume ($Kg \cdot m^{-3}$)
v	is the Darcian velocity ($m \cdot sec^{-1}$)
ρ_f	is fluid density ($Kg \cdot m^{-3}$)
g	is gravitational acceleration ($m \cdot sec^{-2}$)
l	is characteristic microscopic length (m)
L	is characteristic macroscopic length (m)
k_c	is the first-order reaction rate constant (sec^{-1})
t	is time (sec)

The use of the same soil and contaminant in both the model and the prototype yields equality for four dimensionless numbers, π_1, π_3, π_4, and π_5 (Cooke and Mitchell, 1991). For the other four, certain constraints have to be imposed to ensure similitude between the model and prototype. These constraints can be summarized as follows:

- The Reynolds number (π_2) has to be less than unity, so that the flow in the porous medium is laminar both in the prototype and in the model (Bear, 1972). Therefore, the soil that is used in the model should allow for low flow velocities. To calculate the Reynolds number, the average soil grain size, d_{50}, can be used as the average flow channel dimension (Bear, 1979).
- The Peclet number (π_7), relating the two parameters that constitute the coefficient of hydrodynamic dispersion should also be less than unity. If molecular diffusion is dominant in the dispersion process, the equality of Peclet number is no longer necessary (Cooke and Mitchell, 1991).

- The dynamic effects number (π_6) can be neglected in laminar seepage in porous media, because the inertial forces involved are not significant (Cooke & Mitchell, 1991).
- The chemical effects number (π_8) plays an important role in problems where the chemical decay is dominant in the advection-dispersion process. If a flow of a non-reactive pollutant is studied, or rather, if the pollutant analyzed is weakly reactive, the inequality of this number can be neglected. Furthermore, if the experiments, as the ones described in this thesis, are performed for a short duration, the similitude in the chemical effects number is not considered to be an important requirement.

In a flow involving three immiscible phases, if the flow is laminar, the one dimensional fluid velocity for each phase can be expressed as (Knight and Mitchell, 1996)

$$v = -\frac{k_r k \rho_f}{\mu_f} Ng \frac{dh}{dl} \qquad (3.12)$$

where

k	is the intrinsic permeability of the porous medium (m^2)
k_r	is the fluid relative permeability factor for the fluid based on its saturation (*non-dimensional*)
μ_f	is the dynamic fluid viscosity ($Pa \cdot sec$)
$\frac{dh}{dl}$	is the hydraulic gradient (*non-dimensional*)
ρ_f	is the fluid density (kg / m^3)
Ng	is the centrifuge acceleration (m / sec^2)

Arulanadan *et al.* (1988) demonstrated that if the same soil is used both in prototype and in the model, and if the boundary conditions are identical, the ratio between prototype and model fluid velocity may be expressed as

$$v^* = \frac{v_m}{v_p} = \frac{g_m}{g_p} = N \qquad (3.13)$$

where v^* is the fluid velocity scale factor, and the subscripts m and p denote model and prototype, respectively. Thus, the model velocity will be N times greater than the prototype velocity. The centrifuge time-scale factor is

$$T^* = \frac{T_m}{T_p} = \frac{1}{N^2} \qquad (3.14)$$

which is the centrifuge model time that is scaled down by the square of the scale factor. Knight and Mitchell (1996) found that in a multi-phase immiscible flow, the dynamic similitude is achieved in both the model and the prototype if the scale factors of all the forces acting on the system under consideration are equal to unity. Each fluid element is influenced by gravity forces (F_G), pressure forces (F_P), viscosity forces (F_V), and surface tension (F_S). If the resultant of the dynamic forces in the model and prototype is greater than zero, the fluid element will be accelerated. In this hypothesis, the *dynamic equilibrium* of the system of forces acting on the fluid element will be achieved considering the inertia force (F_I) and dynamic similitude will not occur. Given an elementary mass of fluid in a porous medium, Knight and Mitchell (1996) defined the dynamic forces acting on it; such forces can be classified as follows:

Inertial

$$F_I = ma = \rho_f L^3 \frac{L}{T^2} = \rho_f L^4 T^{-2} = \rho_f v^2 L^2 \qquad (3.15)$$

Gravitational

$$F_G = mg = \rho_f L^3 g \qquad (3.16)$$

Pressure

$$F_P = (\Delta p)A = (\Delta p)L^2 \qquad (3.17)$$

Viscosity

$$F_v = \mu_f \left(\frac{dv}{dx}\right) A = \mu_f \left(\frac{v}{L}\right) L^2 = \mu_f vL \qquad (3.18)$$

Surface tension

$$F_S = \sigma L \qquad (3.19)$$

where

m	is the fluid mass (kg)
ρ_f	is the fluid density $(kg \cdot m^{-3})$
a	is the acceleration field $(m \cdot sec^{-2})$
g	is the acceleration due to the Earth's gravity field $(m \cdot sec^{-2})$

Δp	is the change in pressure (between two fluids) (Pa)
A	is area (m^2)
μ_f	is the fluid dynamic viscosity ($Pa \cdot sec$)
v	is the fluid velocity ($m \cdot sec^{-1}$)
dv/dx	is the velocity gradient (s^{-1})
σ	is the surface tension of the fluid ($Pa \cdot sec$)
L	is a characteristic length (m)

Dynamic similitude will occur if the following ratios are all equal to unity:

$$\frac{F_{Gm}}{F_{Gp}} = \frac{F_{Pm}}{F_{Pp}} = \frac{F_{Vn}}{F_{Vp}} = \frac{F_{Sm}}{F_{Sp}} = \frac{F_{Im}}{F_{Ip}} = 1 \qquad (3.20)$$

Assuming the ambient air pressure is zero with respect to the atmospheric pressure, five dimensionless numbers may be defined: *Reynolds*, *Froude*, *Weber*, *Capillary*, and *Bond* numbers. The Reynolds number is defined as the ratio between inertial and viscous forces and can be written as:

$$\pi_2 = \frac{F_I}{F_V} = \frac{\rho_f v l}{\mu_f}$$

It has already been said that it is not similar in model and prototype. Reynolds number must be kept below the critical value ($Re < 1$) for flow in porous media (Bear, 1972) to ensure the validity of Darcy's law. The capillary number is the ratio of viscous forces to surface-tension forces:

$$\pi_9 = \frac{F_V}{F_S} = \frac{\mu_f v}{\sigma}$$

This number is not similar because the velocity in the model is N-times greater than that in the prototype (Knight and Mitchell, 1996). Morrow and Songkran (1981) found that in water flooding tests, the LNAPL trapping is sensitive to the capillary number over the range from 10^{-6}, below which there is no effect on trapping, to 10^{-3}, at which there is no trapping. Knight and Mitchell (1996) showed that in centrifuge tests, if the LNAPL is not subjected to high water velocities, the capillary number similitude is not significant. In this study, LNAPL was released in a water-wet sand and always displaced water or air. The Froude number is defined as

$$\pi_{10} = \frac{F_I}{F_G} = \frac{v^2}{gd}$$

where d is a macroscopic length which represents the average flow channel radius. This number is not similar because the model velocity is N-times greater than that in the prototype. The lack in similitude can be minimized if the model is subjected to small accelerations and the flow is laminar (Knight and Mitchell, 1996). The Weber number is the ratio of surface-tension force to inertial force. It can be written as

$$\pi_{11} = \frac{F_S}{F_I} = \frac{\sigma}{\rho_f d v^2}$$

Such a number is not similar in model and prototype. Considering, however, the insignificance of the inertial effect, and if a laminar flow occurs, the deficiency in similitude can be neglected (Knight and Mitchell, 1996). The Bond number is the ratio of gravity force to capillary or surface- tension force. For two immiscible fluids it is defined as

$$\pi_{12} = \frac{F_G}{F_S} = \frac{\Delta \rho_f \, g r^2}{\sigma}$$

where $\Delta\rho_f$ is the difference in density between the fluids, and r is the particle radius. The acceleration in the centrifuge is N times greater than the acceleration due to the gravity. Thus, the Bond number in the model is N times greater than that in the prototype. This means that the effect of the gravity on the LNAPL blobs is N times greater than that in the prototype, whereas the capillary forces remain the same magnitude. Consequently, the effect of the capillary forces acting on the LNAPL blobs is reduced compared to the real scale case. The final result would be a smaller amount of LNAPL trapped in the unsaturated zone as residual fluid (Knight & Mitchell, 1996). Based on a research using uniform glass beads, Morrow and Songkran (1981) found that no residual LNAPL trapping occurred if the inverse of the Bond number is less than 3. On the other hand, when the inverse Bond number is greater than about 200, buoyancy forces have no effect on the amount of trapped residual non-wetting phase saturation, and the residual saturation depends only upon the capillary number. Knight and Mitchell (1996) found that when fluids with a low density difference, low accelerations and relatively high capillary porous medium are used in centrifugal models, the effect of centrifuge residual LNAPL remobilization may be minimized.

4. PROPOSED EXPERIMENTAL METHODOLOGY

4.1 INTRODUCTION

The primary objective of this study is to utilize a geotechnical centrifuge to obtain a visual record of the time-dependent distribution of LNAPL which is released from a line source to a partially saturated porous granular medium. Due to the requirement of obtaining a visual record of the migration pattern, attention is restricted to a two-dimensional modelling of the problem. Contrary to traditional centrifuge modelling, this choice should allow the visual observation of the LNAPL movement. The proposed technique for producing descriptive representations of the migration patterns involves the use of image processing techniques. The proposed methodology for measuring LNAPL and water content involves the use of "conventional" techniques such as water evaporation, and LNAPL volatilization.

This study can be divided into two parts. First, an unsaturated soil profile is modelled by means of the geotechnical centrifuge. The results of the centrifuge models will be compared to a real scale test. In the second part, LNAPL is released to partially saturated sands. The effect of the porosity on the dynamics of LNAPL movement is investigated. In both parts of the research, models are accelerated in the centrifuge at 20*g* and 30*g*. Table 4.1 lists the dimensions of the models used in the experimental program. According to the scaling laws for geotechnical centrifuge modelling (Arulanadan *et al.*, 1988), the last

column of Table 4.1 provides the dimensions of the models transformed to the prototype scale. In order to compare the results of the modelling performed at 20*g* and 30*g*, geometry and time of the models are converted in prototype scale dimensions.

Table 4.1 Dimensions of the models

	Model at 30g	*Model at 20g*	*Real scale*
Thickness of sand layer	*9 cm*	*13.5 cm*	*270 cm*
Depth of the water table	*7 cm*	*10.5 cm*	*210 cm*
Tank line opening length	*0.1 cm*	*0.15 cm*	*3 cm*
Tank length	*3.33 cm*	*5 cm*	*100 cm*
Tank height	*6 cm*	*9 cm*	*180 cm*
LNAPL volume	*55.54 cm^3*	*125 cm^3*	*1×10^6 cm^3*
LNAPL head	*5.56 cm*	*8.33 cm*	*166.67 cm*
Time of infiltration	*144 minutes*	*324 minutes*	*3 months*

The quality of the modelling results is verified by comparing the data derived from models performed at different accelerations. In order to assess the efficiency of the techniques chosen to measure water and LNAPL content, a set of preliminary experiments was included as part of the experimental program. The overall study would encompass all data in a form that can be used by researchers with interests in centrifuge modelling of three-phase flow.

4.2 THE EXPERIMENTAL FACILITIES

4.2.1 The centrifuge of Delft Technical University, The Netherlands

The experiments were carried out using the Centrifuge of Delft Technical University, The Netherlands. The centrifuge has a symmetric rotating arm which carries two identical swinging baskets (Figure 4.2). These baskets are hinged to the centrifuge arm, so that the model is always perpendicular to the resultant acceleration with a balanced basket. One basket is filled with the actual experimental set-up while the other basket is loaded with a counter weight to balance the centrifuge. Figure 4.3 shows the centrifuge at rest with both swinging baskets.

When the baskets swing out in flight the radius from the axis of rotation to the basket floor is 1.1 *m* (Figure 4.1). The platform of the basket has a working space of $0.45\ m \times 0.35\ m$, while the available height is 0.42 *m*. The samples are all small enough to be handled by one operator and when the loading apparatus is separately mounted at the basket, a sample can easily be slid on the platform and is ready to be tested. Multiple tests can easily be performed in one day. Around the centrifuge a 0.5 *m* protective thick enclosure has been made to act as a shield against parts breaking off or detaching from the centrifuge during flight. Table 4.2 gives the major characteristics of the Delft Technical University centrifuge and Table 4.3 gives the dimension of the swinging basket for the model and the prototype at the maximum acceleration.

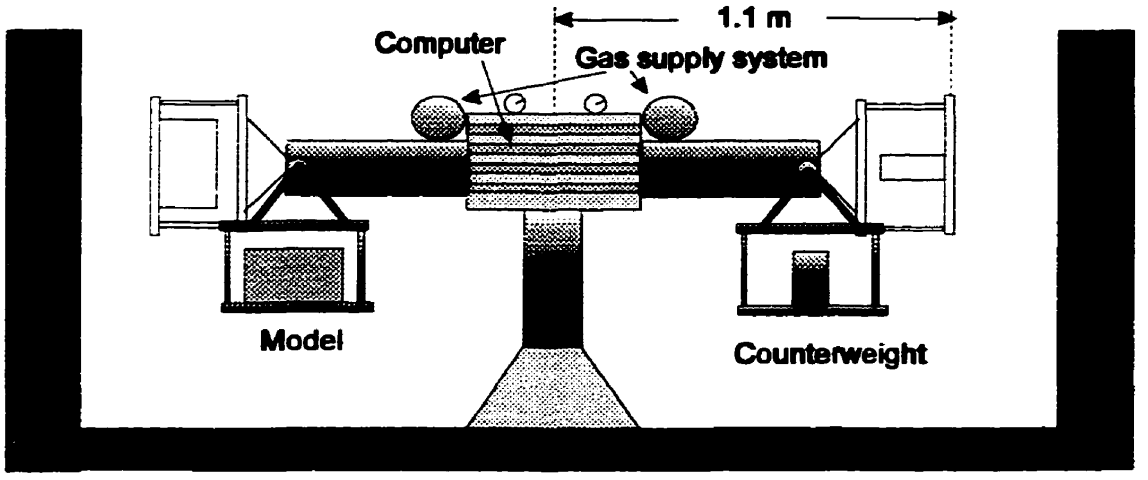

Cross-sectional view

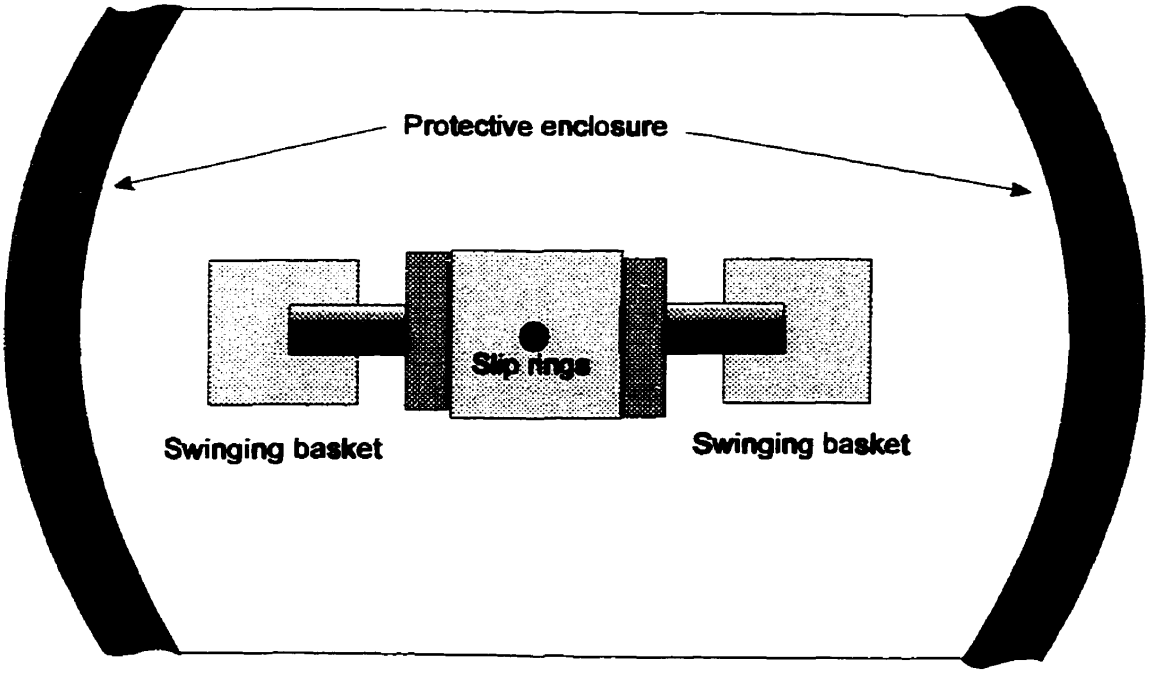

Plan view

Figure 4.1 Cross-sectional and plan view of the geotechnical centrifuge of Delft Technical University.

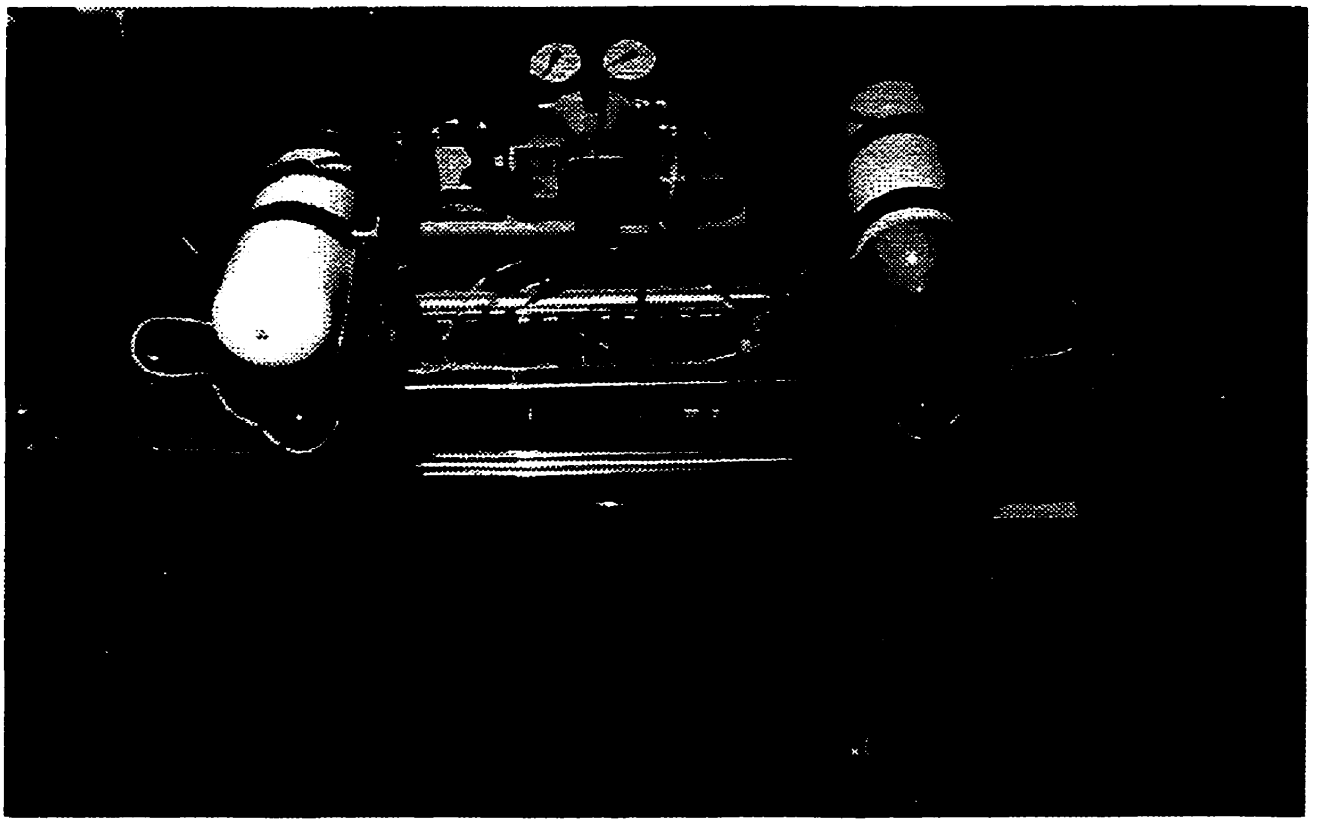

Figure 4.2 The geotechnical centrifuge of Delft Technical University in its stationary configuration.

Table 4.2 Characteristics of the Centrifuge of Delft University of Technology

Characteristic	*Value and unit*
Radius of the centrifuge arm	*1.1 m*
Maximum acceleration	*300 g*
Maximum payload at 300 g	*40 kg*
Maximum capacity	*120 g-kN*
Capacity drive system	*11 kW*

Table 4.3 Dimensions of model and prototype at the maximum acceleration

Dimension swinging basket	*Model*	*Prototype (300g)*
Length	*0.45 m*	*135 m*
Width	*0.35 m*	*105 m*
Height	*0.42 m*	*126 m*

Due to the small size in comparison with centrifuges at L.C.P.C. (France), U.C. Davis (USA), Cambridge (UK), and ISMES (Italy), the cost of operation is low and a large number of test can be performed in a relatively short period. Automated preparation devices such as the computer controlled sand raining device assures a good reproducibility of the samples (Allersma, 1994). The computer controlled sand preparation device produces sand samples with a standard deviation in porosity of less than 0.2% (Allersma, 1994) .

Due to the accuracy, slight differences in tests procedures can be made visible. Several accessories are available to perform advanced "in flight tests"; these include the following:

- sand pouring machine
- two dimensional loading system
- gas supply system for flow rate control
- water circulation system
- vane apparatus
- pile driving hammer

The devices are controlled by a PC compatible single board computer (486, 66MHz processor, 16 Kbytes RAM, 32 Mbytes solid state disk, 1 Giga-Byte HD) which is located in the rotating part of the centrifuge (Figure 4.2). The computer is accessible via slip rings and line driver units. The communication with the on-board mechanical equipment is realized by commercial available AT-slot interface boards. One board contains 8 analog inputs, one voltage controlled output and 32 digital input/output lines. Since the measuring and control signals do not require slip rings, the noise is reduced to a very low level (Allersma, 1994). The interface board is easily accessed via a BASIC program, so that the user can write his/her own software to define a particular test procedure. The limited space for provision of sensors is compensated by using image processing techniques to digitize automatically and on line surface displacements of clay and sand samples. The displacement of objects can also be measured using this technique

4.2.2 Video Equipment

A series of video cameras are used to control the centrifuge and to observe and record the performance of models in the centrifuge . Figure 4.3 gives a schematic view of the equipment in the centrifuge room and the control room.

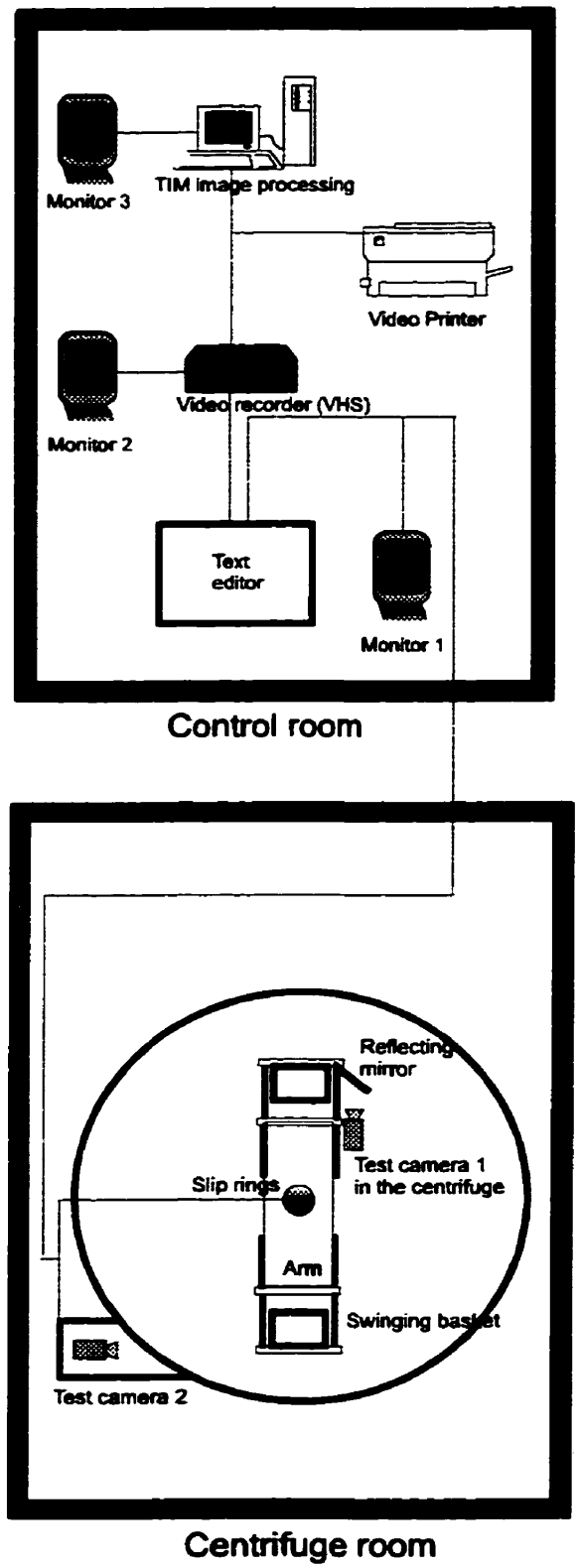

Figure 4.3 Schematic view of the Delft Technical University centrifuge set-up.

Continuous observation of a test conducted in the centrifuge is possible with the available video system. The test in the centrifuge can be watched from two different positions. The first test camera is mounted at the top of the centrifuge swinging basket of the rotating centrifuge. The side of the test box can be seen by a mirror located in front of the model. This camera is a compact *CCD* camera which is capable of resisting the high centrifugal accelerations. The video signals from this test camera are transmitted by cable through the slip rings to the control room. The second test camera is placed outside the rotating centrifuge within the protective enclosure. A flash light illuminates the test sample each time the sample passes the frame of view of the camera at the focal distance, which gives an instantaneous image of the test sample and container. The flash light is triggered by a switch mounted on the rotational axis of the centrifuge. In addition to this external camera there is also the provision for installing a 35 ***mm*** photo camera to generate single pictures of high quality.

The unmodified signal is directly visible on a monitor one. The video signal can be recorded on VHS video recorder system. Before the signal is recorded a text can be added to the video signal to provide information about the test and the recorded image. Monitor two in Figure 4.3 shows what is recorded on the VHS tape, which is the image of the test with the added text. During the centrifuge test there is the provision to make a picture of the video image with a Polaroid video image printer which is also connected to a video recorder. The video recorder is also connected to a computer with a "frame grabber" board. The images can directly be processed with this computer for further analysis. The image processing software package used for this research is the TIM version 1995*. The result of the processed image is shown on monitor one.

* produced by Difa Measuring System BV, Druivenstraat 25, 4816 KB Breda, The Netherlands.

4.2.3 The strong-box

Figure 4.4 illustrates the strong-box used in this research to contain the layer of the porous medium. The device consists of a metal rigid U-frame the sides of which are incorporated with transparent plexiglas. To the author's knowledge, this experimental research program represents the first instance where a transparent sided container was used in the study of the centrifuge modelling of contaminant migration in soil. The low acceleration levels of the tests and the high rigidity of the transparent sides of the strong-box ensured that no significant deformations of the strong-box occurred during flight. A sink at the bottom of the strong-box allowed drainage of the sand sample in flight. The inner part of the strong-box was covered by a synthetic porous fabric having roughly the same hydraulic conductivity of the two sand packages used in the experiments. The porous fabric was necessary to avoid loss of sand during the drainage. The transparent sides of the strong-box were greased with vaseline. The vaseline was used to reduce the boundary friction between Plexiglas and sand, and Plexiglas and LNAPL. The vaseline did not present any problem of refraction of the image of the sand sample image due to the isotropy to natural light. The two transparent sides of the strong-box had scales along the z-direction (vertical) and the x-direction (horizontal) in order to control the dimension of the sand sample and the water table, and to measure the LNAPL plume area at the end of the tests. Figure 4.5 illustrates the orientation of the dimensions of the strong-box. The dimensions of the strong-box are summarized in Table 4.4 and converted in real scale for both the centrifuge accelerations ($20g$ and $30g$) used in this study.

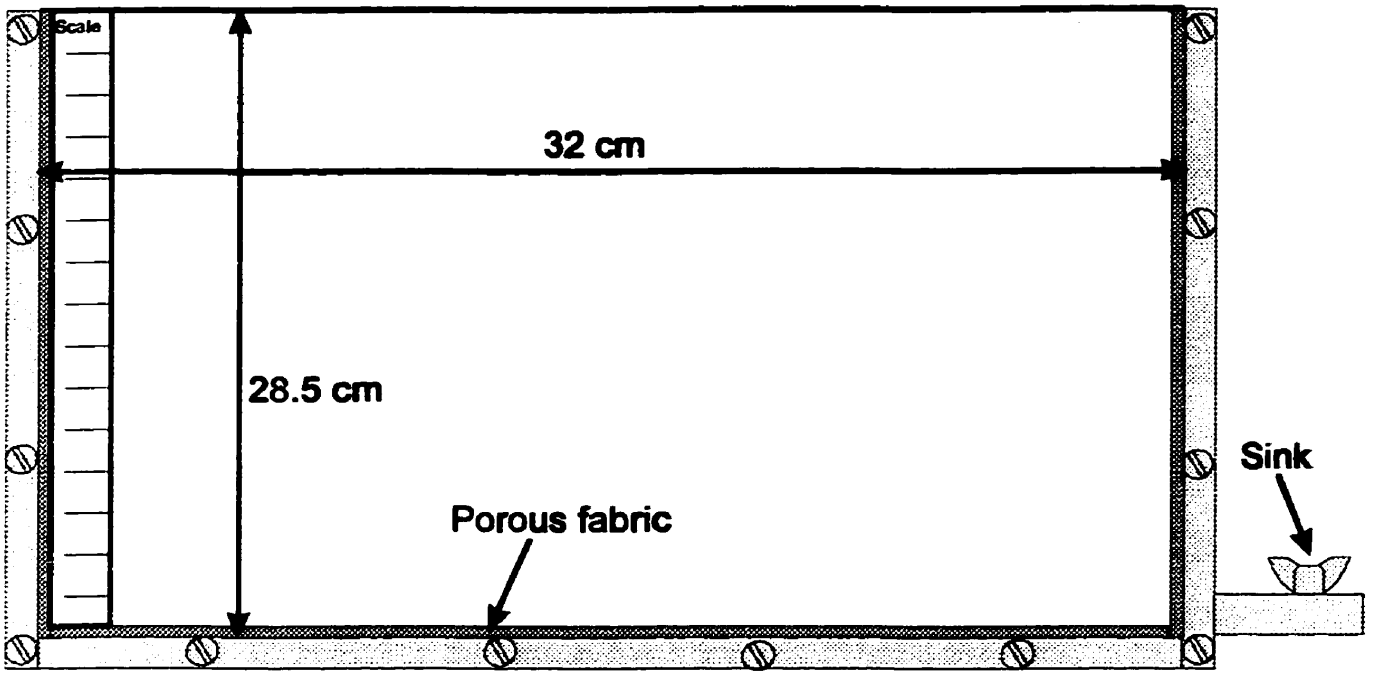

Figure 4.4 View of the strong-box

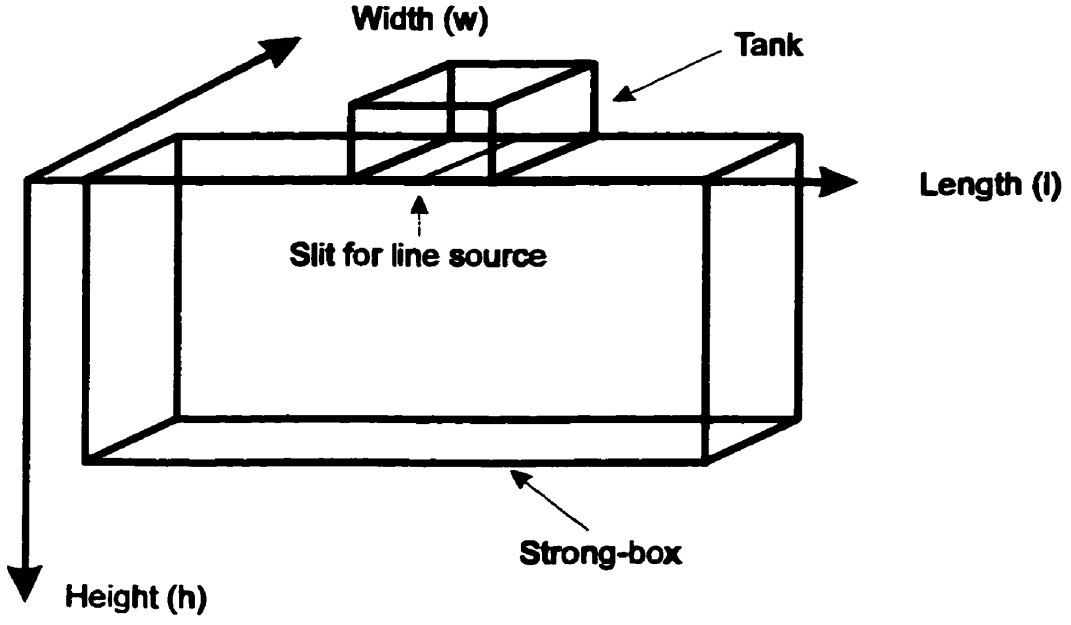

Figure 4.5 Orientation of height, length, and width

Table 4.4 Dimensions of the strong box

Dimension	*Strong-box*	*Real scale (20g)*	*Real scale (30g)*
Length	*32.0 cm*	*640 cm*	*960 cm*
Height	*28.5 cm*	*570 cm*	*855 cm*
Width	*4.0 cm*	*80 cm*	*120 cm*

4.2.4 The device for the release of the LNAPL

Figure 4.6 shows the internal dimensions of the LNAPL containers used in the experiments. In order to prevent the LNAPL from flowing out the containers before the start of the test, the containers were filled with a layer of about 2 mm of water, which was allowed to freeze. The containers were, then, filled with the required quantity of LNAPL and positioned on the top of the sand samples. After accelerating the centrifuge, the layer of ice broke due to the effect of the centrifuge acceleration and the increase in temperature. This methodology enabled the centrifuge to reach the desired velocity before the start of the LNAPL release. The dimensions of the containers are summarized in Table 4.5 and "translated" to the real scale.

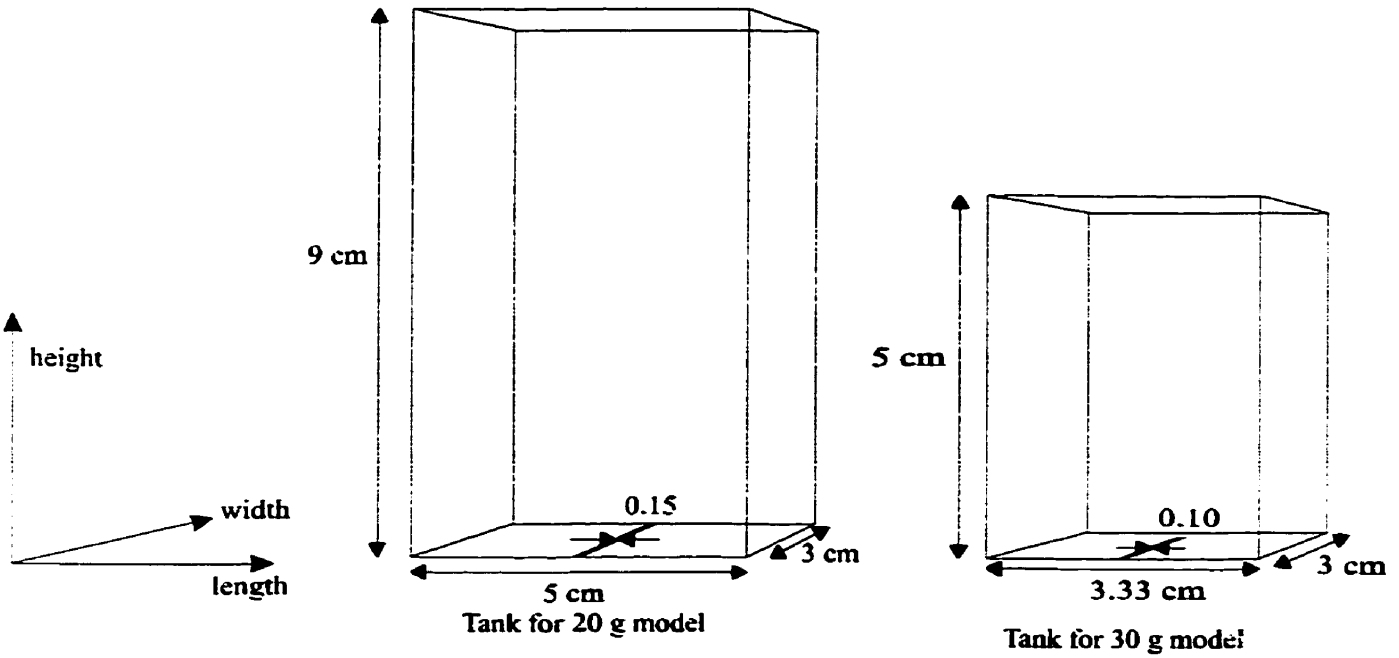

Figure 4.6 The view of the LNAPL tanks

Table 4.5 Container dimensions (* indicates the corresponding real scale dimension for the 20g model only)

Dimension	*Real scale*	*20 g*	*30 g*
Tank linear opening length	*3 cm*	*0.15 cm*	*0.1 cm*
Tank linear opening width	*60 cm**	*3 cm*	*3 cm*
Tank linear opening area	*180 cm^2*	*0.45 cm^2*	*0.3 cm^2*
Tank length	*100 cm*	*5 cm*	*3.33 cm*
Tank height	*180 cm*	*9 cm*	*6 cm*
Tank width	*60 cm**	*3 cm*	*3 cm*
Tank area	*6000 cm^2*	*15 cm^2*	*9.99 cm^2*

From Figure 4.6 and Table 4.5, it can be noted that the dimensions of the LNAPL tanks along the direction of the width are equal. Owing to the use of the same strong-box for both 20*g* and 30*g* models, the width of the LNAPL containers was not scaled with respect to the scaling laws. However, this choice did not alter the similitude between the two-dimensional flow in the 20*g* and 30*g* models. In fact, if the two sand models have the same permeability, the LNAPL flow in the porous medium depends only on the total head. For a one-dimensional Darcy flow, the LNAPL flow rate can be written as

$$dQ = -a\frac{dh}{dt} = \frac{k\,k_r\,\rho\,g}{\mu}\ \frac{h}{L}A \qquad (4.1)$$

where

h is the head of the LNAPL in the container (m)

a is the area of the containers (m^2)

A is the area of the porous medium (m^2)

k is the permeability of the porous medium (m^2)

k_r is the fluid relative permeability factor for the fluid based on its saturation (*non-dimensional*)

L is the length of the porous medium (m)

ρ is the density of the fluid ($kg \cdot m^{-3}$)

μ is the dynamic viscosity of the fluid ($Pa \cdot sec$)

g is the earth's acceleration ($m \cdot sec^{-2}$)

t is time (sec)

According to Figure 4.6, the two terms in (4.1) indicating area can be written as

$$a = l_a \times w_a \qquad (4.2a)$$

$$A = l_A \times w_A \qquad (4.2b)$$

where,

l is the length *(m)*

w is the width *(m)*

Equation 4.1 can be rewritten as

$$dQ = -(l_a \times w_a)\frac{dh}{dt} = \frac{k\rho g}{\mu}\ \frac{h}{L}(l_A \times w_A) \qquad (4.3)$$

Assuming that the vertical component of the LNAPL flow in the two-dimensional centrifuge models is governed by equation (4.3), and satisfies the scaling laws discussed in Chapter 3, the LNAPL flow rate in both models can be written as

$$-(\frac{l_a}{N_{20}} \times w_a)(\frac{dh}{N_{20}} \times \frac{N_{20}^2}{dt}) = (\frac{kk_r\rho g}{\mu} \times N_{20})\ (\frac{h}{N_{20}} \times \frac{N_{20}}{L})(\frac{l_A}{N_{20}} \times w_A) \qquad (4.4a)$$

$$-(\frac{l_a}{N_{30}} \times w_a)(\frac{dh}{N_{30}} \times \frac{N_{30}^2}{dt}) = (\frac{kk_r\rho g}{\mu} \times N_{30})\ (\frac{h}{N_{30}} \times \frac{N_{30}}{L})(\frac{l_A}{N_{30}} \times w_A) \qquad (4.4b)$$

where,

N_{20} is the acceleration factor for the 20g model (20)

N_{30} is the acceleration factor for the 30g model (30)

Dividing the vertical flow rate of the 20g model (4.4a) by the vertical flow rate of the 30g model, we have

$$\frac{dQ_{20}}{dQ_{30}} = 1 \qquad (4.5)$$

Equation (4.5) indicates that the use of the LNAPL containers shown in Figure 4.6 ensures the similitude of the vertical component of the LNAPL flow in the models.

4.2.5 The sand sampling technique

The water and LNAPL contents were measured by means of a sampler specially built for this research program. The Figure 4.7 shows the main characteristics of this sampler. The principle is similar to the samplers that are used to collect undisturbed samples of sand below the water table. The sampling tube is attached to a guide rod. The sampling tube and the guide rod are contained in a external tube. A spring located at the top of the external tube makes the sample tube to return to the initial position. A screw-nut located at the top of the external tube determines the length of the movement of the guide rod and, therefore, of the length of tube and sample extracted. Unfortunately, there is no provision, in the form of vacuum, which can properly retain the water in the sample.

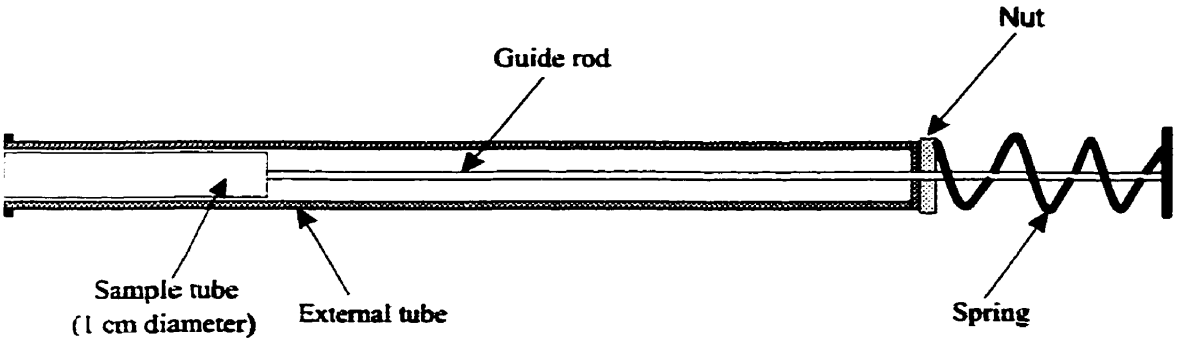

4.7 Cross sectional view of the sampler used

4.2.6 The device for the measurement of the capillary rise at 1g

In order to compare the capillary effects modelled in an accelerated environment to those acting at the prototype scale, it was decided to measure the capillary rise at 1g on the same porous medium used in the centrifuge modelling. Figure 4.8 shows the tool used for measuring the water content and the height of the capillary fringe. The device consists of two coaxial plexiglas cylinders. The internal cylinder is cut in ring segments. The bottom of both the cylinders is closed by a porous fabric which retains the sand. The porous medium is rained within the internal cylinder and saturated. The device is then positioned in a tank filled with water, so that the water level is kept at the base of the cylinders (Figure 4.8). The water in the porous medium is allowed to drain from the base of the cylinder. When the visible capillary fringe reaches equilibrium with the atmospheric

pressure (i.e. when the capillary height is stabilized in the cylinder), each internal ring segment is extracted, weighed, and put in an oven for the measurement of the water content. After the evaporation of the water content, each internal ring segment is weighed again to determine the mass of water which was contained in the porous medium. The derived water contents are correlated to the height above the water level of the tank shown in Figure 4.8.

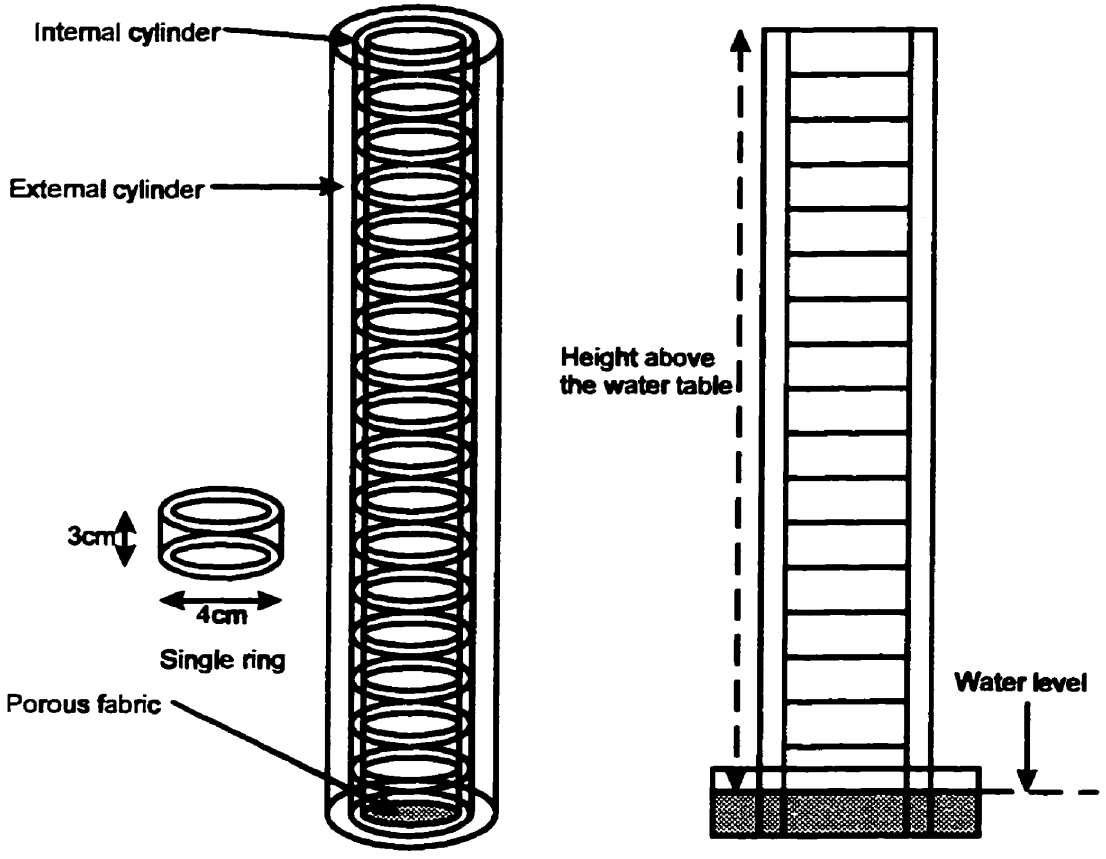

Figure 4.8 Column for capillary fringe's height measurement

4.2.7 The sand rainer device

All models were prepared by raining the sand in the strong-box. A normal sand raining procedure consists of raining the soil from a sand reservoir with a steady flow to the sample container which is mechanically moved on a horizontal bed. The density of the resulting model can be varied by changing the height of fall of the sand. An increase of the height of fall usually results in a higher density.

The Geotechnical Laboratory of Delft Technological University has a sand raining device in which the rate of horizontal movement of the device and the height of fall are computer controlled. Figure 4.9 shows a schematic view of the "sand curtain" device. The "curtain pluviation system" can be considered to be built up of two sub-devices. The first sub-device is the hopper itself (*A*) with the opening system where the sand flow is controlled. The second sub-device (*B*) regulates the horizontal movement of the platform on which the sample container stands. This sample platform moves in a horizontal direction beneath the sand hopper. The sample platform can also be adjusted in the vertical direction to set and correct the height of fall of the sand.

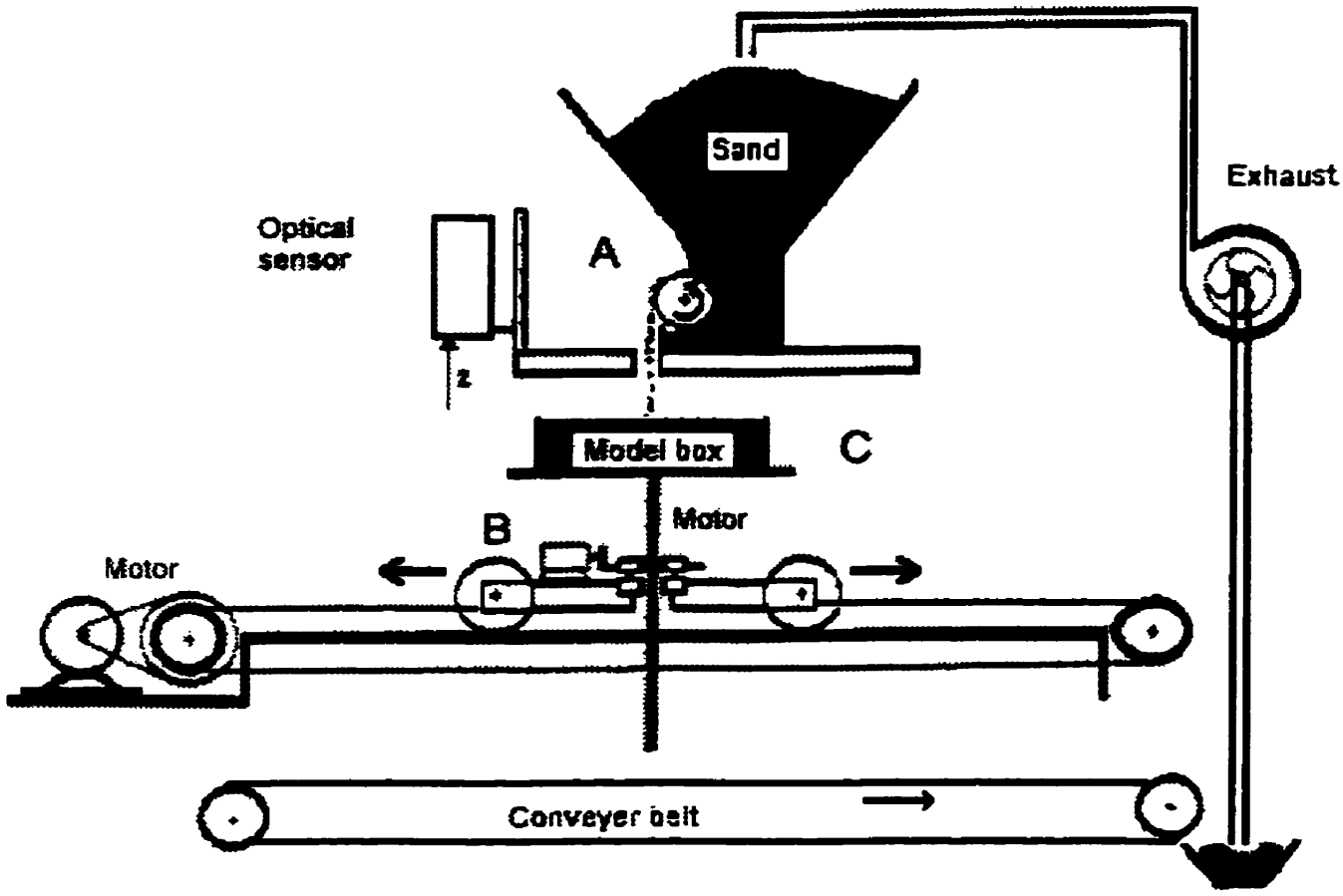

Figure 4.9 Diagram of the sand curtain rainer

Since the sand surface rises progressively due to the accretion, the height of fall becomes variable if the platform C does not move. This results in an non-uniform distribution of porosity. To avoid this, the length of fall is maintained constant during the raining process by automatically adjusting the position of the sample platform C. At the return point of the carriage, the height of the sand is measured, as shown in (Figure 4.9). To avoid sample disturbance during raining, this measurement is carried out optically to an accuracy of $\pm$ 0.1 *mm*. The platform height is reduced until the measured sand surface is at level prior to the instance when two new layers (i.e. layers placed during travel in both direction) were placed.

Further details concerning the sand placement this device are given by Allersma (1990). Details concerning the variations in the porosity achieved by this device are also given by Allersma (1990). Figure 4.10 shows the sand raining machine at the Delft technical University, Geotechnical Laboratory.

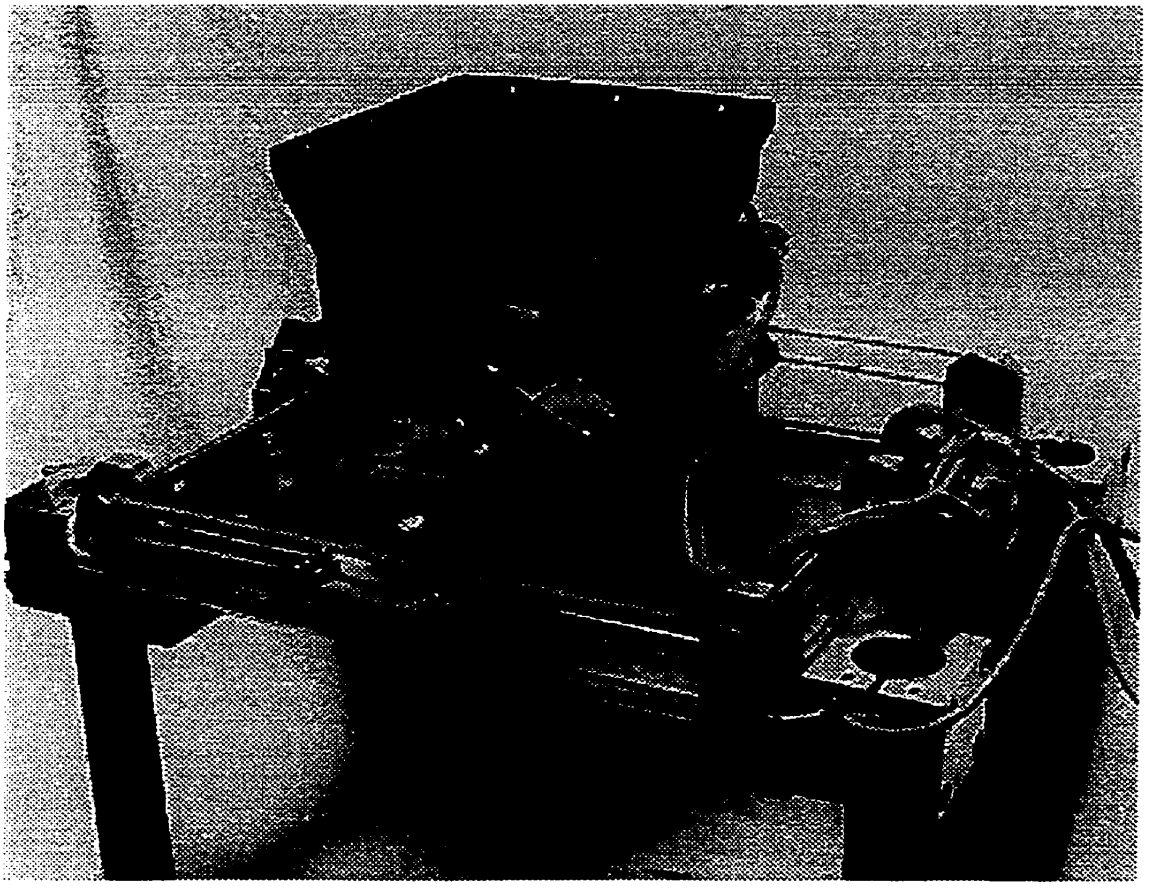

Figure 4.10 The sand raining machine at the Delft Technical University, Geotechnical Laboratory.

4.3 PROPOSED EXPERIMENTAL SYSTEM

4.3.1 Description of the porous media

The experiments were performed using Dutch Fine Sand compacted to a given porosity and possessing the physical parameters shown in Table 4.6. The porosity was calculated at the end of the preparation of each sample, considering the specific weight of the sand used, and the volume occupied by the sand in the model container. The value of standard deviation given in Table 4.6 is due to Allersma (1990) who conducted tests on samples prepared by means of the sand raining machine described in section 4.2.7.

Preliminary tests were carried out to establish if the Dutch Fine Sand satisfied the requirements discussed in Section 3.3 necessary to obtain the similitude between prototype and models. The velocity of water at the maximum acceleration of 30g was $1.16 \times 10^{-4}\ m \cdot sec^{-1}$. This value, combined with an average flow channel given by the D_{50} (Bear, 1972), and with the dynamic viscosity of water at 20 °C (see Table 4.7 after Granet, 1996) gave the Reynolds number for the water flow at 30g equal to 2.32×10^{-2}. Thus, at the maximum acceleration used in this research (30g) the water flow was laminar. The Froude number for the water flow at 30g was equal to 2.29×10^{-7}, which indicates that the inertial effects were negligible when compared with gravitational effects (Knight and Mitchell, 1996). The inverse of the calculated Bond number was *15.2* which is larger than the experimental minimum threshold value found by Morrow and Songkran (1981). The capillary trapping of water was assumed to be uninfluenced by the centrifugal acceleration.

Table 4.6 Soil characteristics

Parameter	*Value*
D_{90} (mm)	5.0×10^{-4} *m*
D_{50} (mm)	2.0×10^{-4} *m*
D_{10} (mm)	1.2×10^{-4} *m*
Uniformity coefficient	*1.58*
Porosity (Dense sand)	*35.9 %*
Porosity (Loose sand)	*41.0 %*
Porosity standard deviation	*<0.2%*
Void ratio (Dense sand)	*0.56*
Void ratio (Loose sand)	*0.69*
Specific weight	*26.5 kN/m³*
Friction angle loose sand	*24-30 degree*
Friction angle dense sand	*33-35 degree*

Table 4.7 Properties of water

Property	*Given Value*
Density at 20 °C	$998.2\ kg \cdot m^{-3}$
Dynamic viscosity at 20 °C	$1.0 \times 10^{-3}\ Pa \cdot sec$
Interfacial tension air-water	$7.28 \times 10^{-2}\ N \cdot m^{-1}$

4.3.2 Description of the chemical-physical characteristics of the LNAPL

For reasons of time, it was decided to use a LNAPL having properties already measured. The LNAPL used in the experiment was a Shell Multigrade motor oil 15W/40 the properties of which are listed in Table 4.8. The information on the oil properties was supplied by the Shell Customer Service in The Hague, The Netherlands. The viscosity was measured by means of a standard Saybolt viscometer, produced by Kaltec Scientific Inc., Novi, Michigan. The interfacial tension was measured by using a Video Intensified Optical Contact Angle meter produced by KSV Instruments Ltd., Helsinki, Finland.

Table 4.8 Properties of LNAPL

Property	*Given Value*
Density at 20 ^{o}C	$950\ Kg/m^3$
Dynamic viscosity at 20 ^{o}C	$1.42 \times 10^{-1}\ Pa \cdot sec$
Dynamic viscosity at 100 ^{o}C	$1.47 \times 10^{-2}\ Pa \cdot sec$
Kinematic viscosity at 25 ^{o}C	$1.49 \times 10^{-4}\ m^2 \cdot sec^{-1}$
Kinematic viscosity at 100 ^{o}C	$1.55 \times 10^{-5}\ m^2 \cdot sec^{-1}$
Viscosity index	135
Flame point	212 ^{o}C
Ice point	-30 ^{o}C
Interfacial tension air-oil	$3.6 \times 10^{-2}\ N \times m^{-1}$
Interfacial tension water-oil	$4.5 \times 10^{-2}\ N \times m^{-1}$

According to the physical properties listed in Tables 4.7 and 4.8, the calculated inverse of the Bond number for the water-LNAPL system was equal to *318.5* at the maximum acceleration of 30g. This number was greater than the threshold (*200*) value indicated by Morrow and Songkran (1981). Thus, buoyancy forces have no effect on the amount of trapped residual non-wetting phase saturation, and residual saturation depends only on the capillary number. However, the capillary number is not significant to the residual LNAPL saturation if the hydrocarbon always displaces water, and if the water is in equilibrium in the porous medium (Knight and Mitchell, 1996). The Reynolds number for the LNAPL was calculated after measuring the velocity of the LNAPL in the sand models during preliminary tests. For the most critical case possible in the centrifuge modelling, (centrifuge acceleration equal to 30g, and loose packing of the sand), the observed velocity of the LNAPL was $2.2 \times 10^{-5}\ m \cdot sec^{-1}$. This velocity produced the Reynolds number equal to 2.97×10^{-5} which was five order of magnitude smaller than the critical value. Due to the small maximum value of velocity, the Froude number was less than 8.2×10^{-9}. At a maximum centrifuge acceleration of 30g, the inertial effect were negligible on the LNAPL chosen for this study.

4.3.3 Preliminary experiments

i) Reliability of the sampler efficiency

The tool used in this study to collect sand samples was described in section 4.2.5. Since the sampler was specially built for this research program, it was decided to test the reliability of the tool. Sand samples of known water content were utilized to "calibrate" the sampler. In order to estimate the magnitude of loss of water after sampling, four

samples of sand were prepared at 35.9 per cent of porosity by raining the sand with the technique discussed in section 4.2.8. Sand possessing the properties listed in Table 4.6 was used in these tests. Two of the samples were completely saturated, the other two were prepared with a water content smaller than the value at saturation. The initial and the final values of water content are indicated in table 4.9 where the water contents, the errors, and the degrees of saturation are expressed in percentage value.

Table 4.9 Test on the sampling technique

Sample	*Saturation*	*Initial Water Content*	*Measured Water Content*	*Error*
1	*100.00*	*20.741*	*20.511*	*1.109*
2	*66.66*	*13.813*	*13.806*	*0.051*
3	*100.00*	*20.741*	*20.483*	*1.244*
4	*66.66*	*13.813*	*13.795*	*0.131*

The water content was determined by drying the samples in an oven (Heraeus model T5050) at a temperature of 125 °C for eight hours. After this period, the samples were taken and measured. The sand was weighed with a balance (Mettler P 163) before and after drying. Table 4.9 lists the values of water content measured at the end of the evaporation. The raw data of tests are reported in Appendix A. From Table 4.9 it can be noted that the error obtained using the sampler described in section 4.2.5 is not greater than two percent, and this was considered acceptable. In particular, the error was greater than one percent for the two samples completely saturated, whereas it was smaller than

one percent for the two samples with a saturation of 66.66 percent; which implies that the sampling methodology produced better results with unsaturated samples than with those saturated. This can be attributed to the fact that in fully saturated samples the sampler was not able to retain the entire water and part of the free water was lost during extraction. This, however, was not a point of concern since the saturated sand was visible in the models and, therefore, the samples taken from within that zone were assumed to be fully saturated.

ii) Efficiency of the water evaporation process

Since it was mandatory to evaporate all the water of the sand samples, the progress of the evaporation process was also observed. Three tests were carried out to observe the loss of water in time using an oven (Heraeus model T5050). Figure 4.11 shows such a relationship between loss of water and time at the temperature of 125 ^{o}C, for different initial values of water content.

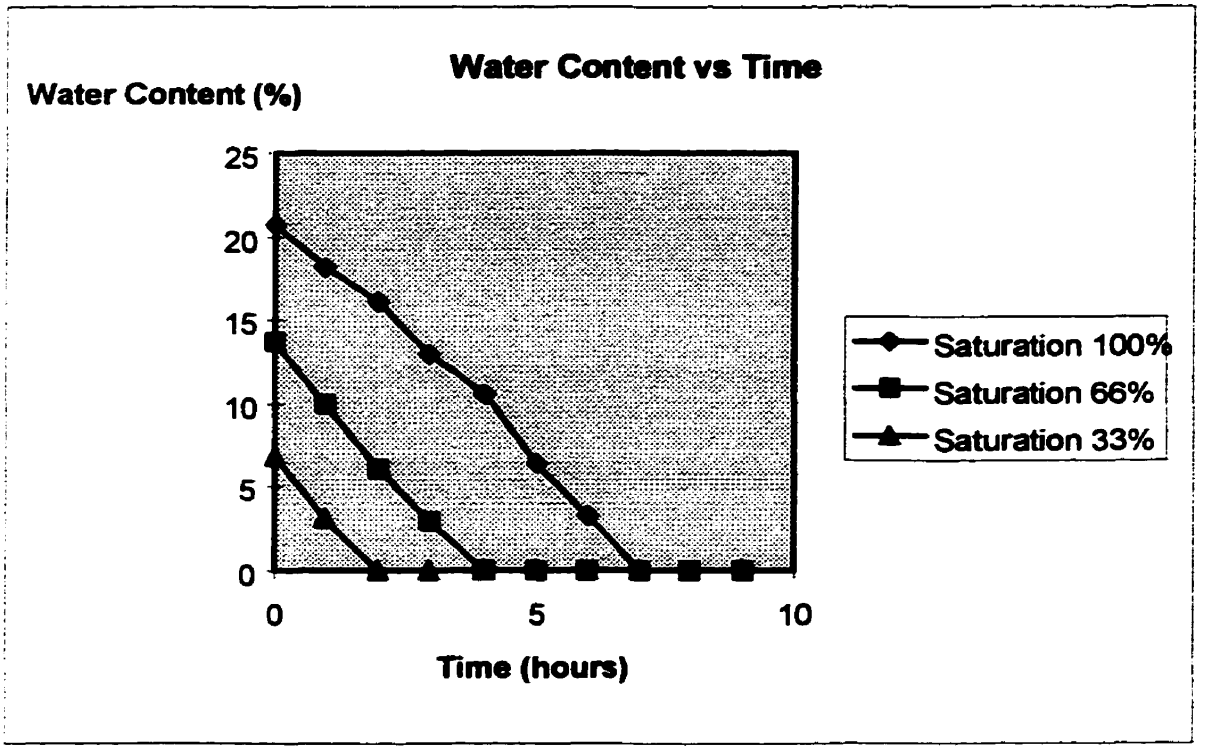

Figure 4.11 Efficiency of the oven at 125 ^{o}C

When compared with the sand samples of the centrifuge tests, these samples have a smaller mass. Gravelle *et al.* (1996) demonstrated that, at a constant temperature, an increase in mass of sand increases the rate of evaporation of water, due to the greater liquid surface area available. Another observation made was that in the partially saturated samples the complete evaporation of the water was faster than in fully saturated sample. From the results shown in Figure 4.11, and from the above considerations, it was concluded that eight hours were sufficient to completely dry out the sample.

iii) Effect of the LNAPL on the water evaporation

In order to measure the water content of sand samples also containing LNAPL , it was necessary to quantify how important the influence of the hydrocarbon was on the efficiency of the moisture content evaporation of the samples. Thus, the relationships between mass of sand, volume of LNAPL, and time required for the volatilization of the entire water content of the sample had to be derived.

The influence of the LNAPL on the moisture evaporation from the sand was tested utilizing four samples whose properties are listed in Table 4.10.

Table 4.10 Water evaporation test

Sample	*Sand (g)*	*Water (g)*	*Water Content (%)*	*Oil (g)*	*Oil Content (%)*
A1	*20.00*	*1.37*	*6.85*	*1*	*5.00*
A2	*20.00*	*2.74*	*13.70*	*1*	*5.00*
B1	*20.00*	*1.37*	*6.85*	*1.5*	*7.5*
B2	*20.00*	*2.74*	*13.70*	*1.5*	*7.5*

The samples were prepared with a total fluid content (water and LNAPL) which did not exceed the total void volume available in the sand samples. Such samples were prepared with a porosity of 35.9 per cent. In Figure 4.12, it is possible to observe the time

dependent progress of the evaporation of the water due to the heating at 125 ^{o}C with time.

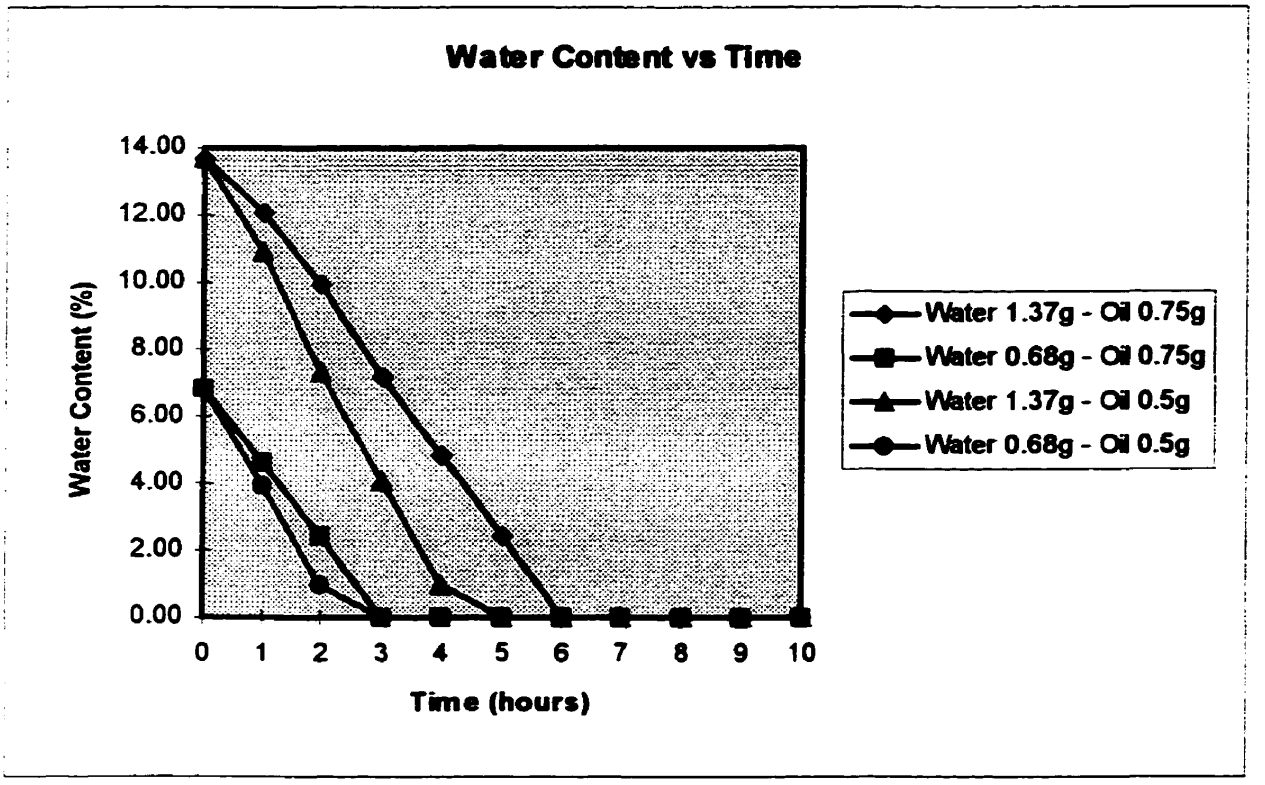

Figure 4.12 Efficiency of the sand drying process in presence of LNAPL

The water content of the samples was measured every hour. The samples were kept in the oven for 10 hours at 125 ^{o}C. The graph in Figure 4.12 shows that at a fixed water content, a higher hydrocarbon content will increase the time required to evaporate the sample water content. A greater LNAPL content produced a higher number of disconnected blobs and the water had a smaller pore volume available to leave the sand.

The samples taken at the end of the centrifuge tests had smaller sand, water, and LNAPL masses. Thus, eight hours were considered sufficient to evaporate the moisture content of the samples.

iv) The measurement of the LNAPL content

Depending upon the facilities available, the measurement of the LNAPL content in the sand sample could be carried out by using any of the following three different methodologies;

- Burn the LNAPL phase in the oven after having evaporated the sample water content.
- Extract the LNAPL by means of the Soxhlet/Rotovapor technique (A.P.H.A., 1995).
- Wash the sample by means of commercial gasoline after the evaporation of the sample water content.

It was possible to use the first methodology, since an oven was available at the Geotechnical Laboratory of Delft Technical University. However, burning hydrocarbons generates hazardous vapors which should be properly treated before emission in the atmosphere. The oven of the Geotechnical Laboratory of Delft Technical University was not equipped with a device capable to treat such fumes. Moreover, in order to burn the LNAPL utilized in this research programme, the use of temperatures greater than 220 ^{o}C were required. The Soxhlet/Rotovapor Extraction (A.P.H.A., 1995) is a codified and fully reproducible methodology, but it was not available either in the Geotechnical Laboratory

or in the Faculty of Civil Engineering of Delft Technical University. The limited budget did not allow the transportation of the samples for measurement of LNAPL at McGill University or at another Institute in The Netherlands. The second method seemed to be less reliable than the first due to the risk of losing part of the soil sample during the washing process. In spite of that, due to the possibility of directly following all the phases of the measurement procedure and to the low cost of the operation, it was decided to measure the LNAPL content by washing the sand with commercial Shell Euro Lead-free gasoline.

In order to establish the washing procedure and test the efficiency of the methodology, the relationships between mass of sand, volume of LNAPL, and time required for the complete volatilization of the whole LNAPL content of the sample had to be derived. Four tests were carried out on sand samples having a fixed LNAPL content of approximately 5 per cent, and a variable solid mass. The technique consisted in a double washing cycle using Shell Euro Lead-free gasoline. In the first washing cycle, the samples, placed in a glass container, were completely submerged into the gasoline. After shaking, the sand settled onto the base of the glass containers, and the gasoline was pumped out of the containers. Afterwards, the samples had been left to settle in a ventilated hood for 16 hours, and measurements of weight were taken every hour. The volatilization was considered complete when no variations in weight were recorded in the successive 8 hours. The difference between the initial and the final sand weight, after the first washing cycle, was attributed entirely to the presence of LNAPL in the sample.

A second washing cycle was performed using the same procedure previously described. After 8 hours, the final hydrocarbon weights were found to be very close to those initial measurements (see Table 4.11).

Table 4.11 Measured weights of the sand micro-samples after washing

Sample	*Sand (g)*	*Initial Oil (g)*	*Oil-First Cycle (g)*	*Oil-Second Cycle (g)*	*Final Error*
A1	*20.003*	*1.002*	*0.932*	*0.991*	*1.098*
A2	*20.005*	*1.008*	*0.917*	*0.987*	*2.083*
B1	*10.001*	*0.511*	*0.455*	*0.499*	*2.348*
B2	*10.007*	*0.503*	*0.463*	*0.494*	*1.789*

The measurement of the hydrocarbon weight by using this technique gave a final error not greater than 2.5 per cent. It was concluded that two soil washing cycles with commercial Shell Euro Lead-free gasoline were sufficient to dissolve all traces of LNAPL present in the samples.

v) Measurement of the variation of the porosity in the models

The use of a geotechnical centrifuge is a powerful and fast tool to analyze phenomena that may be difficult to reproduce at 1*g*. However, in order to obtain reliable results, all the aspects of the modelling technique required to be checked before and during the experimental program. During the preliminary phase of this study, the major drawback encountered was the settlement of the sand model in flight. The sand samples were prepared outside the centrifuge under earth's 1*g* gravity field by the method mentioned in section 4.2.7. During flight, the increase of the self weight caused the settlement of the

sand and, consequently, a change in porosity. In seepage phenomena, porosity plays an important role on the hydraulic characteristics of the porous medium. For this reason, it was decided to quantify the settlement of the sand due to the increased acceleration. The change in porosity was calculated by measuring the vertical settlement (z) of the sand surface of the sample. The settlement was measured with a Linear Variable Displacement Transducer (LVDT) (model 7DCDT-1000 produced by Hewlett Packard). This transducer was able to measure only the vertical settlement. The sand samples were placed in the container shown in Figure 4.13.

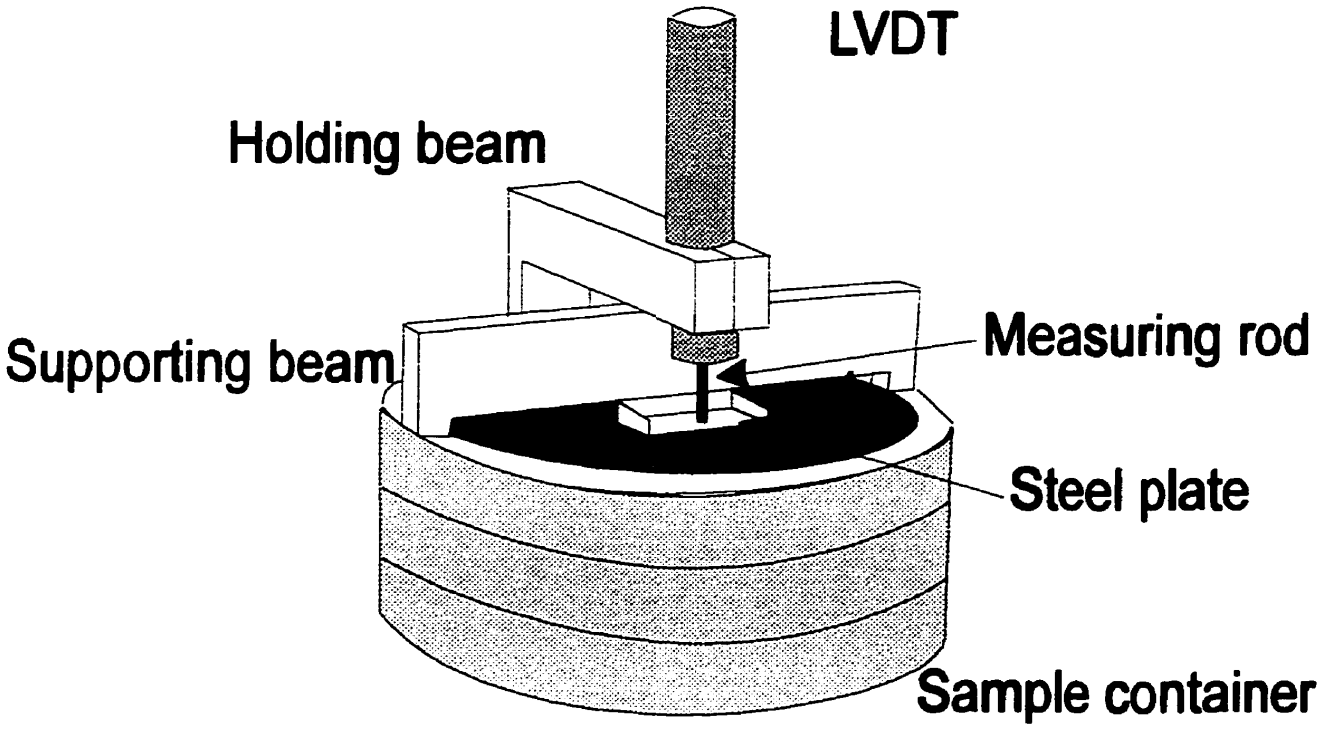

Figure 4.13 LVDT mounted on the top of the sand container (Stuit, 1995)

Stuit (1995) found an experimental relationship for the settlement in time. In that research, tests up to 120 g were carried out. At the maximum value of gravity, the relationship between settlements in time is given by

$$z = z_0 + C\,ln\left(\frac{t}{t_0}\right) \qquad (4.6)$$

where

z is the settlement (*mm*)

z_0 is the settlement at the reference time t_0 (*mm*)

t is the time (*sec*)

t_0 is the reference time, which is time required for the centrifuge to reach the required gravity's acceleration (*sec*)

C is a settlement constant which depends on soil type, density, and acceleration of gravity (*mm*)

One test was performed for 15 minutes on a sand sample 135 *mm* high possessing a porosity equal to 35.9 percent. A duration of 120 seconds was necessary to bring the centrifuge to 20*g*. The sand settlement measured at this time was equal to 1.19 *mm*. At the end of the test, the final sand settlement was measured and the settlement constant C was calculated as 0.074 *mm*. Since the 20*g* models of this study would have been accelerated for about two hours (7200 seconds), the theoretical vertical settlement was found to be approximately 1.5 *mm*. Thus, the change in volume of the 20*g* sand model would be 1.1 percent after 2 hours. A similar test was carried out at 30*g* for 15 minutes on a sand sample 90 *mm* high possessing identical porosity to the previous sand sample. The settlement at the reference time (100 seconds) was 0.98 *mm* and the settlement constant was 0.16 *mm*. The theoretical settlement after the time required for the 30g

models (18000 seconds) was calculated equal to 1.8 *mm*. For the 30*g* models, the difference between initial and final volume would be approximately 2 percent.

4.4 EXPERIMENTAL PROCEDURE

The experimental procedure adopted for the testing of each model used in the research program and for the study of capillary rise tests conducted at 1g are outlined in the following sections.

4.4.1 The measurement of the capillary rise at 1g

The tool utilized for this test is described in section 4.2.6. The procedure followed in this test is summarized as follows:

1. First, the cylinder of plexiglas shown in Figure 4.8 was weighed. Since the cylinder did not fit in the sand raining device, the sand was rained by using a funnel. The sand raining was stopped when the weight of the porous material reached the required value. The volume of the sand in the cylinder was measured and the density was adjusted using a vibrating tool.
2. The sand was saturated by very gradually percolating water upwards from the base of the cylinder. The flow rate utilized was equal to $9.0 \times 10^{-9}\ m^3 \times sec^{-1}$. When the sand was completely saturated, the cylinder was placed in the basket shown in Figure 4.8, in which there was a layer of water *3 cm* high.
3. The water was left to drain through the base of the cylinder. The decrease of the height of the saturated zone with time was visible since the cylinder was transparent. The capillary height was observed every 12 hours. When no macroscopic variations were

recorded for more than 24 hours, the equilibrium between water and air was considered to be achieved.

4. The internal cylinder was extracted from the external cylinder. Each ring segment was weighed and placed in the oven. After 12 hours the ring segments were extracted and weighed, and the water content determined.

4.4.2 Preparation of the centrifuge models

The basic steps involved in the preparation of the sand models in the experimental facility are summarized in the following:

1. The strong-box was placed on the platform C (Figure 4.9) of the sand raining device. The height of the fall for the sand was regulated according to the desired value of porosity (Allersma, 1990). The sand raining device was stopped when the desired height of the model was achieved.
2. At the end of the sand raining, the strong-box was connected (Figure 4.5) to an automatic pump. This device was able to deliver a fluid, contained in a reservoir, at a constant flow rate. The flow rate utilized was $9.0 \times 10^{-9}\ m^3 \cdot sec^{-1}$. According to the average flow channels of the sand (Table 4.4), this flow rate does not introduce any disturbance of the sand.
3. When the water reached the top of the sand in the model, the pump was stopped and the model was ready for centrifuge testing.

4.4.3 Modelling of the unsaturated profile in the centrifuge

To model an unsaturated profile in the centrifuge, the following procedure was used:

1. The models prepared as described in section 4.4.2 were weighed and transported to the centrifuge room. The strong-box was then placed on one of the two swinging baskets of the centrifuge facility (Figure 4.2), and the other was loaded with a counterweight. The cameras were focused on the strong-box and the stroboscopic light regulated.
2. The centrifuge was started and accelerated to the required value of angular velocity. The progress of the experiments was recorded and photographs were taken every 10 minutes. These photographs were saved directly on the hard disk of the controlling computer bypassing the video-recorder. This procedure gave pictures of a better quality than those developed from the *VHS* cassette. The temperature in the centrifuge room was kept constant at 20 ^{o}C.
3. At the termination of an experiment, the centrifuge was stopped and the strong-box was extracted from the swinging basket. The model was then transported to the Soil Mechanics Laboratory of Delft Technical University for sampling.
4. The sampling procedure involved the extraction of small sand samples every 30 *cm* (real scale dimensions) commencing from the surface of the sand. The sampling of the models was carried out following the division in layers indicated in Figure 4.14. The samples were taken from the central zone of the model. The length of the samples was 1.5 cm at 20 g, and 1 cm at 30 g. After extraction from the model, the samples were placed into a glass containers and weighed. After evaporation, the samples were weighed again and the water content was determined.

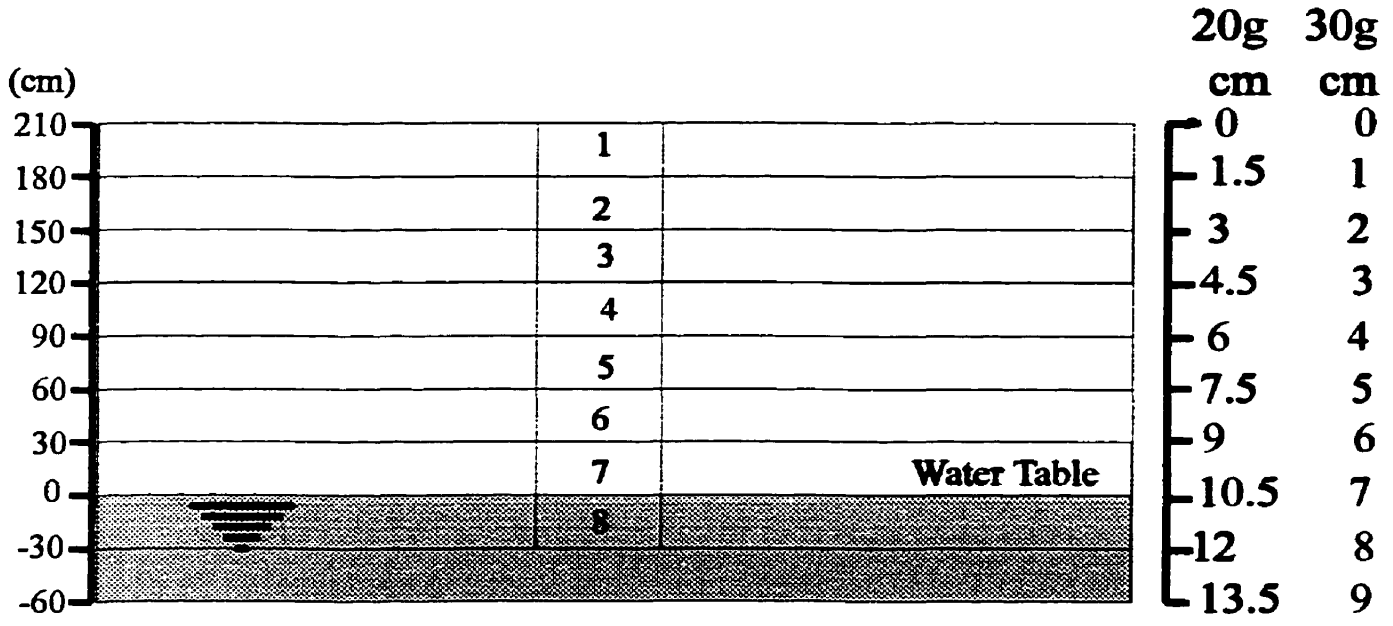

Figure 4.14 Position of the samples in the model

4.4.4 Modelling of the LNAPL release in the centrifuge

The LNAPL release modelling was carried out on sand models prepared as described in section 4.4.2. After the modelling of the unsaturated profile (section 4.4.3), the steps followed in this part of the experimental program were as follows:

1. In order to increase the visual contrast between contaminated sand and non-contaminated sand, the LNAPL phase was marked with commercial black oil color.
2. The LNAPL containers described in section 4.2.4 were filled with the LNAPL and placed on the upper surface of the sand models.
3. The centrifuge was started and brought to the required value of angular velocity. The progress of the experiments was recorded on VHS and pictures were taken every 10 minutes.

4. At the termination of an experiment, the centrifuge was brought to rest and the strong-box was quickly (within 3 minutes) extracted from the swinging basket. The sand models were then transported to the Soil Mechanics Laboratory of Delft Technical University for sampling purposes.
5. The sampling technique was carried out following the division in layers and zones indicated in Figure 4.15.

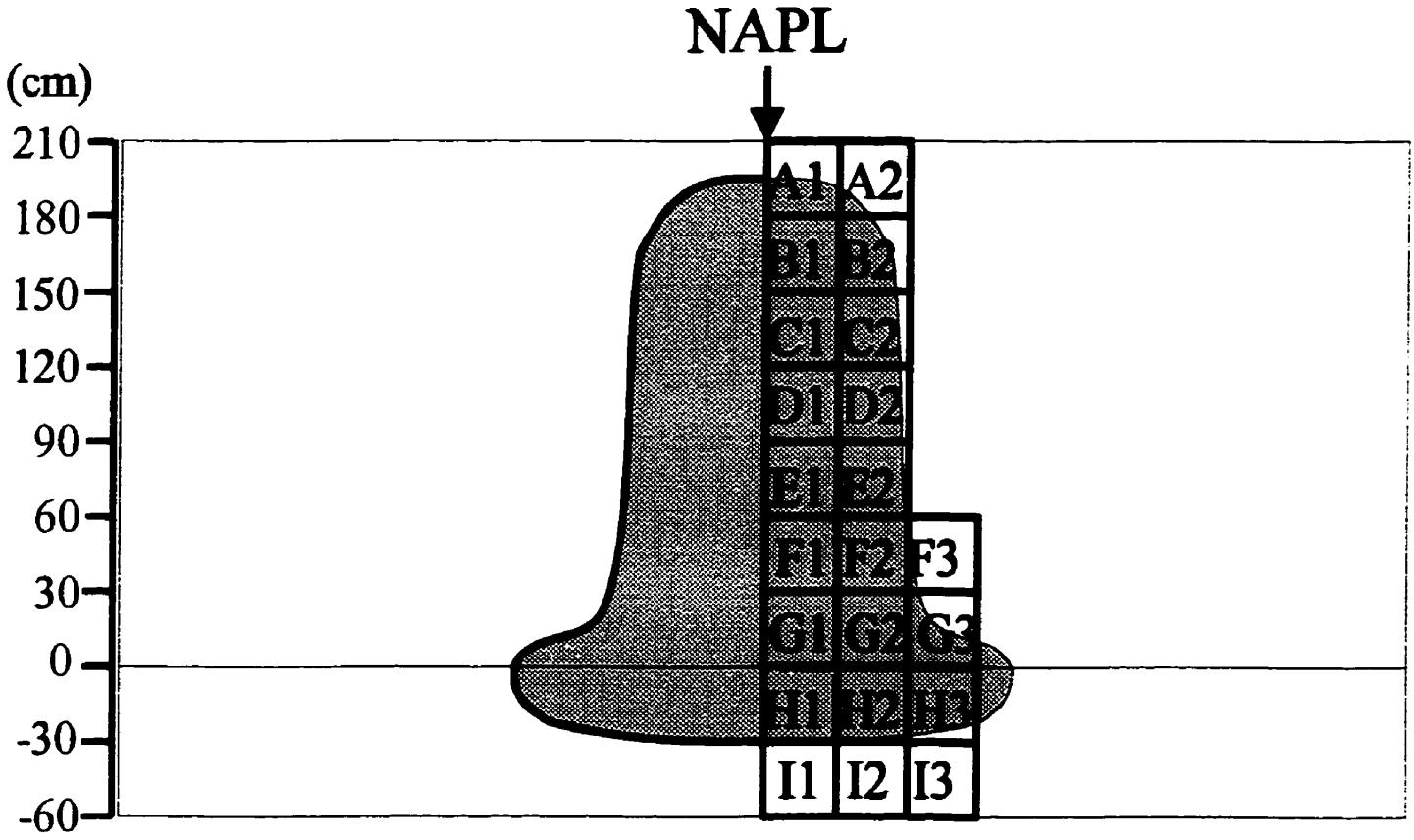

Figure 4.15 Division in layers and zones of the sand samples

The measurement in Figure 4.15 are given in actual scale dimensions. To locate the samples, plumes traced after preliminary tests were used. Such tests gave a good indication about the expected size and shape of the plumes at the end of the simulations. A decision was made to take samples along three vertical directions (columns). The first one (1) was next to the axis of symmetry of the plume which passes through the linear opening of the LNAPL container. The second sample column (2) was adjacent to the first one, and the third sample column (3) was positioned in the zone where the plume spread out laterally over the capillary fringe. In order to respect the scaling relationships between models, a cylindrical sampler of scaled diameter was to be used. In this study, the use of the same sampler gave samples which were representative of different scaled soil volumes. Samples of the 30 g test corresponded to a bigger real scale soil volume than those of the 20 g test. The lack in similitude caused a loss in detail for the results of the 20 g test, since the numerical values were representative of smaller soil volumes (real scale dimensions).

6. The samples taken were weighed and placed in the oven to remove the moisture. After 12 hours the samples were weighed and the water content calculated.
7. After evaporating the moisture content of the sand, the samples were washed with a commercial gasoline as described in section 4.3.3. The samples were weighed and the LNAPL content determined.

5. EXPERIMENTAL PROGRAM

5.1 GENERAL

The modelling of the suction-moisture profile was conducted on sand models prepared at an initial value of porosity equal to 35.9 percent. The models were accelerated to 20*g* and 30*g*. The results of the centrifuge modelling were compared with the suction-moisture profile obtained from a 1*g* test. The purpose of these tests was to demonstrate the accuracy with which the unsaturated profile of sand ca be modelled by using the centrifuge and the 1*g* test. The modelling of the LNAPL release was conducted on sand models prepared at two different values of porosity, 35.9 and 41.0 percent . The purpose of this part of the study was to observe the LNAPL migration through an unsaturated sand, to gain an understanding of the hydrodynamics processes associated with three-phase flows simultaneously influenced by gravity, diffusive, suction, and inertial effects, and to evaluate the effect of the porosity on the dynamics of the LNAPL flow.

This Chapter presents the results obtained for all the experiments and the observations made from these results and from comparisons between the different testing conditions. The experiment schedule for the centrifuge models and the 1*g* test is shown in Table 5.1.

Table 5.1 Experiment schedule of the centrifuge modelling

Model No.	*Objective*	*Porosity*	*Gravity*
1	Unsaturated profile	*35.9 %*	*1g*
2	Unsaturated profile	*35.9 %*	*20g*
3	Unsaturated profile	*35.9 %*	*20g*
4	Unsaturated profile	*35.9 %*	*30g*
5	Unsaturated profile	*35.9 %*	*30g*
6	LNAPL release	*35.9 %*	*20g*
7	LNAPL release	*35.9 %*	*30g*
8	LNAPL release	*41.0%*	*20g*
9	LNAPL release	*41.0%*	*30g*

5.2 EXPERIMENTAL RESULTS AND OBSERVATIONS

5.2.1 Model of the unsaturated profile in sand

The magnitude of the capillary forces was measured at 1*g* on dense sand which was prepared at a porosity of 35.9 per cent. At equilibrium conditions, the height of the capillary fringe was measured on the plexiglas cylinder and was found to be approximately 42 *cm*.

The water content was then measured for each ring segment of the cylinder and plotted against the height of the ring segment above the water level (Figure 4.8). The measured degree of saturation profile is shown in Figure 5.1, where, the height above the water table (the bottom of the column) is plotted against the degree of saturation.

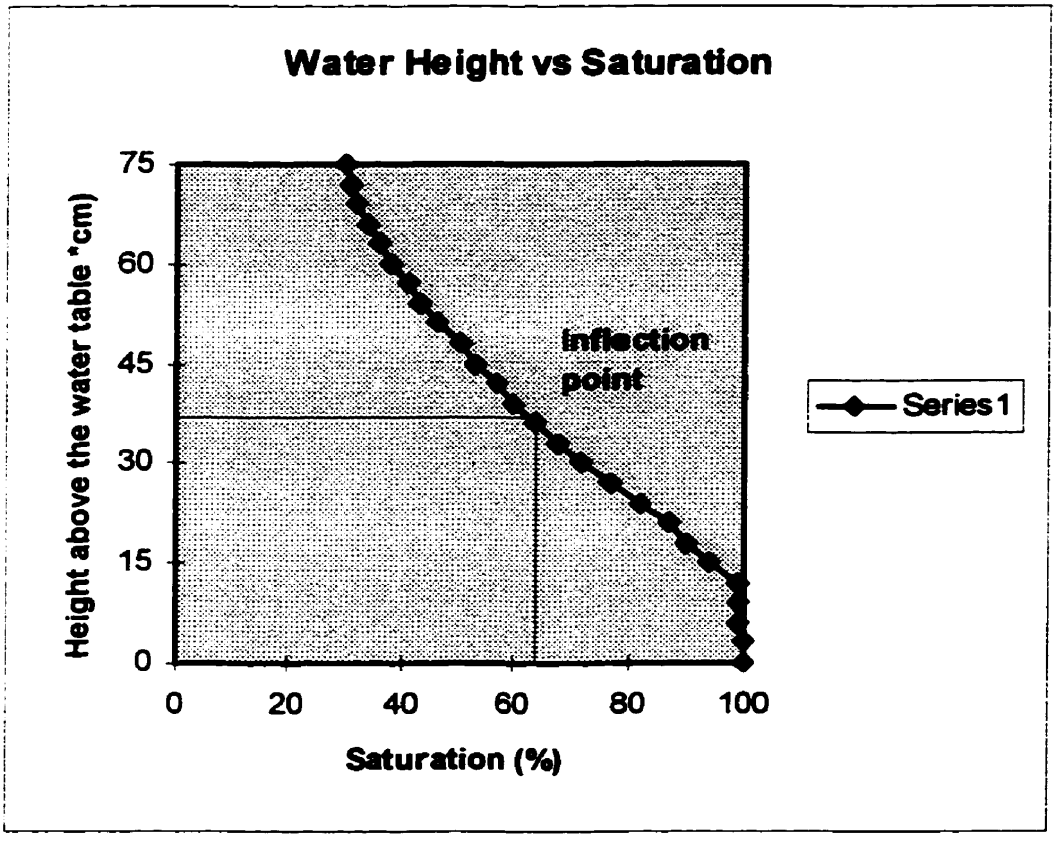

Figure 5.1 Saturation profile in 1g test on dense sand

The inflection point can be located about 40 *cm* above the water table and gives an indication of the limit of the capillary fringe (Bear, 1972). This value is very close to the direct measurement made on the Plexiglass column.

Four models (two at 20*g* and two at 30*g*) were used to study the profile of the saturation distribution. Each sand model was tested twice at the same value of gravity to ensure that the procedure was reproducible. Figure 5.2 shows the position of the saturated zone at the end of the 30*g* test identified as the darker strip at the base of the strong-box whose thickness was estimated to be 3.5 *cm*. The desired height of the water table in the strong-box was achieved by adjusting the maximum height of the outflow pipe connected to the sink of the strong-box.

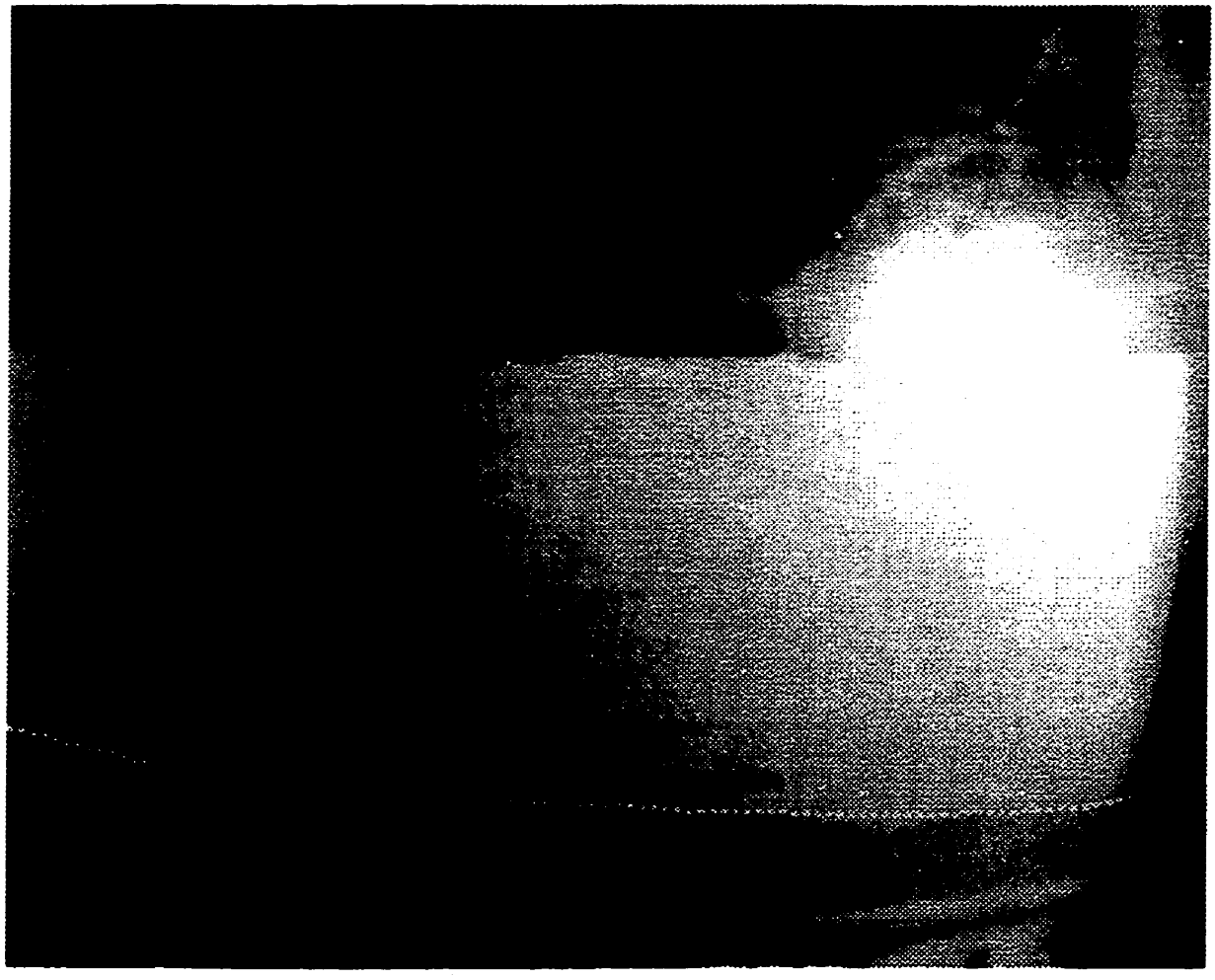

Figure 5.2 The saturated sand at the end of the 30g model

In Figure 5.3, the unsaturated profiles obtained for the four centrifuge models and the 1*g* test are shown.

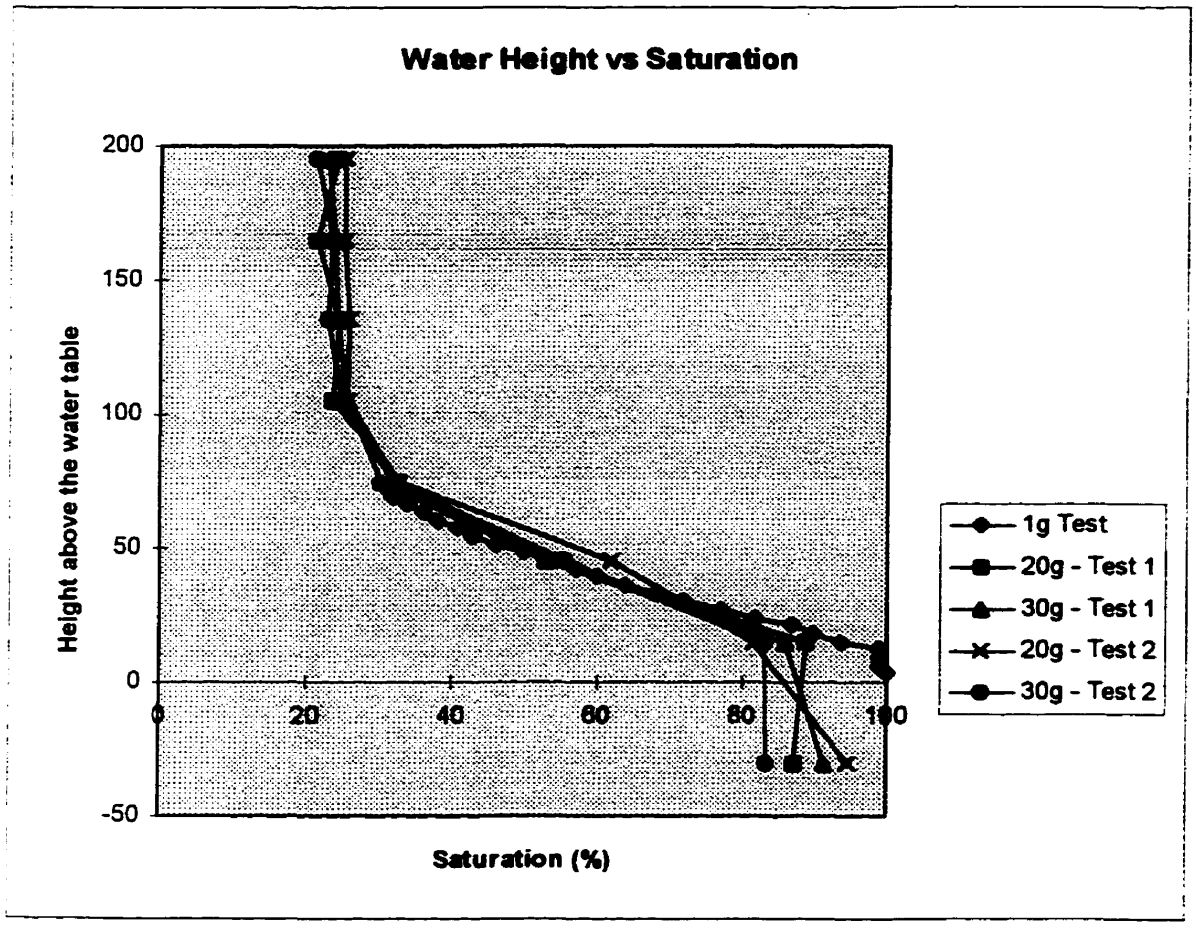

Figure 5.3 Saturated profiles

In Figure 5.3, the position of the sample with respect to the water table is plotted against the water saturation. The vertical model dimensions were converted into prototype scale dimensions. The water saturation was calculated using the final average void ratio (the raw data for the four models and the 1*g* test are listed in the Appendix A). The four profiles show a good agreement between each other, especially in the vadose zone. The

"*modelling of models*" concept indicates that the unsaturated profiles obtained are reproducible, since the results obtained at different *g*-levels are similar. The four saturation curves of the centrifuge tests also correlate well with the saturation curve for the 1*g* test, which is much more detailed due to the higher number of measurements carried out (every three cm). Despite the difference in detail, all the curves are similar in the range of the funicular zone, and show the same trend in decreasing saturation values.

The major differences between the saturation curves are in zones that are located below the water table. There are two explanations for these unexpected results, the first being that the sampling technique gave more reliable results for unsaturated samples when compared with the saturated ones. Another possibility was that the actual porosity was smaller than the value considered in the sand model calculated at the end of the tests. In flight, the centrifugal acceleration which applies to the model is directly proportional to the radius of the centrifuge (equation (3.8f)). In flight, the centrifugal acceleration at the base of the model was 8.5 percent greater than at the top for the 30*g* test, and 11.8 per cent for the 20*g* test. Thus, the calculated saturation was smaller than the actual value.

The soil-moisture characteristic curve is a parameter which also gives information about the pore size distribution of the soil. Owing to the poor gradation of the sand used in this work, a larger range of matrix potential over which the water content changes was expected. In their study, Cooke and Mitchell (1996) obtained a larger matrix potential variation range. It is, however, difficult to compare tests conducted under different conditions.

5.2.2 LNAPL release to dense sand

After reproducing the unsaturated profile, the second part of the study consisted of simulating a LNAPL spill into the unsaturated sand. The LNAPL quantity released was the equivalent of *1000 L* at the prototype scale. Two models were studied by using the Dutch Dune sand prepared at dense packing (porosity of 35.9 %), and tested at 20*g* and at 30*g*. The sand models were prepared following the methodology described in section 4.2.7. The LNAPL flow was monitored by means of the camera located on the beam of the centrifuge. From the results shown in Figure 5.4, 5.5, and 5.6, it is possible to observe the progress of the LNAPL movement in the experiment performed at 20*g*. The pictures were processed by means of the software TIM.

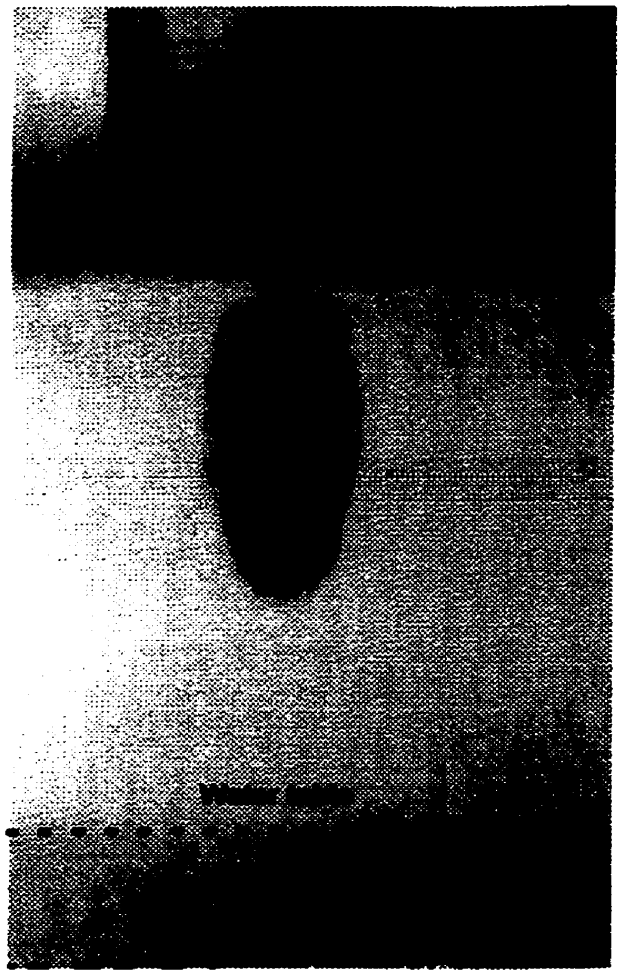

Figure 5.4 Plume development in the 20*g* test after centrifuge time of 72 minutes (prototype time of 20 days).

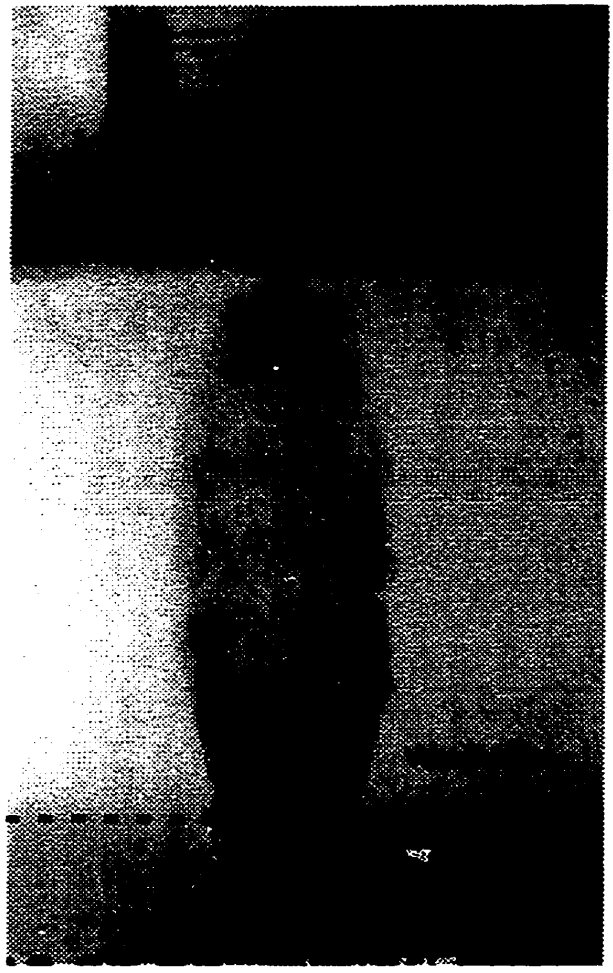

Figure 5.5 Plume development in the 20*g* test after centrifuge time of 180 minutes (prototype time of 50 days).

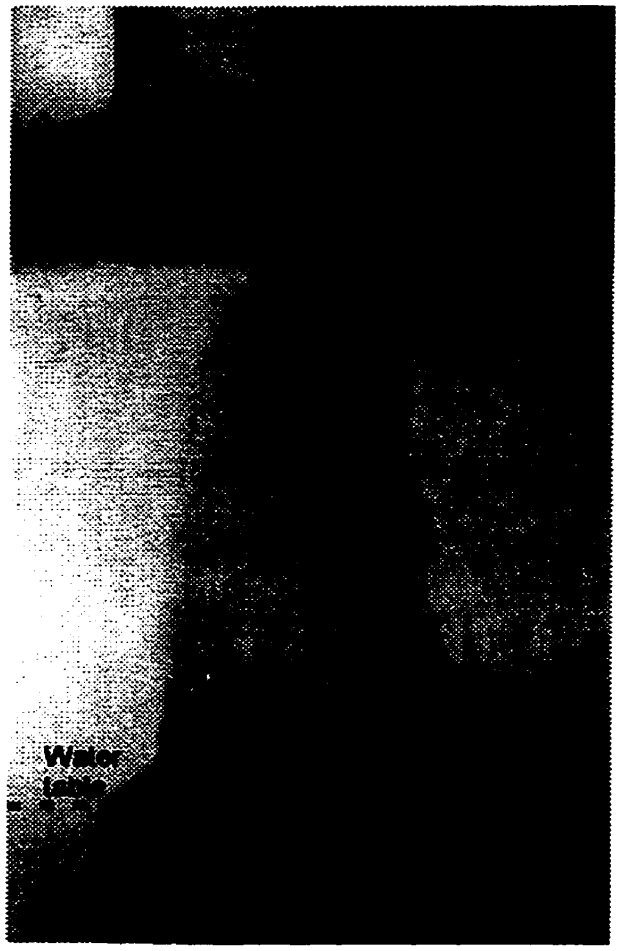

Figure 5.6 Plume development in the 20*g* test after centrifuge time of 252 minutes (prototype time of 70 days).

Converting the results of the 20*g* test to the prototype scale, it is evident that after three months the LNAPL reached the water table at a depth of 210 *cm*. Comparing the three views (Figures 5.4, 5.5, and 5.6) we observe that, at the end of the simulation time, the shape of the LNAPL plume is influenced by the variation in the degree of saturation with depth. The LNAPL plume spread out laterally over the capillary fringe. Due to the limited space available for any downward movements, the plume was forced to move horizontally. Owing to the LNAPL accumulation, the capillary fringe and the water table is depressed under the weight of the LNAPL phase.

Figures 5.7, 5.8, and 5.9, illustrate the measured water and LNAPL content along the columns 1, 2, and 3, respectively. The raw data concerning water and LNAPL content are presented in the Appendix A.

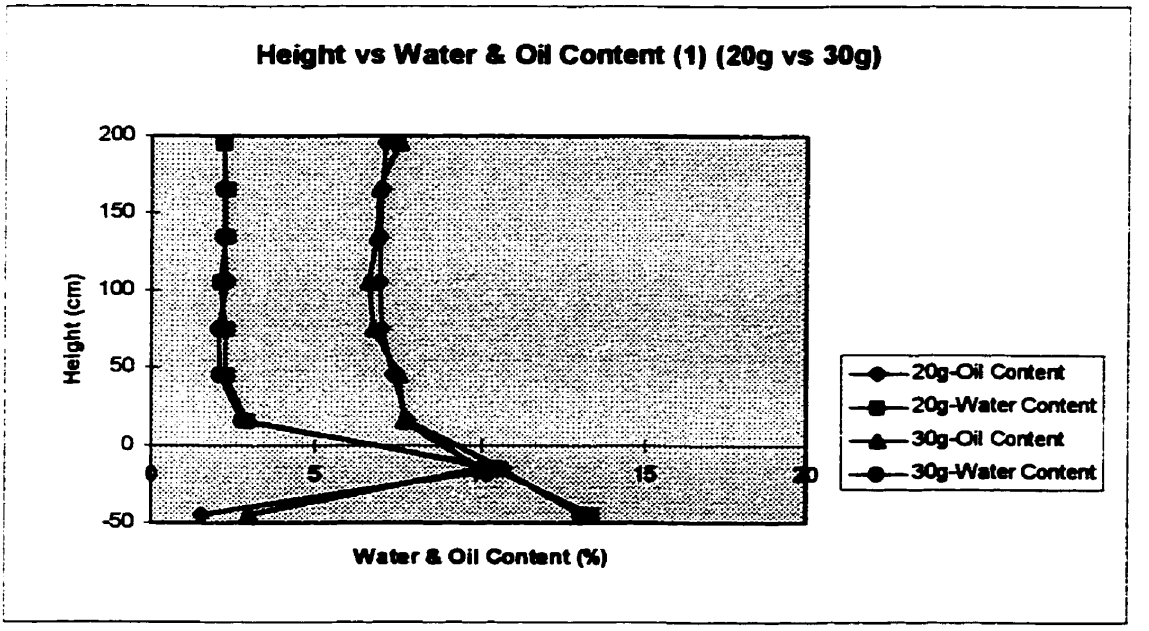

Figure 5.7 Oil and Water Content along column 1

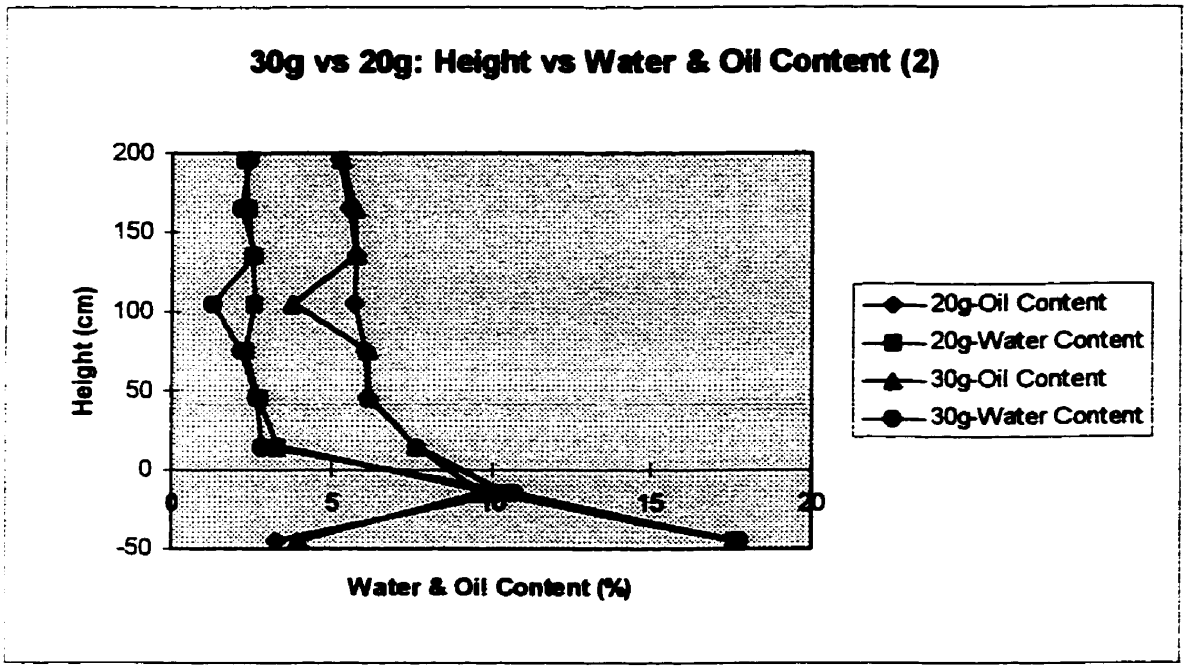

Figure 5.8 Oil and Water Content along column 2

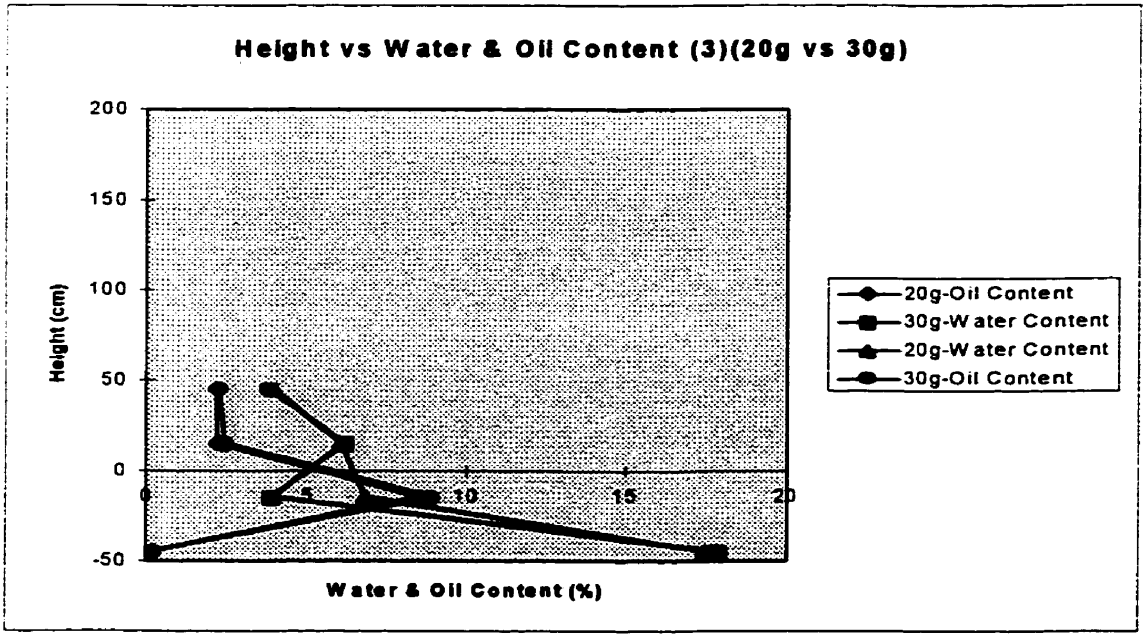

Figure 5.9 Oil and Water Content along column 3

Figures 5.7, 5.8, and 5.9 demonstrate a good correlation between the results of the three different tests. In the column 2, at 110 *cm* above the water table there is a large difference in the values of water and oil content between the 20*g* model and the 30*g* model. Since the difference was measured both for the water and for the LNAPL content, and the magnitude of the difference is almost the same for the two phases, the lack of similitude could be due to the lack of accuracy in the sampling technique rather than due to errors in the reproducibility of the model.

Comparing the suction-moisture profiles shown in Figure 5.3 and those shown in Figures 5.7, 5.8 and 5.9, it can be seen that the presence of LNAPL decreases the water content of the sand and depresses the water table. The capillary fringe almost disappears because of the weight of the mobile LNAPL phase. At similar heights above the water table, the LNAPL content is lower in column 2 than in column 1. For both the columns, and for both the models, a LNAPL content equal to zero was expected for the samples I1 and I2 , which are those taken at the bottom of the model. Instead, the LNAPL content measured was small but not zero. This behavior could be due to a partial emulsification of the LNAPL in the water. The variation of the LNAPL content in the plume for the two models is shown in Figure 5.10. The numbers written in the larger font are related to the simulation carried out at 30*g*, and the values written in the smaller font are related to the 20*g* test.

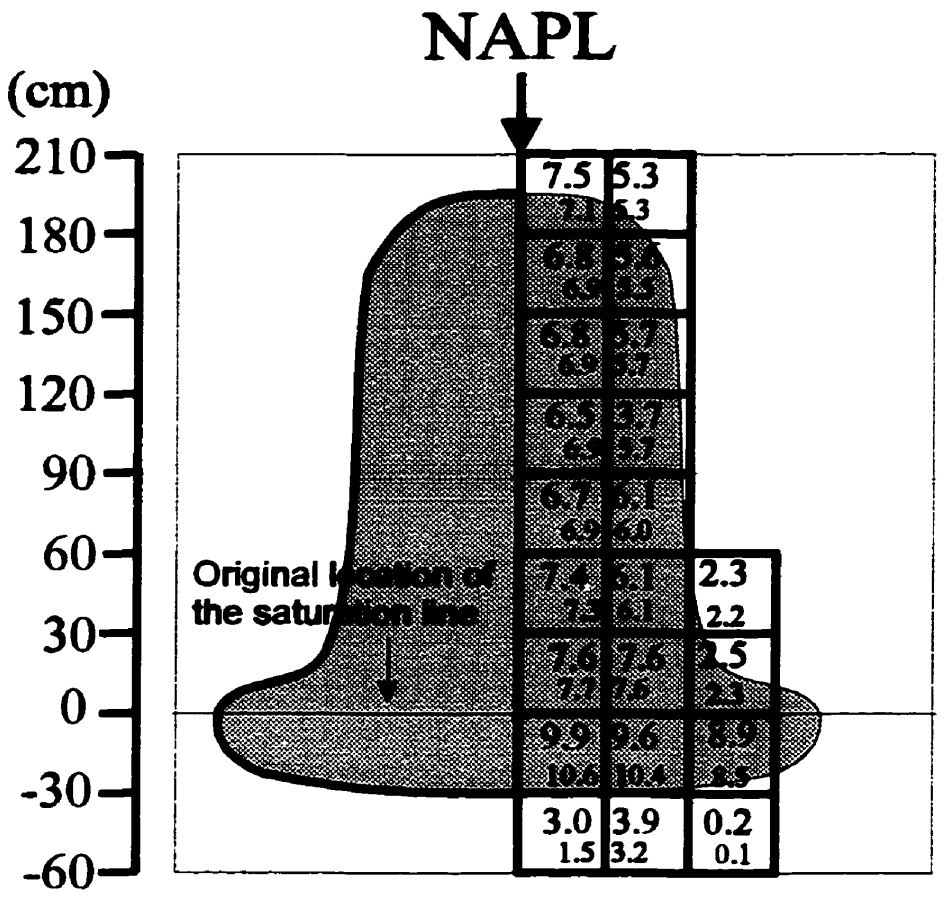

Figure 5.10 Measured Oil Content

The plumes obtained at the end of the two tests are shown in Figure 5.11. The plume areas were traced on paper sheets, scanned and converted into real scale dimensions. Figure 5.12 shows the movement of the plume with time for the 30*g* test.

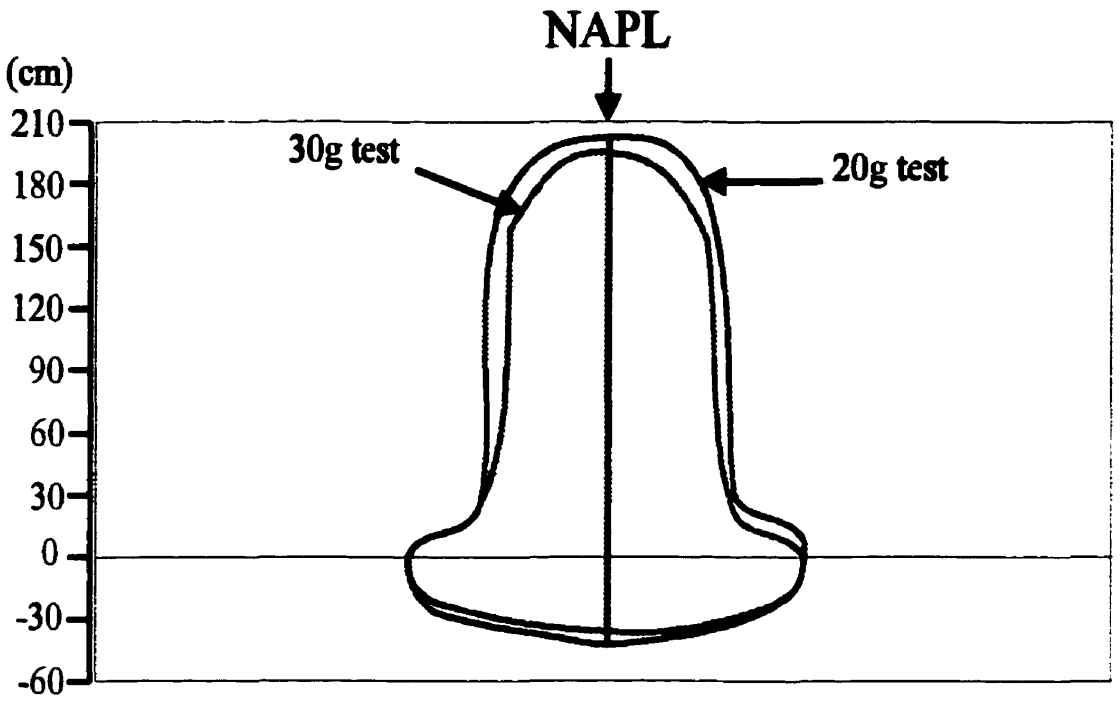

Figure 5.11 Shapes of the plumes at the termination of the tests.

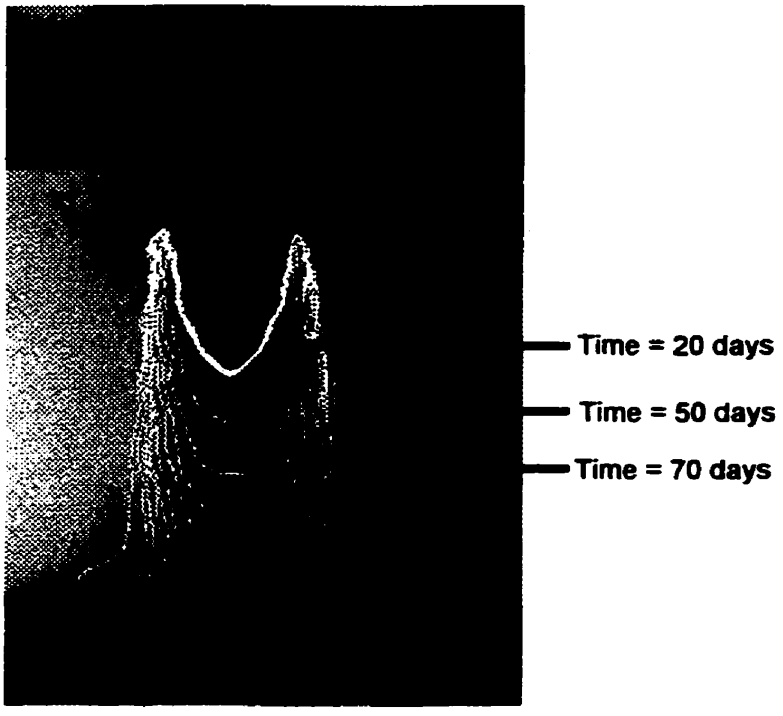

Figure 5.12 Movement of the plume in time

Despite errors made in the transformation of the measures from one scale to another, the two plumes in Figure 5.11 are very similar and have significantly different shapes only in proximity of the surface of the model. This could be attributed to the placement of the LNAPL container on the sand surface. In fact, since the container was pressed on the sand exerting a slight manual pressure, the difference in pressure intensity could result in a difference in penetration of the tank into the surface of the sand. The upper part of the LNAPL plumes might be influenced by the difference in the elevation of the LNAPL container relative to the surface if the sand.

However, there is excellent correlation between the vertical location of the light non-aqueous phase liquid plumes. This is a further confirmation that a three-fluid flow can be correctly modelled by means of the centrifuge if the initial and boundary conditions are properly reproduced. The vertical flow is fully influenced by the gravity and along the horizontal direction, due to the absence of gravitational effects, the flow is driven by advection/dispersion and matrix suction effects. As seen in section 3.3, advection/dispersion can be correctly modelled because of the similitude of the dimensionless numbers π_3 and π_4 . Mitchell and Stratton (1994) demonstrated that the horizontal flow of model and prototype are similar due to the concentration gradients, which cause diffusion, being identical in the model and the prototype. The horizontal length scale of the LNAPL diffusion is similar in the model and the prototype because both the soil area and the transport time are scaled down by the square of the linear scaling

factor, which is N^2. Therefore, the horizontal fluid movement due to diffusive effects is similar in both the model and the prototype.

The similarity of the matrix suction effect is complicated by many other factors. Goforth *et al.* (1991), indicated that there is no advantage to the modelling of unsaturated flow in a gravity accelerated environment using soils where transport phenomena are dominated by suction gradients. Mitchell and Stratton (1994) gave a geometric comparison to support the existence of the similitude. In the centrifuge model, the volume of the LNAPL is scaled down by the cube of the modelling scale factor and the holding capacity of the porous medium is reduced accordingly. Since the horizontal transport is directly affected by the quantity of light non-aqueous phase liquid present, which in turn is affected by the vertical transport, the ultimate distance of horizontal migration by matrix suction will be similar, for both model and prototype, if the vertical transport is similar. Time in the model is scaled down by the square of the modelling scale factor and lateral matrix suction gradients are similar at similar fluids contents. The area contaminated, which is also scaled down by the square of the modelling factor, will be similar in model and prototype at any given time. Thus, rate of horizontal contaminant movement due to the matrix suction gradient will be similar in model and prototype, if the LNAPL trapping mechanism is not disturbed by high velocities of the wetting phase. The laboratory results of vertical movements, derived from the tests performed in connection with this research, support the discussion given above and enhances the reliability of the model.

In the models used in this study, the hydraulic potential gradient was dominant in the first part of the LNAPL release. Due to the decrease of the total head of the LNAPL in the tank with time, suction gradients dominated the final part of the tests. As discussed previously, diffusive and matrix suction effects are similar in models and the prototype if the vertical transport is similar. Thus, transient unsaturated flows can be modelled in the centrifuge under both conditions. Since many real scale cases of superficial hydrocarbon release cause transient flows, the centrifuge model can provide useful information about the phenomenon.

5.2.3 LNAPL release to loose sand

The third part of this study consisted of modelling a LNAPL superficial release to a loose sand. Models of Dutch Dune sand were prepared with an initial porosity of about 41 %. This value was obtained by decreasing the falling height of the sand raining device (section 4.2.7). The goal of this part of the study was to study the effect of a change in the porosity of the granular medium on the flow velocity, the plume volume, and the LNAPL concentration in the sand. Two tests were carried out, one at 20*g*, and one at 30*g*. Figure 5.13, 5.14, and 5.15 illustrate the plume configuration at 20, 50, and 70 days (prototype time) for the 30*g* test, respectively.

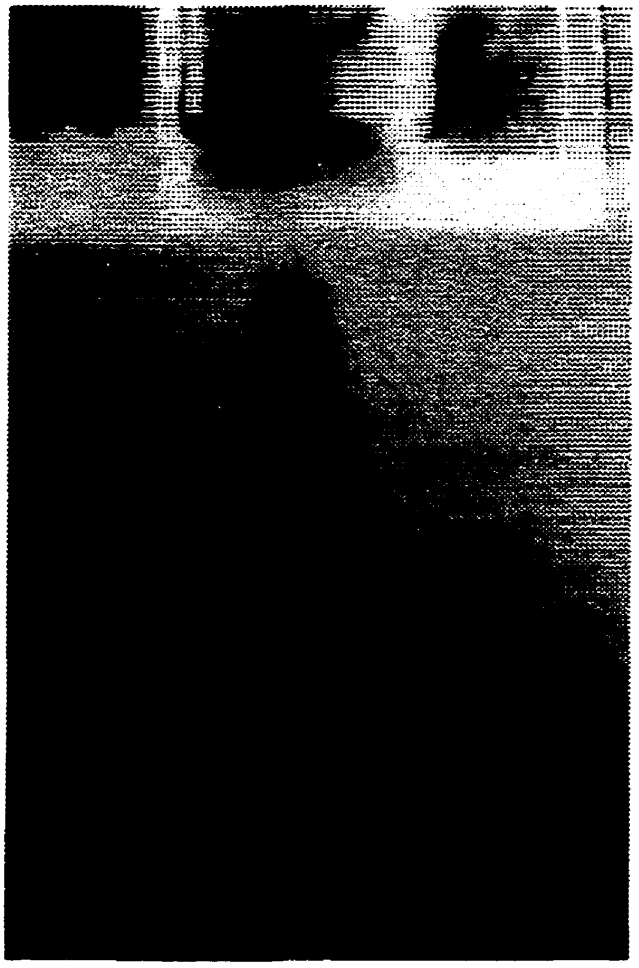

Figure 5.13 Plume development in the 30*g* test after centrifuge time of 32 minutes (prototype time of 20 days).

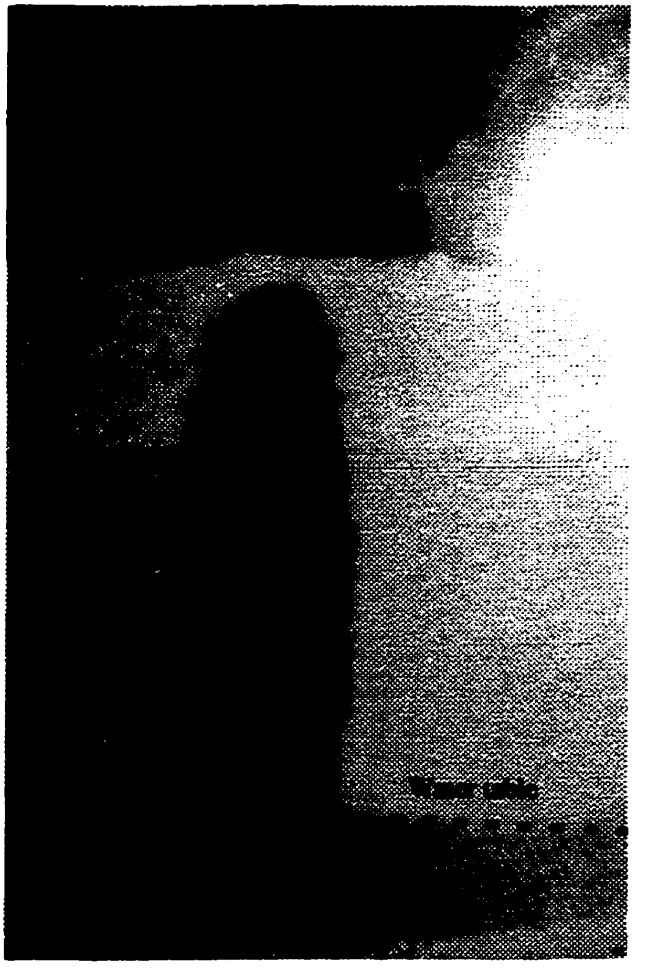

Figure 5.14 Plume development in the 30*g* test after centrifuge time of 80 minutes (prototype time of 50 days).

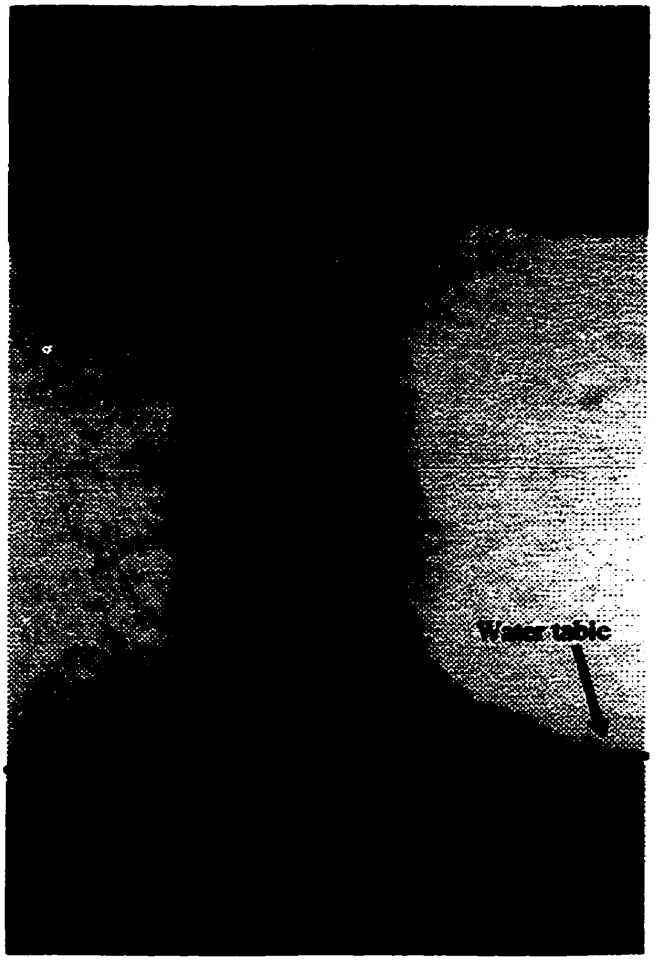

Figure 5.15 Plume development in the 30*g* test after centrifuge time of 112 minutes (prototype time of 70 days).

Comparing these photographs with Figures 5.4, 5.5, and 5.6, the differences between the plumes become evident; in the loose sand, the plume spread out laterally over a wider region. The final shapes of these plumes were traced on the side of the strong-box, scanned, and redrawn with graphics software. Figure 5.16 shows the traces of the plumes for the models consisted of dense sand and loose sand. Water and LNAPL contents are shown in Figure 5.17, 5.18, and 5.19. The vertical dimensions (distance from the water table) are converted in real scale dimensions. Figure 5.20 shows the LNAPL contents distribution in the plume. In Figure 5.20, numbers written in bigger font indicate the results of the 30 g test, whereas those in smaller font indicate the results of the 20 g tests.

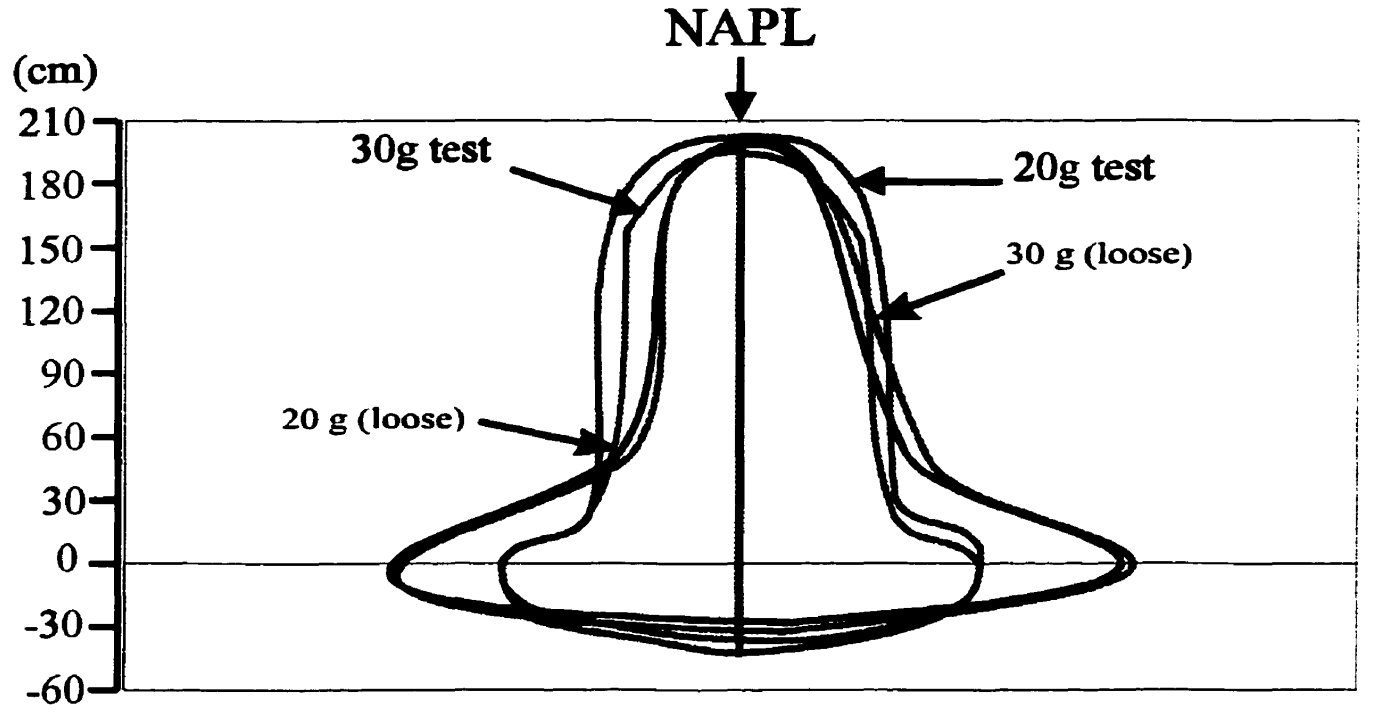

Figure 5.16 Traces of the plumes recorded at the termination of the centrifuge tests.

Time for the 20*g* tests: 324 minutes equivalent to 3 months.

Time for the 30*g* test: 144 minutes equivalent to 3 months.

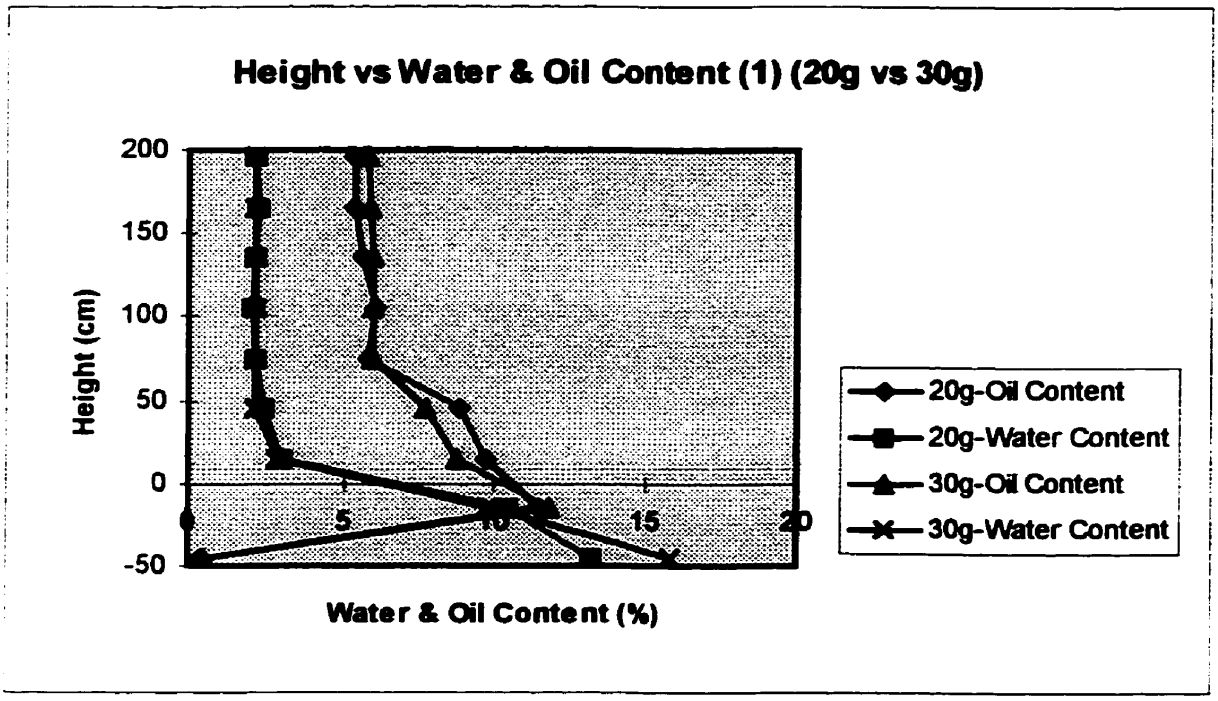

Figure 5.17 Water and LNAPL content in the column 1

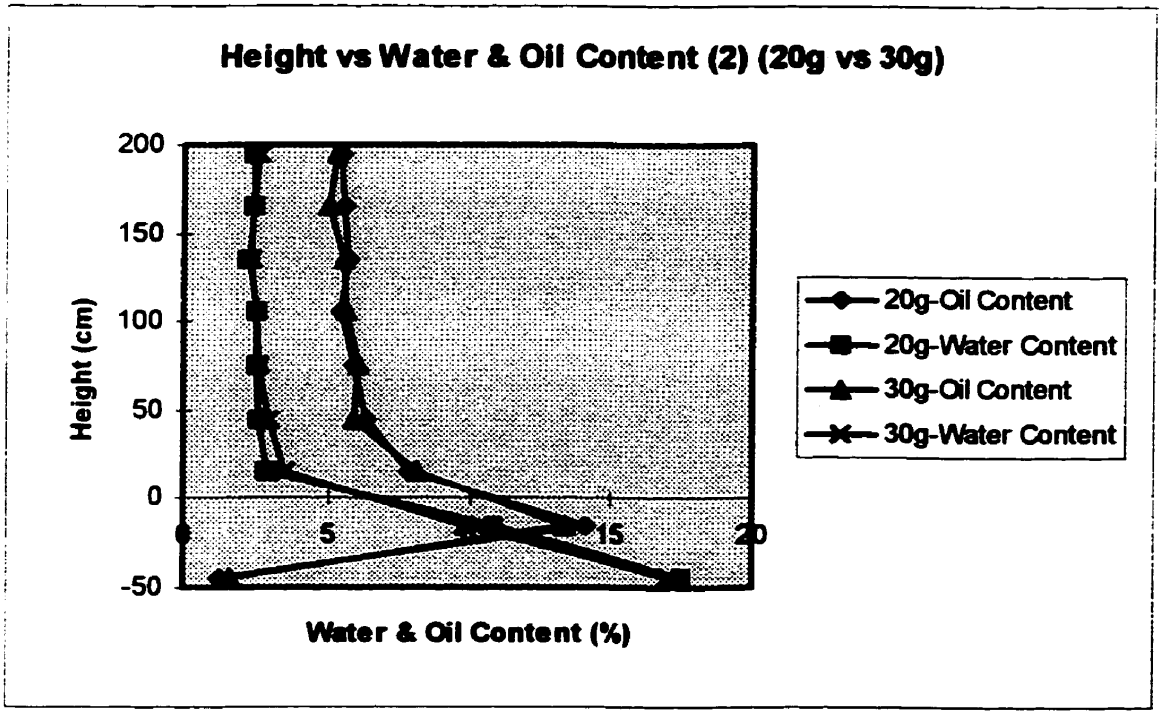

Figure 5.18 Water and LNAPL content in the column 2

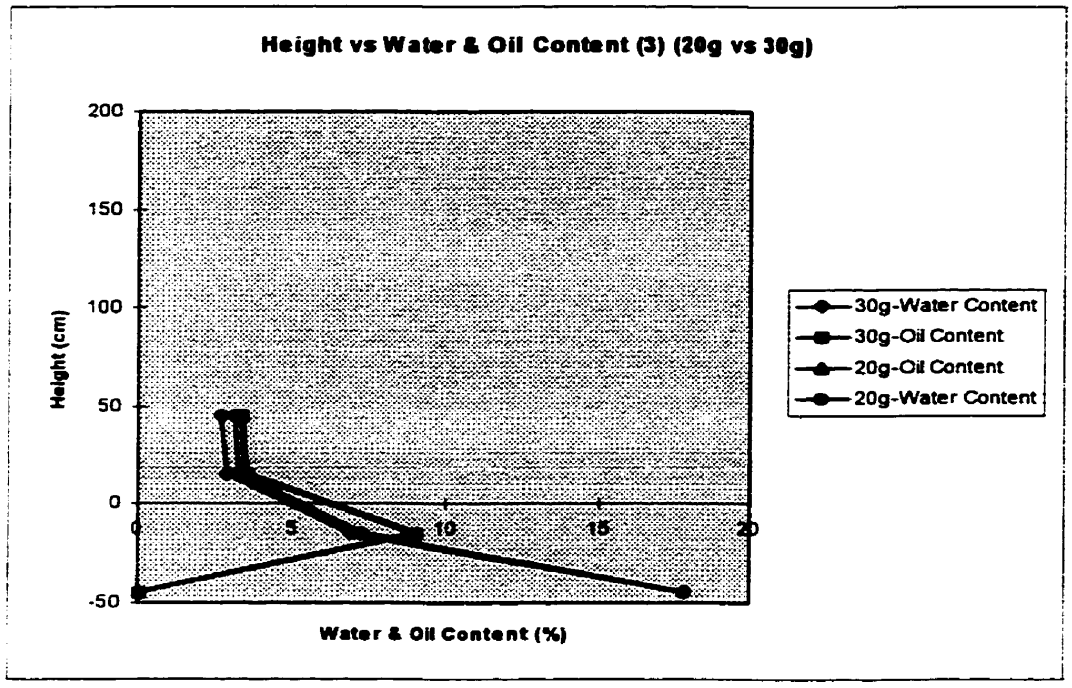

Figure 5.19 Water and LNAPL content in the column 3

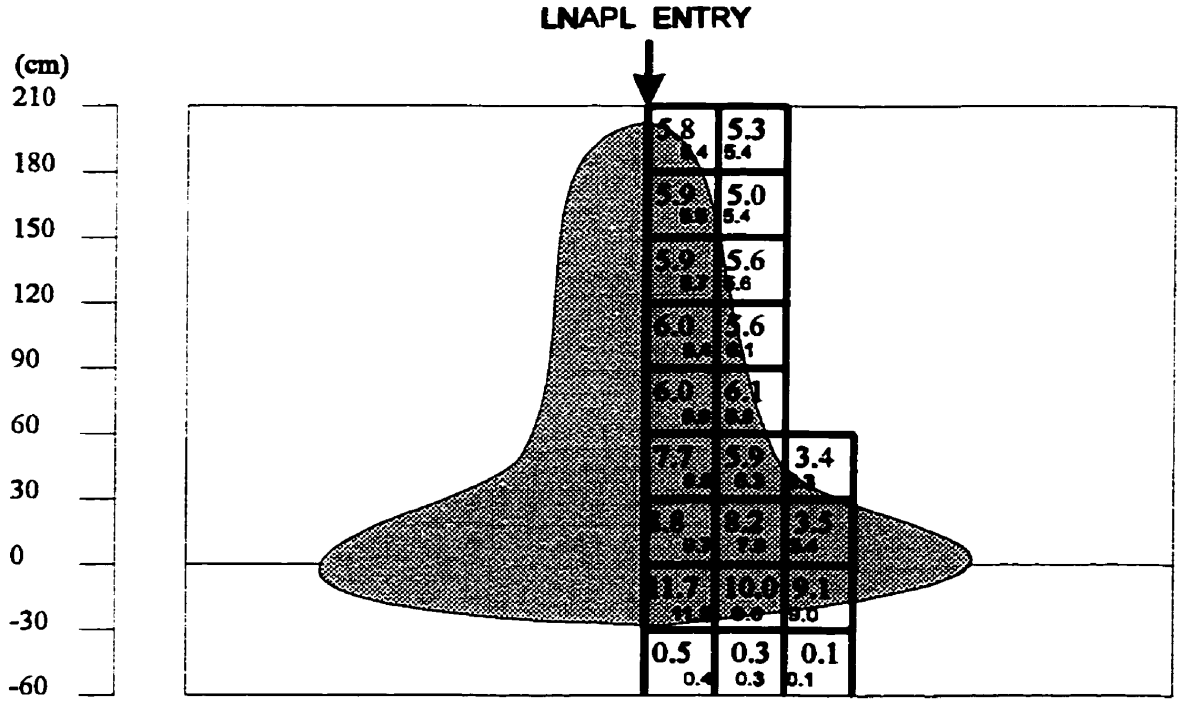

Figure 5.20 Measured LNAPL content (larger fonts for the 30g test and smaller font for the 20g test

The agreement between the results of the 20 g and 30 g tests is generally elevated. Only the LNAPL content curves in the first column demonstrated some differences in vicinity of the capillary fringe. Small quantities of LNAPL were measured under the plumes due to a slight emulsification of it. The velocity of infiltration of the LNAPL in the loose sand was greater than that in the dense sand. The LNAPL flowed out the container in about 85 days (prototype time) for the dense sand tests, and in about 70 days (prototype time) for the loose sand tests. Consequently, the amount of time necessary for the LNAPL to accumulate on the water table was shorter in dense sand than in loose sand. It was concluded that the porous medium exerted less resistance during the LNAPL downward infiltration. The intensity of the capillary forces acting in the loose sand was smaller than those acting in the dense sand. Thus, the water content throughout the unsaturated zone was smaller and the matrix suction effect on the infiltrating LNAPL was also reduced. In the unsaturated zone, the same distance from the water table along the same soil column will give a greater LNAPL content in dense sand than that in loose sand (see, for example, Figure 5.10, and 5.20). The opposite trends were observed in the saturated zone. From these observations, it is clear that a larger void volume is available for the LNAPL infiltration, and less intense surface tension forces exert an influence on the vertical movement of the LNAPL. With respect to the dense sand models, a smaller LNAPL volume was trapped as residual hydrocarbon in the vadose zone and the LNAPL movement driven by the gravity was favoured. Thus, the hydrocarbon could infiltrate through the sand with greater ease and accumulate above the water table. The horizontal dimensions of the plumes in the funicular zone were almost the same than those for the plumes achieved in tests involving dense sand.

5.3 OVERALL EXPERIMENTAL OBSERVATIONS

The overall objectives of this thesis were satisfied by the use of new a model methodology which could be used to examine complex three-phase flow phenomena in a porous medium. The major observations noted throughout the experimental research program can be summarized as follows:

1. The suction-moisture profile in unsaturated sand can be modelled in a gravity accelerated environment using the same soil of the prototype. The comparison of the results of the centrifuge tests and the 1*g* test confirms that the suction effects in the funicular zone are properly reproduced.
2. Despite the lack of similitude for some dimensionless numbers governing the phenomenon, a superficial LNAPL release can be modelled in a geotechnical centrifuge obtaining similar results at different gravity accelerations. Thus, it is possible to obtain useful information about the hydrocarbon migration in partially saturated sand.
3. A two-dimensional LNAPL flow was modelled in a transparent strong-box. This technique allowed direct observations of the infiltration progress.
4. This study confirms that the advective/dispersive and the suction gradients can be properly modelled in a centrifuge model. The similitude of the horizontal dimensions of the plume indicates that the gravity independent movement is similar at different gravity accelerations.
5. Porosity is one of the parameters which governs the LNAPL flow dynamics. The amount of trapped LNAPL in the vadose zone depends on the void size. An increase in

porosity causes a decrease in the suction gradient. As a consequence, the water content will decrease in the pendular zone and the influence of the capillary forces on the infiltrating hydrocarbon will also be reduced.

6. In loose sands, the LNAPL can migrate more easily towards the saturated zone. With the same conditions and after equal time, the volume of hydrocarbon directly in contact with the water table will be higher in loose than in dense sand. On the other hand, the amount of trapped hydrocarbon in the vadose zone will be higher in dense than in loose sand.
7. Converting the centrifuge experiments to the prototype scale, after three months, the equivalent of 1000 L LNAPL flowed through the soil and reached the water table located 210 cm beneath the sand surface. A small amount of LNAPL was also detected in the saturated zone outside the plume.

5.4 RELIABILITY OF THE RESULTS DERIVED FROM PREVIOUS CENTRIFUGE STUDIES

Recently, a large number of studies have been produced on the three-phase flow in porous media by using centrifuge modelling. Each research focused on some of the parameters governing the multi-phase flow, utilized different centrifuges, and modelled different porous media, boundary, and initial conditions. For this reason, it is extremely difficult to compare the results of the previous studies to those obtained in this research programme.

However, the theoretical aspects discussed and the techniques carried out in previous research can increase the confidence on the results obtained in this study. In fact, the use of fundamental modelling procedures of previous studies, such as limiting the maximum acceleration to 30*g* or using a LNAPL possessing density close to unity, ensured that the basic mechanical laws governing the transport process were satisfied. The different geometry of the models and release technique of the LNAPL utilized in this research, produced further information by using a modelling technology that, according to the confidence shown by previous investigators is regarded as reliable.

Illangasekare *et al.*(1991) modelled a one-dimensional multi-phase flow in silt and sand under different conditions of saturation. They compared the results obtained with the centrifuge modelling to a simple one-dimensional three-parameters mathematical model. The parameters for the mathematical model (effective immiscible fluid phase conductivity, effective capillary suction head at the fluid front, and volume fraction of the immiscible fluid phase behind the front) were derived from a bench test. The centrifuge acceleration used was 20*g*. The results of the centrifuge models showed a significant correlation to the numerical results and the research demonstrated that gravity driven fluid movement was correctly modelled.

A three-dimensional flow in the centrifuge was studied by Goforth *et al.* (1991). They restricted their attention to the measurement of the intrinsic permeability and saturated hydraulic conductivity in a water flow. The soils used in that study were sand, and silty sand, the maximum centrifuge acceleration was 24.4*g*. The authors found that the

measurement of the intrinsic permeability in the centrifuge demonstrate an excellent correlation with the results obtained from 1*g* tests, but they express their doubts about the reliability of modelling flows dominated by soil suction gradients.

Knight and Mitchell (1996) demonstrated that, in multi-phase flow, the horizontal fluid movements (diffusive and capillary effects) were properly modelled in the centrifuge. In this study, the porous medium was a fine sand; silicon oil was chosen as LNAPL, and three-dimensional models were accelerated up to 30 g. Results obtained from the centrifuge modelling and a numerical model were compared and found to be in good agreement. The confidence of the authors on the results of that research was high, since the use of different centrifuge accelerations produced consistent results. In particular, it was demonstrated that when the gravity gradient is not negligible, suction and diffusion gradients depended on the gravity driven flow. Thus, an accurate modelling of the gravity induced flow should ensure an accurate modelling of soil suction and diffusion gradients.

According to these previous studies, the author attaches a high level of confidence on the results obtained in this thesis, since the horizontal and vertical dimensions of the plumes derived from the separate tests were very similar. The geometric considerations were supported by the measurements carried out at the end of the tests which, despite the lack of significant precision, produced consistent water and LNAPL contents.

5.5 RELATIONSHIP BETWEEN CENTRIFUGE RESULTS AND PROTOTYPE SITUATION

The two-dimensional release of LNAPL from a line source attempts to model a situation that can be encountered at a long cracked storage tank or a cracked pipeline which are situated in the partially saturated zone. The geometry of the problem is illustrated in the Figure 5.21, where the dimensions (in 1*g* scale) and the different levels of saturation of the sand are also indicated.

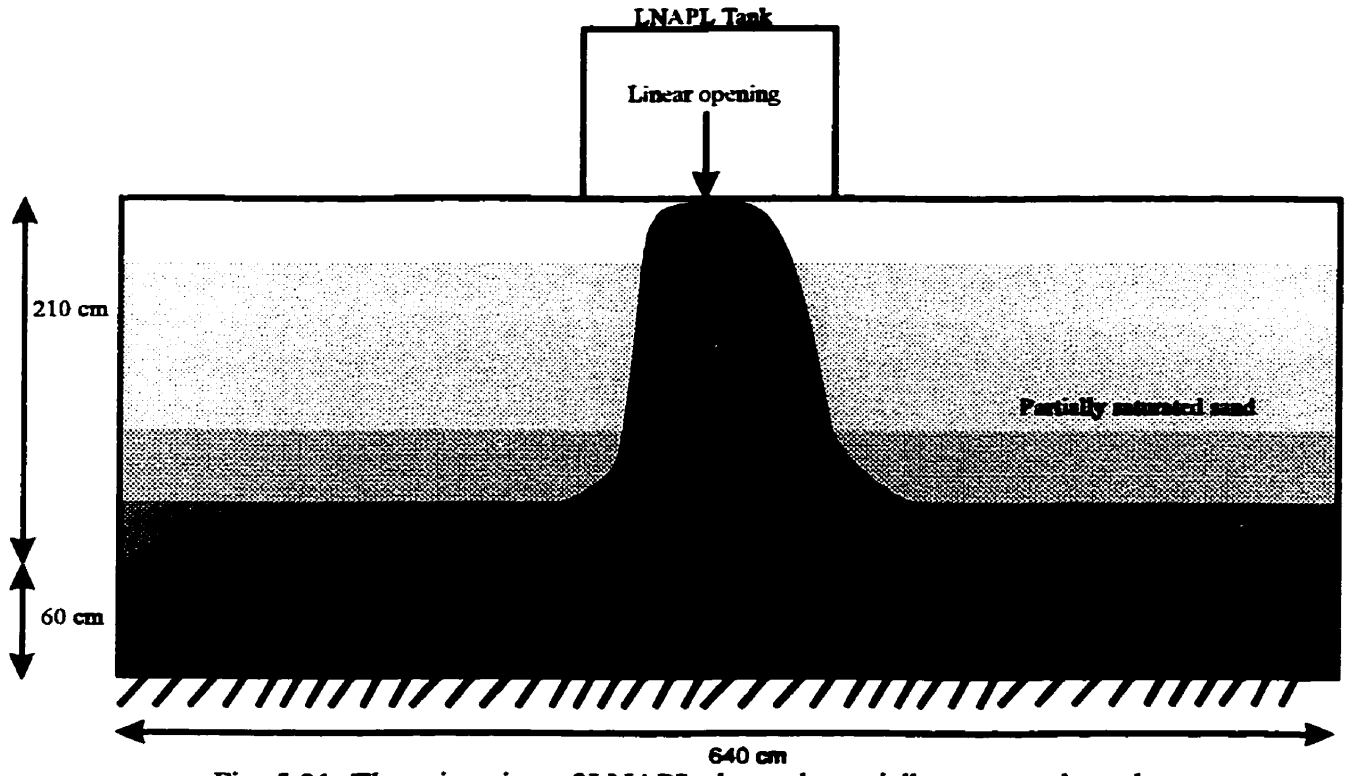

Fig. 5.21 The migration of LNAPL through partially saturated sand.

Table 5.2 Dimensions of the models

	Model at 30 g	*Model at 20 g*	*Prototype*
Thickness of sand layer	*9 cm*	*13.5 cm*	*270 cm*
Depth of the water table	*7 cm*	*10.5 cm*	*210 cm*
Tank line opening length	*0.1 cm*	*0.15 cm*	*3 cm*
Tank length	*3.33 cm*	*5 cm*	*100 cm*
Tank height	*6 cm*	*9 cm*	*180 cm*
LNAPL volume	*55.54 cm^3*	*125 cm^3*	*1×10^6 cm^3*
LNAPL head	*5.56 cm*	*8.33 cm*	*166.67 cm*
Time of infiltration	*144 minutes*	*324 minutes*	*3 months*

Table 5.2 summarizes the model dimensions converted to the prototype scale. According to the results of the centrifuge experiment, the LNAPL reaches the water table located 210 *cm* below the upper sand surface by seepage through dense and loose sand after approximately 3 months. If the sand is loose, a greater amount of LNAPL will accumulate on the water table, whereas if the sand is dense more LNAPL will remain trapped in the unsaturated zone. In the first case, the remediation of the prototype situation is very difficult since the hydrocarbon flows quickly toward the water table and after three months is already part of the ground water system. In the second case, the trapped LNAPL will be an important source of pollution for percolating water and in cases involving a rise in the water table. Remediation, however, will be possible since the volume of trapped LNAPL is greater.

6. CONCLUSIONS

The primary objective of this thesis was to develop a centrifuge modelling technique which would allow the direct observation of the movement of a multigrade motor oil lighter than water in a partially saturated zone and to complement such observations with conventional measurements of hydrocarbon and water content in the various zones at the termination of centrifuge tests. The use of the transparent strong-box is regarded as a new development in the experimental procedure. The geotechnical centrifuge of the Geotechnical Laboratory of Delft Technical University was used to achieve this objective. The experiments conducted in the centrifuge corresponded to a prototype scenario involving a deposit of Dutch Dune sand having an impervious boundary located at 270 *cm* below the ground surface. Over the first 60 *cm* from the ground level of the sand deposit, a static aquifer was present. The volume of the spill corresponded to 1000 L and the duration of the spill corresponded to three months. The simulation was carried out at two different values of gravity acceleration, $20g$ and $30g$ and the results obtained were compared by transforming all the dimesions to the prototype scale. Sand deposits prepared at two different porosities was used.

The results have shown the importance of the porosity as a governing parameter in immiscible fluid flow by demonstrating how the non-aqueous phase liquid flow is dependent on the pore dimensions. The increase in porosity favoured the vertical flow of the LNAPL and decreased the suction gradient. Horizontal LNAPL movement caused by

advection/dispersion and matrix suction were considered to be properly modelled due to the similitude in the plume horizontal dimensions. In the saturated zone, LNAPL traces were detected. For the model with the unsaturated profile, the centrifuge results were compared with a $1g$ test. Owing to the reduced prototype dimensions, a further development might be to perform a full scale test to validate the results derived from centrifuge tests for the LNAPL release. The supplementary experiments scheduled in the experimental program were performed in order to provide the basic understanding required for the interpretation of the results obtained at the end of the centrifuge models.

The LNAPL content and water content measurements were carried out by recovering core samples from the centrifuge models. In spite of the good agreement between the results obtained, the hydrocarbon distribution could be measured more efficiently by means of image processing. By using such a technique, the researcher will be able to calibrate and monitor the progress of infiltration of the LNAPL into the various regions of the unsaturated sand, continuously. This thesis provides the first preliminary step for further development of a centrifuge modelling technique which might prove to be an effective tool in accurate observations of the movement of immiscible fluids such as LNAPL in unsaturated porous media.

7. REFERENCES

Abdul, A.S., (1988). Migration of petroleum products through sandy hydrogeologic systems. *Ground Water Monitoring Review*, **8** (4): 73-81.

Abriola, L.M., Pinder, G.F. (1985). A multiphase approach to the modeling of porous media contamination by organic compounds 1. Equation development. *Water Resources Research*, **21**(1): 11-18.

Allersma, H.G.B. (1990). Centrifuge research TU Delft: Computer controlled sand pluviation machine. *Internal report no.325.*Geotechnical Laboratory, Delft Technical University.

Allersma, H.G.B. (1991). Using image processing in centrifuge research. *Centrifuge 91.* (eds. Ko, McLean), Balkema, Rotterdam, The Netherlands: 551-559.

Allersma, H.G.B. (1994). The University of Delft geotechnical centrifuge. *Centrifuge94*, (eds. Leung, Lee, Tan), Balkema, Rotterdam, The Netherlands: 47-52.

Allersma, H.G.B., Hospers, B., den Braber, M.G., (1996). Centrifuge tests on the sliding behaviour of spudcans. *Proceeding of the 49th Canadian Geotechnical Conference:* 199-206.

American Public Health Association (1995). Standard methods for the examination of water and wastewater, 19th edition. A.P.H.A., Washington DC.

Arulanadan, K., Thompson, P.Y., Kutter, B.L., Neegoda, N.J., Muraleetharan, K.K., and Yogachandran, C. (1988). Centrifuge modeling of transport processes for pollutants in soils. *Journal of Geotechnical Engineering ASCE*, **114**(2): 185-205.

Baehr, A.L., (1987). Selective transport of hydrocarbon in the unsaturated zone due to aqueous and vapor partioning. *Water Resources Research.* **23** (10): 1926-1938.

Bear, J. (1972). *Dynamics of Fluids in Porous Media.* American Elsevier Inc., New York, N.Y..

Bear, J. (1979). *Hydraulics of Groundwater*. McGraw-Hill, New York, N.Y..

Boon, M.P., Craig, W.H., (1978). Model ground anchors under gravitational and centrifugal accelerations. *Revue Francaise de Geotechnique*, **3**: 18-23

Cook, B., and Mitchell, R.J., (1991). Physical modelling of a dissolved contaminant in an unsaturated sand. *Canadian Geotechnical Journal*, **28**(4): 829-833.

Corapcioglu, M.Y., Baehr, A.L., (1987). A compositional multi-phase model for groundwater contamination by petroleum products: 1 Theoretical considerations. *Water Resources Research.* **23** (1): 191-200.

Corapcioglu, M.Y., Hossain, M.A., (1986). Migration of chlorinated Hydrocarbons in Groundwater. *Hydrocarbons in Ground Water: Prevention, Detection, and Restoration, National Water Well Association:* 33-52.

Fetter, C.W., (1993). *Contaminant Hydrogeology*. Macmillan Publishing Company, New York, N.Y..

Goforth, G.F., Bloomquist, D., Townsend, F.C., (1991). Saturated and unsaturated fluid flow in a centrifuge. *Centrifuge 91.* (eds. Ko, McLean), Balkema, Rotterdam, The Netherlands: 497 - 502.

Gravelle, C.F., Knight, M.A., and Mitchell, R.J., (1996). Measurement of two-fluid saturation in a fine to medium sand. *Canadian Geotechnical Journal*, **33** (4):1014-1017.

Granet, I., (1996*). Fluid Mechanics*. Prentice-Hall International Inc., Englewood Cliffs, N.J..

Illangasekare, T.H., Znidarcic, D., Al-Sheridda, M., Reible, D.D., (1991). Multiphase flow in porous media. *Centrifuge 91.* (eds. Ko, McLean), Balkema, Rotterdam, The Netherlands: 517 - 525.

Knight, M.A., Mitchell, (1996). Modelling of light nonaqueous phase liquid (LNAPL) releas into unsaturated sand. *Canadian Geeotechnical Journal*, **33** (4): 913-925.

Mandel, J., D'Escartha, Y., Halphen, B., Habib, P., Luong, M.P., Zarka, J., (1975). Theoretical and experimental study of the stability of underground cavities. *Symposium Franco-Polonais. Problemes de rheologie et de mechanique des sols, Nice*: 225-270.

Mikasa, M., Takada, N., (1973). Significance of centrifugal model test in soil mechanics. *Proceeding of the 8th International Conference in Soil Mechanics and Foundation Engineering*,. **1.2**: 273-278.

Mitchell, R.J., (1991). Centrifuge modelling as a consulting tool. *Canadian Geotechnical Journal*, **28**(1): 162-167.

Mitchell, R.J. (1994). Matrix suction and diffusive transport in centrifuge models. *Canadian Geotechnical Journal*, **31**(2): 357-363.

Mitchell, R.J., Stratton, B.C., (1994). LNAPL penetration into porous media. *Centrifuge 94*. (eds. Leung, Lee, Tan), Balkema, Rotterdam, The Netherlands: 345 - 350.

Morrow, N.R., and Songkran, B., (1981). Effect of viscous and buoyancy forces on non-wetting phase trapping in porous media. *Surface Phenomena in Enhanced Oil Recovery*. Plenum Press, New York, N.Y.: 387- 411.

Parker, J.C., (1989). Multiphase flow and transport in porous media. *Reviews of Geophysics*, **27** (3): 311-328.

Phillips, E., (1869). D'equilibre des solides elastiques sembables. *C.R. Academy Scientifique de Paris*, Vol. 68: 75-79.

Pinder, G.F., Abriola, L.M., (1986). On the simulation of Nonaqueous Phase Organic Compounds in the subsurface. *Water Resources Research*, **22** (9): 109S-119S.

Pokrovskii, G.I., Fiodorov, I.S., (1936). Studies of soil pressures and deformations by means of a centrifuge. *Proceeding of the 1st International Conference in Soil Mechanics and Foundation Engineering*, **1**: 70.

Schwille, F., (1981). Groundwater pollution by fluids immiscible with water. *The Science of the Environment*, **21**:173-185.

Schwille, F., (1984). Migration of organic fluids immiscible with water in the unsaturated zone. *Pollutants in Porous Media* . Springer-Verlag, Berlin, Germany: 27-48.

Schwille, F., (1988). *Dense chlorinated solvents in porous and fracturated media*. Lewis Publisher, Chelesea, Mich..

Stone, H.L., (1973). Estimation of three-phase relative permeability and residual oil data. *Journal of Canadian Petroleum Technology*, **12**(4): 53-61.

Stuit, H.G., (1995). *Sand in the Geotechnical Centrifuge*. PhD Thesis. Delft University of Technology.

Yamaguchi, H., Kimura, T., Fujii, N., (1977). On the scale effect of footings in dense sand. *Proceeding of the 9th International Conference in Soil Mechanics and Foundation Engineering*, **1.1**: 795-798.

APPENDIX A - RAW DATA

TEST OF THE SAMPLING TECHNIQUE:

Samp.	*W. Solid (g)*	*Vol. Solid (cm^3)*	*Vol. Void (cm^3)*	*Initial w*	*Satur.*	*Measured w*	*Error*
1	4.367	1.617	0.906	20.741%	100%	20.511%	98.891%
2	4.692	1.738	0.973	13.813%	66%	13.806%	99.949%
3	8.172	3.027	1.695	20.741%	100%	20.483%	98.756%
4	8.464	3.135	1.755	13.813%	66%	13.795%	99.870%

TEST OF THE EFFICIENCY OF THE DRYING OUT PROCESS (SUCTION-MOISTURE PROFILE) :

time (h)	*Ws (g)*	*Vs (cm^3)*	*Vv (cm^3)*	*Ww 100(g)*	*w*	*Ww 66(g)*	*w*	*Ww 33(g)*	*w*
0	10	3.704	2.074	2.074	20.741%	1.369	13.689%	0.684	6.844%
1	10	3.704	2.074	1.815	18.145%	0.996	9.960%	0.313	3.129%
2	10	3.704	2.074	1.607	16.065%	0.612	6.123%	0.005	0.045%
3	10	3.704	2.074	1.300	13.003%	0.294	2.939%	0.000	0.000%
4	10	3.704	2.074	1.058	10.580%	0.000	0.000%	0.000	0.000%
5	10	3.704	2.074	0.644	6.438%	0.000	0.000%	0.000	0.000%
6	10	3.704	2.074	0.323	3.226%	0.000	0.000%	0.000	0.000%
7	10	3.704	2.074	0.000	0.000%	0.000	0.000%	0.000	0.000%
8	10	3.704	2.074	0.000	0.000%	0.000	0.000%	0.000	0.000%
9	10	3.704	2.074	0.000	0.000%	0.000	0.000%	0.000	0.000%

SUCTION-MOISTURE PROFILE TESTS:

30 g Test 1

Container	*C*	*Location*	*C+S+W*	*S+W*	*C+S*	*W*	*S*	*W%*	*S30*
1	82.601	0=1	96.201	13.600	95.581	0.620	12.980	0.0478	21.222
2	82.682	1=2	97.086	14.404	96.405	0.681	13.723	0.0496	22.048
3	82.652	2=3	97.253	14.601	96.551	0.702	13.899	0.0505	22.440
4	82.613	3=4	97.183	14.570	96.453	0.730	13.840	0.0527	23.435
5	82.624	4=5	97.052	14.428	96.202	0.850	13.578	0.0626	27.814
6	82.661	5=6	98.350	15.689	96.804	1.546	14.143	0.109	48.567
7	82.620	6=7	99.336	16.716	96.801	2.535	14.181	0.179	79.423
8	82.322	7=9	99.552	17.230	96.806	2.746	14.484	0.190	84.234

30 g Test 2

Container	C	Location	C+S+W	S+W	C+S	W	S	W%	S30 2
1	82.601	0=1.5	97.208	14.607	96.480	0.728	13.879	0.0525	25.290
2	82.682	1.5=3.0	94.697	12.015	94.101	0.596	11.419	0.0522	25.165
3	82.652	3.0=4.5	98.503	15.851	97.694	0.809	15.042	0.0538	25.931
4	82.613	4.5=6.0	97.667	15.054	96.908	0.759	14.295	0.0531	25.600
5	82.624	6.0=7.5	97.971	15.347	97.003	0.968	14.379	0.0673	32.458
6	82.661	7.5=9.0	97.094	14.433	95.452	1.642	12.791	0.1284	61.893
7	82.620	9.0=10.5	98.773	16.153	96.435	2.338	13.815	0.1692	81.596
8	82.322	10.5=13.5	98.159	15.837	95.554	2.605	13.232	0.1969	94.920

20 g Test 1

Container	C	Location	C+S+W	S+W	C+S	W	S	W%	S20
1	82.601	0=1.5	96.128	13.527	95.480	0.648	12.879	0.050	24.259
2	82.682	1.5=3.0	96.596	13.914	96.011	0.585	13.329	0.044	21.161
3	82.652	3.0=4.5	97.503	14.851	96.783	0.720	14.131	0.051	24.566
4	82.613	4.5=6.0	97.921	15.308	97.205	0.716	14.592	0.049	23.658
5	82.624	6.0=7.5	97.971	15.347	97.003	0.968	14.379	0.067	32.458
6	82.661	7.5=9.0	98.094	15.433	96.552	1.542	13.891	0.111	53.521
7	82.620	9.0=10.5	98.950	16.330	96.402	2.548	13.782	0.185	89.138
8	82.322	10.5=13.5	98.259	15.937	95.815	2.444	13.493	0.181	87.331

20 g Test 2

Container	C	Location	C+S+W	S+W	C+S	W	S	W%	S20
1	82.601	0=1.5	96.051	13.450	95.482	0.569	12.881	0.044	21.298
2	82.682	1.5=3.0	96.650	13.968	96.001	0.649	13.319	0.049	23.494
3	82.652	3.0=4.5	97.450	14.798	96.780	0.670	14.128	0.047	22.865
4	82.613	4.5=6.0	97.958	15.345	97.203	0.755	14.590	0.052	24.950
5	82.624	6.0=7.5	97.952	15.328	97.001	0.951	14.377	0.066	31.892
6	82.661	7.5=9.0	98.153	15.492	96.550	1.603	13.889	0.115	55.647
7	82.620	9.0=10.5	99.951	17.331	97.401	2.550	14.781	0.173	83.179
8	82.322	10.5=13.5	100.250	17.928	97.607	2.643	15.285	0.173	83.370

1 g Test

Saturation (%)	Height (cm)
30	75
31	72
32	69
34	66
36	63
38	60
41	57
43	54
46	51
50	48
53	45
57	42
60	39
64	36
68	33
72	30
77	27
82	24
87	21
90	18
94	15
99	12
99	9
99	6
100	3
100	0

TEST OF THE EFFICIENCY OF THE DRYING OUT PROCESS (SPILL SIMULATION) :

Time (hours)	*Ws (g)*	*Vs*	*Vv*	*Ww 66 (g)*	*w*	*Ww 33 (g)*	*w*
0	10	3.70	2.07	1.37	13.69	0.68	6.84
1	10	3.70	2.07	1.09	10.91	0.39	3.94
2	10	3.70	2.07	0.73	7.34	0.10	0.98
3	10	3.70	2.07	0.41	4.07	0.00	0.00
4	10	3.70	2.07	0.10	1.00	0.00	0.00
5	10	3.70	2.07	0.00	0.00	0.00	0.00
6	10	3.70	2.07	0.00	0.00	0.00	0.00
7	10	3.70	2.07	0.00	0.00	0.00	0.00
8	10	3.70	2.07	0.00	0.00	0.00	0.00
9	10	3.70	2.07	0.00	0.00	0.00	0.00
10	10	3.70	2.07	0.00	0.00	0.00	0.00

SPILL SIMULATION DENSE SAND

20 g Column 1

C	*Location*	*C+S+W+O*	*C+S+O*	*C+S*	*S+W+O*	*S+O*	*S*	*W*	*O*	*w%*	*oil%*
82.604	A1	85.784	85.719	85.513	3.18	3.115	2.909	0.065	0.206	0.022	0.071
82.650	B1	85.849	85.782	85.578	3.199	3.132	2.928	0.067	0.204	0.023	0.070
82.622	C1	85.284	85.228	85.059	2.662	2.606	2.437	0.056	0.169	0.023	0.069
82.620	D1	85.185	85.135	84.972	2.565	2.515	2.352	0.050	0.163	0.021	0.069
82.483	E1	85.462	85.399	85.209	2.979	2.916	2.726	0.063	0.190	0.023	0.070
83.224	F1	85.498	85.450	85.298	2.274	2.226	2.074	0.048	0.152	0.023	0.073
82.530	G1	85.395	85.318	85.117	2.865	2.788	2.587	0.077	0.201	0.030	0.078
83.262	H1	85.601	85.401	85.196	2.339	2.139	1.934	0.200	0.205	0.103	0.106
82.491	I1	85.333	85.002	84.964	2.842	2.511	2.473	0.331	0.038	0.134	0.015

20 g column 2

C	*Location*	*C+S+W+O*	*C+S+O*	*C+S*	*S+W+O*	*S+O*	*S*	*W*	*O*	*w%*	*oil%*
82.604	A2	85.056	85.004	84.888	2.452	2.400	2.284	0.052	0.116	0.023	0.051
82.650	B2	85.101	85.045	84.918	2.451	2.395	2.268	0.056	0.127	0.025	0.056
82.622	C2	85.233	85.171	85.034	2.611	2.549	2.412	0.062	0.137	0.026	0.057
82.620	D2	85.716	85.633	85.454	3.096	3.013	2.834	0.083	0.179	0.029	0.063
82.483	E2	85.315	85.255	85.102	2.832	2.772	2.619	0.060	0.153	0.023	0.058
83.224	F2	85.575	85.516	85.386	2.351	2.292	2.162	0.059	0.130	0.027	0.060
82.530	G2	85.839	85.762	85.588	3.309	3.232	3.058	0.077	0.174	0.025	0.057
83.262	H2	86.758	86.402	86.031	3.496	3.140	2.769	0.356	0.371	0.129	0.134
82.491	I2	86.612	86.114	86.021	4.121	3.623	3.530	0.498	0.093	0.141	0.026

20 g column 3

C	*Location*	*C+S+W+O*	*C+S+O*	*C+S*	*S+W+O*	*S+O*	*S*	*W*	*O*	*w%*	*oil%*
82.530	F3	83.955	83.903	83.873	1.425	1.373	1.343	0.052	0.030	3.872	2.2338
83.230	G3	85.632	85.495	85.444	2.402	2.265	2.214	0.137	0.051	6.188	2.30352
83.290	H3	85.831	85.743	85.550	2.541	2.453	2.260	0.088	0.193	3.894	8.53982
82.510	I3	84.006	83.780	83.777	1.496	1.270	1.267	0.226	0.003	17.837	0.23678

30 g column 1

C	*Location*	*C+S+W+O*	*C+S+O*	*C+S*	*S+W+O*	*S+O*	*S*	*W*	*O*	*w%*	*oil%*
82.604	A1	84.475	84.437	84.309	1.871	1.833	1.705	0.038	0.128	0.022	0.075
82.650	B1	84.806	84.762	84.626	2.156	2.112	1.976	0.044	0.136	0.022	0.069
82.622	C1	83.930	83.903	83.821	1.308	1.281	1.199	0.027	0.082	0.023	0.068
82.620	D1	84.067	84.036	83.949	1.447	1.416	1.329	0.031	0.087	0.023	0.065
82.483	E1	84.442	84.404	84.283	1.959	1.921	1.800	0.038	0.121	0.021	0.067
83.224	F1	85.443	85.400	85.248	2.219	2.176	2.024	0.043	0.152	0.021	0.075
82.530	G1	84.365	84.318	84.191	1.835	1.788	1.661	0.047	0.127	0.028	0.076
83.262	H1	84.460	84.355	84.256	1.198	1.093	0.994	0.105	0.099	0.106	0.100
82.491	I1	84.091	83.911	83.869	1.600	1.420	1.378	0.180	0.042	0.131	0.030

30 g column 2

C	*Location*	*C+S+W+O*	*C+S+O*	*C+S*	*S+W+O*	*S+O*	*S*	*W*	*O*	*w%*	*oil%*
82.680	A2	84.000	83.970	83.905	1.320	1.290	1.225	0.030	0.065	0.024	0.053
82.610	B2	84.055	84.025	83.949	1.445	1.415	1.339	0.030	0.076	0.022	0.057
82.660	C2	84.178	84.141	84.060	1.518	1.481	1.400	0.037	0.081	0.026	0.058
82.320	D2	84.584	84.555	84.474	2.264	2.235	2.154	0.029	0.081	0.013	0.038
82.570	E2	84.142	84.110	84.021	1.572	1.540	1.451	0.032	0.089	0.022	0.061
83.260	F2	84.497	84.466	84.396	1.237	1.206	1.136	0.031	0.070	0.027	0.062
83.300	G2	84.718	84.681	84.583	1.418	1.381	1.283	0.037	0.098	0.029	0.076
82.490	H2	85.486	85.220	84.979	2.996	2.730	2.489	0.266	0.241	0.107	0.097
83.190	I2	88.831	88.010	87.825	5.641	4.820	4.635	0.821	0.185	0.177	0.040

30 g column 3

C	*Location*	*C+S+W+O*	*C+S+O*	*C+S*	*S+W+O*	*S+O*	*S*	*W*	*O*	*w%*	*oil%*
82.530	F3	83.655	83.613	83.588	1.125	1.083	1.058	0.042	0.025	3.970	2.363
83.230	G3	84.571	84.496	84.466	1.341	1.266	1.236	0.075	0.030	6.068	2.527
83.290	H3	84.891	84.803	84.578	1.601	1.513	1.288	0.088	0.225	6.832	8.911
82.510	I3	85.466	85.025	85.033	2.956	2.515	2.523	0.241	0.008	17.479	0.217

SPILL SIMULATION ON LOOSE SAND

20 g column 1

C	*Location*	*C+S+W+O*	*C+S+O*	*C+S*	*S+W+O*	*S+O*	*S*	*W*	*O*	*w%*	*oil%*
82.604	A1	84.985	84.937	84.809	2.381	2.333	2.205	0.048	0.128	0.022	0.058
82.650	B1	85.214	85.162	85.021	2.564	2.512	2.371	0.052	0.141	0.022	0.059
82.622	C1	84.198	84.166	84.079	1.576	1.544	1.457	0.032	0.087	0.022	0.060
82.620	D1	84.373	84.338	84.241	1.753	1.718	1.621	0.035	0.097	0.022	0.060
82.483	E1	84.852	84.804	84.673	2.369	2.321	2.19	0.048	0.131	0.022	0.060
83.224	F1	85.833	85.781	85.598	2.609	2.557	2.374	0.052	0.183	0.022	0.077
82.530	G1	84.775	84.718	84.541	2.245	2.188	2.011	0.057	0.177	0.028	0.088
83.262	H1	84.799	84.675	84.526	1.537	1.413	1.264	0.124	0.149	0.098	0.118
82.491	I1	84.599	84.311	84.301	2.108	1.82	1.81	0.288	0.01	0.159	0.006

20 g column 2

C	*Location*	*C+S+W+O*	*C+S+O*	*C+S*	*S+W+O*	*S+O*	*S*	*W*	*O*	*w%*	*oil%*
82.604	A2	84.001	83.970	83.899	1.397	1.366	1.295	0.031	0.071	0.024	0.055
82.650	B2	84.057	84.025	83.953	1.407	1.375	1.303	0.032	0.072	0.025	0.055
82.622	C2	84.173	84.141	84.059	1.551	1.519	1.437	0.032	0.082	0.022	0.057
82.620	D2	84.601	84.555	84.455	1.981	1.935	1.835	0.046	0.100	0.025	0.054
82.483	E2	84.149	84.110	84.019	1.666	1.627	1.536	0.039	0.091	0.025	0.059
83.224	F2	84.496	84.466	84.392	1.272	1.242	1.168	0.030	0.074	0.026	0.063
82.530	G2	84.738	84.681	84.523	2.208	2.151	1.993	0.057	0.158	0.029	0.079
83.262	H2	85.406	85.220	84.979	2.144	1.958	1.717	0.186	0.241	0.108	0.140
82.491	I2	88.969	88.010	87.941	6.478	5.519	5.450	0.959	0.069	0.176	0.013

20 g column 3

C	*Location*	*C+S+W+O*	*C+S+O*	*C+S*	*S+W+O*	*S+O*	*S*	*W*	*O*	*w%*	*oil%*
82.53	F3	83.939	83.903	83.859	1.409	1.373	1.329	0.036	0.044	2.7	3.3
83.23	G3	85.558	85.495	85.42	2.328	2.265	2.19	0.063	0.075	2.9	3.4
83.29	H3	85.899	85.743	85.541	2.609	2.453	2.251	0.156	0.202	6.9	9.0
82.51	I3	84.242	83.98	83.979	1.732	1.47	1.469	0.262	0.001	17.8	0.1

30 g column 1

C	*Location*	*C+S+W+O*	*C+S+O*	*C+S*	*S+W+O*	*S+O*	*S*	*W*	*O*	*w%*	*oil%*
82.604	A1	85.783	85.719	85.559	3.179	3.115	2.955	0.064	0.160	0.022	0.054
82.650	B1	85.848	85.782	85.621	3.198	3.132	2.971	0.066	0.161	0.022	0.054
82.622	C1	85.281	85.228	85.089	2.659	2.606	2.467	0.053	0.139	0.021	0.056
82.620	D1	85.185	85.135	84.991	2.565	2.515	2.371	0.050	0.144	0.021	0.061
82.483	E1	85.459	85.399	85.239	2.976	2.916	2.756	0.060	0.160	0.022	0.058
83.224	F1	85.499	85.450	85.268	2.275	2.226	2.044	0.049	0.182	0.024	0.089
82.530	G1	85.395	85.318	85.071	2.865	2.788	2.541	0.077	0.247	0.030	0.097
83.262	H1	85.601	85.401	85.181	2.339	2.139	1.919	0.200	0.220	0.104	0.115
82.491	I1	85.333	85.002	84.991	2.842	2.511	2.500	0.331	0.011	0.132	0.004

30 g column 2

C	*Location*	*C+S+W+O*	*C+S+O*	*C+S*	*S+W+O*	*S+O*	*S*	*W*	*O*	*w%*	*oil%*
82.604	A2	84.004	83.970	83.901	1.400	1.366	1.297	0.034	0.069	0.026	0.053
82.650	B2	84.057	84.025	83.959	1.407	1.375	1.309	0.032	0.066	0.024	0.050
82.622	C2	84.175	84.141	84.061	1.553	1.519	1.439	0.034	0.080	0.024	0.056
82.620	D2	84.601	84.555	84.452	1.981	1.935	1.832	0.046	0.103	0.025	0.056
82.483	E2	84.150	84.110	84.017	1.667	1.627	1.534	0.040	0.093	0.026	0.061
83.224	F2	84.496	84.461	84.392	1.272	1.237	1.168	0.035	0.069	0.030	0.059
82.530	G2	84.751	84.681	84.518	2.221	2.151	1.988	0.070	0.163	0.035	0.082
83.262	H2	85.391	85.220	84.989	2.129	1.958	1.727	0.171	0.231	0.099	0.134
82.491	I2	88.941	88.010	87.921	6.450	5.519	5.430	0.931	0.089	0.171	0.016

30 g column 3

C	*Location*	*C+S+W+O*	*C+S+O*	*C+S*	*S+W+O*	*S+O*	*S*	*W*	*O*	*w%*	*oil%*
82.53	F3	83.945	83.903	83.858	1.415	1.373	1.328	0.042	0.045	3.2	3.4
83.23	G3	85.567	85.495	85.418	2.337	2.265	2.188	0.072	0.077	3.3	3.5
83.29	H3	85.907	85.743	85.539	2.617	2.453	2.249	0.164	0.204	7.3	9.1
82.51	I3	84.006	83.78	83.779	1.496	1.27	1.269	0.226	0.001	17.8	0.1